2016

Molecular Basis of Mechanosensitivity

Josefina Ines del Marmol

MOLECULAR BASIS OF MECHANOSENSITIVITY

A Thesis Presented to the Faculty of

The Rockefeller University

in Partial Fulfillment of the Requirements for

the degree of Doctor of Philosophy

by

Josefina Inés del Mármol

June 2016

MOLECULAR BASIS OF MECHANOSENSITIVITY

Josefina Inés del Mármol, Ph.D.

The Rockefeller University 2016

Mechanosensation is arguably the least understood of all senses. For most physiological processes, the first response to membrane stress is thought to be the opening or closing of mechanosensitive channels[1], but the clonal nature of the first mechanotransducers is still largely unknown. The objective of my research was to identify molecules involved in mechanosensory transduction by both studying known channels as well as performing screens to identify previously uncharacterized channels.

Shortly before my research began, Daniel Schmidt from the MacKinnon Lab showed that certain voltage gated potassium channels, not previously associated with mechanosensation, are in fact remarkably sensitive to membrane tension in isolated membrane patches[2]. I therefore began investigating the possibility of voltage gated potassium channels being mechanosensitive in physiological contexts. Results using hypo-osmotic swelling provided additional support that Paddle Chimaera and Kv2.1 are indeed mechanosensitive in cellular contexts[3]. Given the close structural similarity between voltage gated potassium channels and other ion channel families, I extended these studies to include sodium and calcium selective voltage gated ion channels using patch inflation, swelling, poking, and stretching. However the sodium selective voltage gated channel, Nav1.7, and calcium selective voltage gated channels, Cav1.2 and Cav1.3, were not found to display major mechanosensitive properties.

In a complimentary approach, I performed a screen of 10 different cell lines using the poking assay to identify novel molecules involved in mechanical transduction. My results identified multiple undescribed slow-inactivating mechanosensitive currents in cell lines from a variety of sources including numerous cancer cell lines, human stem cells and mouse stem cells. Further work using transcriptome analysis, bioinformatic techniques, and electrophysiological recordings identified that the pore forming subunit responsible for the slow-inactivating mechanosensitive conductances in mouse embryonic stem cells is Piezo1, a mechanosensitive channel canonically known for displaying fast-inactivating kinetics. With very few modulators known to date[4,5], the mechanism by which Piezo1 could produce slow inactivating currents was not known.

To address possible novel sources of modulation of Piezo1 currents, I performed transcriptome analyses that identified 2 potential candidates including one novel protein subsequently confirmed to modify the behavior of Piezo1 *in vitro*. This protein, Plp2, is a small transmembrane protein of undescribed function that amplifies the magnitude and slows down the kinetics of Piezo1 in heterologous expression. The other protein, Cd63, is also a transmembrane protein that only amplifies the magnitude of Piezo1 currents, with no modification of its kinetics, in heterologous expression.

Given the remarkably large set of functions that have been attributed to Piezo channels[6,7,8,9] in the very few years since its discovery, and how little we still know of its functional mechanisms, the identification of novel modulators provides a crucial next step in elucidating the molecular basis of mechanosensation.

To my mentors, past and present, Amanda Ernitz and Rod MacKinnon.

Acknowledgements

I would like to first and foremost thank Professor Rod MacKinnon for his never-ending support, commitment to excellence, careful guidance, encouragement, and impeccable research ethics.

I would also like to especially thank the members of my scientific committee, Cori Bargmann and Sandy Simon, for having always been available for advice and support, and for having so carefully reviewed every step of my scientific endeavors at the Rockefeller University.

A great number of people in the MacKinnon lab have enriched my life in the past years, both scientifically and socially. For this I particularly thank Ernie, Steve, Zhenwei, Kouki, Xiao, Jill, Chris, Weiwei and Rich. I thank all other members of the MacKinnon lab, past and present, for forming such a fantastic group of work.

The Dean's Office has been always available for all types of help and advice, for which I thank Sid, Emily, Cris, Marta, Kristen and Stephanie.

A number of faculty members of the Rockefeller University have made an indelible impact in my career, not just because of their exciting scientific production but also through their willingness to chat and offer advice. I would like to thank Vanessa Ruta, Leslie Vosshall, Sebastian Klinge, Ali Brivanlou, Jue Chen, Winrich Freiwald, and David Gadbsy for their much-welcomed advice.

Mis padres, Olga y José, merecen todos mis agradecimientos por haber siempre amorosamente provisto todas las chances para mi aprendimiento, progreso y éxito. Les agradezco también por el apoyo y cuidado contínuo, aún en la distancia.

I emphatically thank my wonderful and supportive husband, Jeff, for his unimaginable patience and tiredless editing. Along with my new family, Janice, Jerry, Gwyn, Ani, Randy, Mike, Sofi, Riley, Ben and Alex, they have rapidly formed an indispensable part of my life, and I thank them all for having made me feel so at home in this strange country.

Sin mis maravillosas amigas hubiera mandando todo al cratzo hace muchísimo tiempo, agradezco especialmente a Sol, Vicky, Anita, Lu, Sole, Molly, Flor, Lali, Marian, Gaby y Apus. La mejor parte de haberme metido en esta profesión demente es haberlas encontrado!

A number of wonderful people have made the past years especially enjoyable, I would like to thank Bea, Maurice and Noel; María and James; Katie, Steve, Luke and Taylor; Courtney and Mike; Lydia and Rich; and Raffi. I sincerely hope you all someday move to wherever it is I move to, so that we can continue the weekly take-out dinners, BBQs, and movie nights.

Agradezco a mi familia querida, mi hermana y Pep, mis tíos Bibi, Cristina, Pelusa, Hugo y Nelly, y mis primos, especialmente Vivi y Cris, por el cariño y apoyo en la distancia.

Y a mis imprescindibles amigos de toda la vida, Rox, Sol, Maru, Tana, Gre y Sabri, les agradezco por tantos años de amistad, que resiste tanto tiempo y distancia.

Lastly, I gratefully acknowledge the fantastic support that I received from the Rockefeller University and the Howard Hughes Medical Institute throughout these years.

Table of Contents

List of Figures

1. Background

At first sight, the field of mechanosensory biology lacks a certain homogeneity that other sensory phenomena provide. Whereas the sense of sight deals with the various ways by which animals process electromagnetic waves, while taste and olfaction handle the probing of our chemical surroundings; force-sensation gives rise to a vast and disparate array of sensory phenomena[10]. Undoubtedly we feel touch and pressure through mechanosensory perception, but we also hear sounds, feel thirst, and taste the texture of foods through mechanosensation as well[11]. Underlying all of these stimuli, from the homeostatic regulation of a cell's volume to the proprioception of an elephant's limbs, is force-sensation. A closer inspection reveals that mechanosensitivity is an even more widespread feature than our intuition first tells us. To some extent all cells are exposed to a diversity of mechanical forces arising from flow, cell to cell contact, migration, stretch and more, even when those cells are not specialized as mechanosensors. One must posit that cells, being so exquisitely sensitive to the chemical nature of their environment, will be equally equipped to respond to the mechanical aspects of it.

With this perspective in mind it is unsurprising that the ability to sense and respond to force is a rather ancient feature. Mechanotransduction machineries are found in most bacteria and Archaea[12], where they aid cells in dealing with osmotic gradients that develop as part of the natural exposure to their environments (i.e. over-hydration due to heavy rain or de-hydration due to sun exposure).

1.1. Early evidence for the molecular basis of mechanotransduction

In a foundational experiment made by Corey and Hudspeth in 1979[1], application of mechanical stimulation to the hair bundle of a frog's hair cells produced an electrical response in 40μs at room temperature. This first observation of the latency of mechanical responses contrasted with that of the visual system[13], two orders of magnitude larger, and imposed some limitations to the molecular machinery underlying the mechanical response. A second messenger system, such as that at work in the visual system, is largely incompatible with a time frame of such short length. Mechanosensory ion channels, conversely, would fit the observations quite nicely.

Fifteen years later, Kung and colleagues molecularly identified the first of such a class: the mechanosensitive channel of large conductance, MscL[12]. MscL provides bacterial cells with the ability to avoid catastrophic rupture after exposure to very low osmolarity solutions (such as rain water). Cells swell immediately and, when failing to otherwise control their volume, open MscL channels that function as last-resort release valves, extruding water and solutes as large as 40Å in diameter[14]. To this day, the cloning and characterization of MscL remains the gold standard for the assertive identification of *bonafide* mechanosensory ion channels. Knockout and rescue experiments in *E.coli* cells conclusively determined the MscL gene to be a necessary part of the transduction machinery. Furthermore, when a vector containing the MscL sequence was used to drive expression in a reticulose-lysate expression system, MscL mechanosensitive channel activity was observed, determining the gene construct to be sufficient to generate the mechanosensitive phenotype. And lastly, MscL

protein retained full activity when purified and reconstituted in liposomes, a cell-free system with no other components than MscL protein and lipids, indicating that the mechanical transduction mechanism resides alone in the protein-lipid interaction[12,14,15].

A myriad other stretch-gated electrical responses has been observed in multiple other systems, but further identification of other candidate mechanosensitive ion channels has proven difficult, due to distinct properties that separate mechanical senses from others.

1.2. Technical challenges of identifying mechanosensory ion channels

In contrast to the retina or the olfactory and gustative epithelia, there is no one large, densely populated organ uniquely devoted to mechanosensory transduction. Arguably, an example would be the skin, but such organ is in charge of a multiplicity of roles and exhibits a diffuse localization that contains at least 5 different sensory termini, all sparsely located among non-sensory cells[16,10]. One could also contest that the auditory system is an entire organ devoted to mechanosensory transduction, with the hair cells of the cochlea tightly packed; but there are only some 15,000 of them. In contrast, mammals have tens to hundred million olfactory receptors, and over 120 million photoreceptors – orders of magnitude more than the auditory system[17].

But a more fundamental reason for the delay in research is rather technical: for the sense of taste or olfaction, the stimulus is a chemical cue that is most often sensed in a concentration-dependent manner. In the case of mechanosensation, the nature of the stimulus is less obvious. Here the stimulus

is a force applied with some angle either to the membrane, the extracellular matrix or a combination of both, depending on cell type and physiological role. Finding appropriate techniques to probe such systems has proven exceptionally challenging. There are multiple generally established ways to probe cells for mechanosensitivity; a brief review of the most popular ones outlines their characteristics:

Hypo-osmotic shock consists of decreasing the osmolarity of the media in which cells are submerged. This causes an initial swelling of the cells that impinges stress on the plasma membrane. Depending on cell type, different cascades of events can follow, but the initial tension on the plasma membrane can potentially lead to opening of mechanosensitive ion channels that can be assessed by either electrophysiological or optical imaging techniques[16,18]. Simplicity and adaptability to high throughput approaches are by far the biggest advantages of this technique, which unfortunately also has several drawbacks. The time frame of the process is often in the order of seconds if not more (depending on the solution exchange system), which largely exceeds the time scale in which most ion channels are known to operate. As a result, a multiplicity of signaling events are likely activated and ion channels may potentially be open not through direct tension in the membrane but via second messengers. In the end, a positive readout in a hypo-osmotic shock experiment is certainly an indication of ion channel activation, but not necessarily due to tension.

Cells can also be stretched directly without osmolarity changes. The most popular way to accomplish stretching is to grow them on elastic silicone membranes that can then be manipulated by an *ad hoc* device[19,20]. Unfortunately

this approach is not amenable to electrophysiological recordings as the cells move significantly during the manipulations and is therefore mostly used in conjunction with optical imaging. But further complications occur due to the fact that not all ion channels can be probed using imaging. Calcium channels have been studied using several appropriate dyes (Fura-2, G-CaMPs) whereas potassium and sodium channels lack a dye of comparable qualities. Additionally, it is technically very difficult to stretch the cells while maintaining them in or around the same field of view. Furthermore, the random orientation of cells on the surface makes the stimulation rather non-uniform among cells rendering the technique relatively non-quantitative.

In the past few years a cell 'poking' technique gained relevance, consisting of individually stimulating cells with a round-end probe controlled by a piezo-actuator while a second probe located at a distant part of the cell performs patch-clamp recordings[18,21]. The poking probe can normally complete its movement in a few milliseconds thus reducing the time scale of the experiment by orders of magnitude. The superiority of this technique lies in the ability to unequivocally elicit tension-gated behavior in real time, while also highlighting channel parameters such as kinetics in a completely physiological environment. Certain quantitative aspects of this technique are unfortunately still questionable. The stimulating probe is comparatively large and positioned more or less randomly over the cell, such that the location of the stimulation is hard to control. Even when 'poking' repeatedly in the same location cells move and accommodate making it difficult to accurately and reliably land the probe at the exact same location. Additionally, even cells of the same kin have different volumes and

morphologies, making comparisons of depth of poking relatively uninformative. Throughput is unavoidably low, as is the limitation of any recording mediated by electrophysiology. Despite all of these drawbacks, cell poking has emerged as the cornerstone tool of modern studies.

Finally, typical screens for mechanosensation involve excising a gigaseal membrane patch containing the channel of interest and applying pressure to elicit changes in gating[22]. However, gigaseal patch formation *per se* imposes tension on the attached membrane, due to the interaction of lipids with the glass pipette (which in turn accounts for the seal effect required for the technique)[23]. Due to this effect, largely ignored in past studies, channels are not under basal tension even before stimulation begins. For the case of bacterial MscL, which is presumed to support several dynes of tension per squared centimeter[24], the additional tension of lipid-glass adherence (estimated in the order of one dyn/cm2) will not significantly alter its properties. But this technique is not suited for channels with sensitivity ranges near or below one dyn/cm2, raising the possibility that ultra sensitive stretch-activated channels may be overlooked through this technique because they are probed in their saturating range of tension.

The nature of most of the techniques detailed above is still largely qualitative. The cell-intact techniques (hypo-osmotic, stretch, and poking) offer little light on the range of tension or regime required for activation. Lacking a reliable membrane tension reporter, we have no means of knowing how much tension each treatment provides, nor how it is distributed on the cell surface.

1.3. A brief review of the strongest candidates for bonafide tension-gated ion channels.

Despite the large number of macroscopic mechanosensory currents observed and mechanosensory behaviors in animals and cells that have been described in the past ~40 years, only a few candidate ion channels and molecules withstood rigorous tests.

Drosophila larvae respond to the gentle poke of an eyelash with a set of stereotypical behaviors including waves of contractions, a response mediated by Class III dendritic arborization neurons[25]. Jan and Jan's group elegantly demonstrated that NOMPC, a member of the TRP ion channel family, was necessary to mechanically activate these neurons. Even more interesting, the expression of NOMPC in a different set of neurons not involved in mechanical perception rendered them mechanically activated. Heterologous expression of NOMPC in a drosophila cell line exhibited mechanically gated currents with millisecond latency, further cementing its role as mechanotransducer. Although protein purification and reconstitution in a cell-free system has not yet been attempted, the Jan group proved that mutations in the pore region of NOMPC change several conductance parameters of the mechanically activated currents, situating NOMPC as the likely pore-forming subunit of the mechanotransducing machinery[25].

Jawed vertebrates express a type of potassium channel named two-pore domain potassium channels (K2P) for their unique architecture. This ion channel family is polymodally activated with a few members, TREK-1 and 2, and TRAAK, being activated by membrane stretch[26]. The MacKinnon group took a closer look at human TRAAK, a project in which I had a small participation.

Human TRAAK channels are activated by hypo-osmotic shock, cell poking, and pressure applied to an excised patch[27]. Protein purification and reconstitution in lipid vesicles with no other cell component exhibited similar mechanosensitive properties, indicating that TRAAK is a *bonafide* stretch-gated ion channel[26]. Several hypotheses have been postulated for the physiological role of this exclusively neuronal channel, but no conclusive literature can be cited. Despite the lack of behavioral information, structural and mechanistic studies conclusively demonstrated that human TRAAK and TREK-1 and 2 are finely tuned to mechanical activation.

The recent discovery of a structurally unique family of ion channels, the Piezos, infused new energy into the field[21,28]. Mouse Piezo1 and Piezo2 exhibit rapidly inactivating mechanical current in response to poking stimulation in heterologous expression systems, as well as endogenously in sensory neurons (Piezo2) and neuroblastoma cells (Piezo1)[21]. Hypo-osmotic shock and gigaseal patch pressurization also elicit clear channel activity. Piezo2 expression is necessary to generate mechanical activation in a subset of sensory neurons, the dorsal root ganglia (DRG) neurons, and recent physiological studies conclusively demonstrated Piezo2 to be the long sought mammalian light-touch mechanotransducing receptor[7]. In addition to its expression in sensory neurons, Piezo2 was shown to be expressed in Merkel cells, a type of epithelial cells (non neuronal) located in the epidermal layer of the skin, where it confers mechanical activity to the cell-neurite complex innervated by sensory afferents[29,30]. Piezo1 has been shown to be involved in endothelial blood flow sensation[31,32], erythrocyte volume regulation[33,34,35], renal tubular cell function[5], and

osteoclastogenesis[36], among others. Furthermore, the drosophila orthologue dmPiezo has recently been implicated as the nociceptor channel in larvae[8]. This list for the role of Piezos is not exhaustive and we are likely to find increasing roles for these channels as research progresses.

A large number of other channels has been linked to mechanosensory processes through forward genetic screens and homology searches. The DEG/ENaC family in *C.elegans* deserves special mention. *C.elegans* responds to a poking stimulus with an escape response mediated by a pair of anterior and posterior receptive neurons (ALM and PLM). Sodium channel members of the DEG/ENaC (degenerin/epithelial sodium channels) family, MEC-4 and MEC-10, are required for the correct expression of this response, but are not able to elicit channel activity when expressed heterologously[37,17]. Two *Drosophila* orthologues of DEG/ENaC channels, Pickpocket and Balboa, share similar features: their correct expression is necessary in larvae sensory neurons to transduce mechanical stimulation, but their heterologous expression does not elicit channel activity[38,39]. Mammalian orthologues, the acid-sensing channels (ASIC), have an even less clear involvement in mechanical transduction[40,41].

Lastly, the large family of transient receptor-potential (TRP) channels, also polymodally regulated, has been extensively linked to mechanotransduction processes. Two invertebrate members, NOMPC in Drosophila[25] and TRP-4 in *C. elegans*[42], have emerged as strong candidates for mechanosensory channels, but the evidence of direct mechanical gating or heterologous expression of other TRP channels is inconclusive.

Ultimately two models have been suggested for mechanically gated channels[11]: one proposes that mechanosensitive channels are being held in position by the cytoskeleton or other tethering molecules, which would perceive the mechanical stimuli and transmit them onto the channel by touching or moving its gating apparatus. The other suggests lipid-protein interactions to be at the core of mechanosensation: at any given time, channels are subject to a complex force profile at the interface with lipids, and any change in that profile (either by a change in lipid composition, membrane fluidity or by bending the membrane) would be immediately perceived by the channel, causing a change in its gating properties. Such fine coupling between the channel and the surrounding lipids would allow minute sensing of the mechanical state of the membrane.

Evidence supporting both models has been found. MscL channels have been found to maintain full functionality when reconstituted into lipid bilayers in the absence of any other membrane protein or cytoskeleton component, indicating that it is a *bonafide* mechanotransducer that requires no more than lipid-channel interactions[15]. On the other hand, the MEC complex of protein found in *C.elegans* requires a plethora of intracellular subunits and extracellular matrix components for its proper functioning, pointing to a complex mechanism that exceeds that of mere protein-lipid interactions[37,43,44]. Most likely, both mechanisms have been explored by nature to cover the vast range of phenomena that involve mechanical stimulation, lending further complexity to the study of mechanosensation.

1.4. Identifying new mechanosensory ion channels

There has been undoubtedly major progress, but there is still a large gap in matching the extensive list of mechanosensory processes with the associated candidate channels. Logic dictates two possible non-exclusive solutions: there are either new ion channels to be discovered, or some of the channels that we already know are mechanosensitive. For my thesis work I chose to use complimentary approaches to study both possibilities with the aim of identifying new molecules involved in mechanosensory processes. The following two chapters will discuss these approaches, results, and the possible implications on the molecular biology of mechanosensation.

2. Examining Known Ion Channels for Mechanosensitive Properties

2.1. Introduction

One of the most recent channels identified as having mechanosensory properties is the eukaryotic 'paddle chimera', a member of the voltage-gated potassium (Kv) channel family. Potassium channels are well known for their voltage- and ligand-gated activities, and their physiological roles are clearly established in many cases. Recent work performed in the MacKinnon laboratory has shown that the gating properties of several Kv channels are markedly influenced by both the chemical composition and mechanical state of the lipid membrane[2]. Both head group charge density and tail chemistry of the lipids in the bilayer were shown to modulate activity. Furthermore, their reconstitution in different systems (bilayers or oocytes) and the use of different patch configurations (on-cell, whole-cell, inside-out or outside-out patches) unveiled changes in gating only explicable when taking into consideration membrane tension as a variable. Other channels, for example voltage-dependent sodium (Nav) channels, are also known to exhibit altered gating properties in gigaseal patches compared to the intact (unpatched) cell membrane[45], possibly due to the increased tension in the patched membrane.

The first subject of my study was potassium channel Paddle Chimaera, which consists of the Kv1.2 channel with the voltage paddle of Kv2.1, a channel that expresses very well and on which preliminary studies on the gating dependence on the mechanical state of the membrane were conducted. The preliminary results from our lab were obtained on excised patches of membrane,

a relatively non-physiological regime to study tension influence on ion channel behavior. I therefore decided to translate the studies into whole cell modalities: hypo-osmotic swelling and cell poking.

Interesting results obtained with potassium channels prompted me to analyze other related ion channels. Voltage-gated potassium channels are members of the 6 trans-membrane (6TM) ion channel superfamily, whose members share a similar transmembrane architecture (although with different degrees of concatenation and subunit stoichiometry)[46]. This family includes calcium and sodium selective voltage-gated ion channels among others. I analyzed a few members of each family.

Voltage-gated sodium channel Nav1.7 is highly expressed in nociceptive neurons at the dorsal root and trigeminal ganglia and is critically involved in pain sensation[47]. Certain Nav1.7 mutations in humans cause a pain-insensitive phenotype, a severe rare condition that can have catastrophic consequences[48]. Both its localization and link to nociception make it an interesting target, therefore I performed studies on this channel next.

Several voltage-gated calcium channels have been linked to mechanosensation[49,50,51,52]. Given the large driving force for calcium ions to enter the cell, and the extensive signaling cascades that follow calcium uptake, it is expected that even minute changes in channel gating could have enormous effects in cell activity. Structurally, voltage-gated calcium channels are composed of a pore-forming subunit (*alpha* subunit) and multiple accessory subunits that are, in many cases, required for channel functioning (*beta*, *alpha2delta* and *gamma*)[53,54,55,56]. Different combinations of subunits are expressed in different

cells and tissues. The *alpha* subunit forms the pore and shares structural similarity with the 6TM ion channel superfamily; it is also the ligand-binding subunit. Interaction with *beta* subunits, soluble intra-cytoplasmatic proteins, aids in surface expression but can also modify the voltage-activation curve. *Alpha2delta* subunits, a combination of an intracellular unipass membrane protein (*delta*) with a highly glycosylated soluble protein (*alpha2*) also aids in the trafficking process. Finally, *gamma* subunits, multipass transmembrane proteins, are postulated to inhibit calcium channel activity, but their expression and functional activity are less clear. I focused on the L-type calcium channel Cav1.2 found in smooth and cardiac muscle, endocrine cells, and neurons[57] and the L-type calcium channel Cav1.3, also found in smooth and cardiac muscle cells but also in sensory neurons such as hair cells[58,59].

I hypothesized that the high mechanical sensitivity of potassium channels could be more than a mere biophysical curiosity, and that potassium channels and other already known channels may play a role in certain mechanosensitive signaling processes, themselves acting as mechanotransducers. Since voltage-gated potassium, sodium, and calcium channels are vital for cellular and neuronal physiology they are not likely to be linked to mechanosensation by loss-of-function mutagenesis screens. This may partially account for why a role for theses channels as mechanosensors has been missed. Therefore I set out to explore mechanosensitivity of voltage-gated potassium channels, and extended the study to members of other 6TM ion families.

2.2. Results

2.2.1. Voltage-gated potassium channels

Voltage-gated potassium channel Paddle Chimaera (PChim) was expressed in Sf9 cells, an insect cell line with very little endogenous voltage-gated current. For hypo-osmotic shock experiments, electro-physiological recordings begin with cells in an iso-osmotic bath solution where baseline channel activity is recorded. Bath solution is then exchanged into hypo-osmotic solution (usually ~70% of the initial osmolarity of the cells), continuously monitoring ion channel activity. Cells can then sometimes be returned to the original osmolarity, if the gigaseal connection has not been deteriorated by the manipulation, to assess reversibility of the process. To study currents, cells are held in voltage-clamp mode at -80mV and stepped to +50mV in 10mV steps, after which they are returned to -80mV. The current level during the depolarization is a result of the number of channels opened and the driving force at each voltage. Channels that inactivate with a certain delay are amenable to analysis by their tail currents[60]. Tail currents, the currents observed immediately after cells are returned to -80mV while the channels are still open, reflect the open probability of the immediately preceding voltage step, and are therefore a better assessment of channel opening. Figure 1 shows two independent exemplary trials of hypo-osmotic swelling of PChim. Conductance increases by a ~20%, but most noticeably, the activation threshold shifts ~15mV to the left, turning the channel more active at lower voltages. The capacitance of the cells was monitored as well to verify that the conductance increase is not simply due to an addition of membrane with more channels[61].

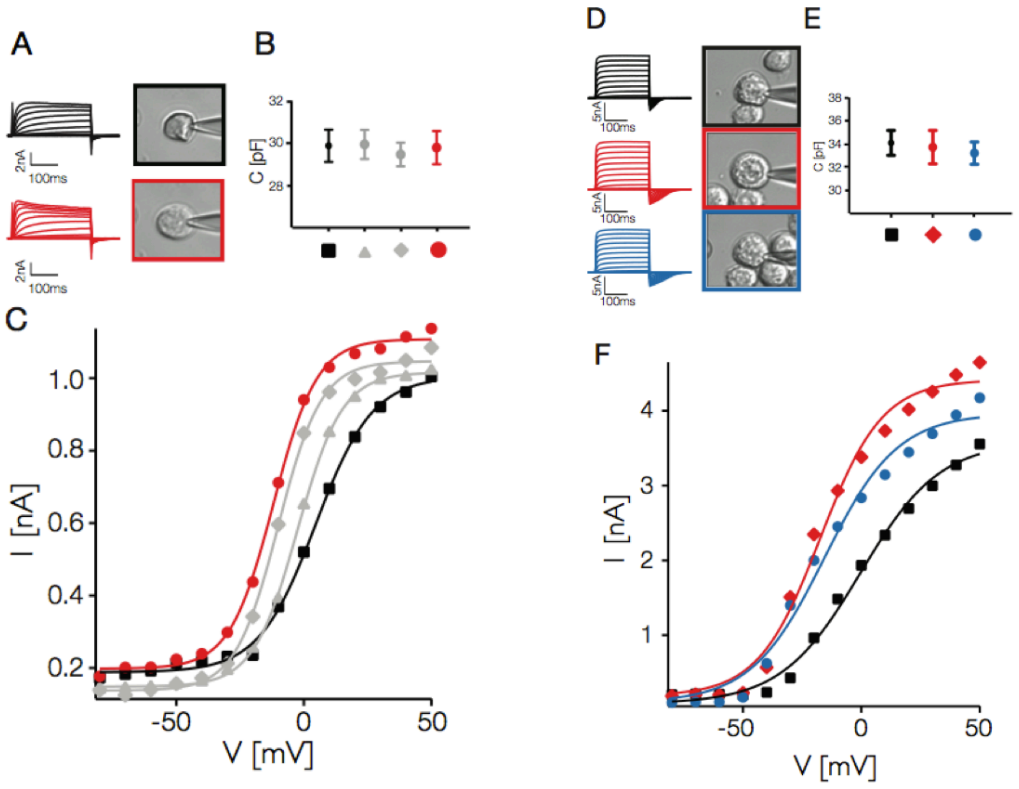

Figure 1. Effect of swelling on PChim in Sf9 cells. Whole-cell patch recordings of Paddle Chimera expressed in Sf9 cells during perfusion with iso-osmotic (initial volume, black) and hypo-osmotic (peak volume, red). B, estimation of the cell capacitance in traces corresponding to initial (black), intermediate (grey) and peak volume (red) state: C (pF): 29.9 ± 0.8, 30.0 ± 0.7, 29.5 ± 0.6, 29.9 ± 0.8. C, Boltzmann functions (solid lines) fit data from (A) with Vm (mV): Black, before swelling: 4.61 ± 0.78. Grey, intermediate swelling states: -2.44 ± 0.26 and -10.05 ± 0.57. Red, peak volume state: -11.95 ± 0.55. D, Whole-cell patch recordings of Paddle Chimera expressed in Sf-9 cells during consecutive perfusion with iso-osmotic solution (black), hypo-osmotic solution (red), and immediately after peaking volume, iso-osmotic solution (blue). (E), estimations of the cell capacitance. C (pF): 34.1 ± 1.1, 33.8 ± 1.4, 33.2 ± 0.9. (F), Boltzmann functions (solid lines) fit data from (D) with Vm (mV): Black, before swelling: -0.35 ± 2.09. Red, during peak volume: -18.56 ± 1.99. Blue, returned to iso-osmotic solution: -17.57 ± 2.63.

Similar results were obtained with voltage-gated Kv2.1 channel, although a more modest shift in voltage was observed (data not shown). The results of hypo-osmotic swelling of Kv PChim are very robust, as results were similar from several independent trials, allowing me to conclude that Kv PChim responds to swelling by hypo-osmotic stimulation.

To support the initial findings of hypo-osmotic stimulation I attempted to use the 'poking' assay. PChim was expressed in Sf9 cells and held at different voltages while poking stimulation was performed in 50ms steps. Most trials did not exhibit any mechanosensitive behavior. Figure 2 shows the few cases of a positive response to poking. As these studies were being conducted, a paper published by the Delmas group reported modest activity of some Kv channels also using this assay[62]. The magnitude of the responses I observed was similar to that reported; however, in my hands this assay produced responses too infrequently to be asserted as positive.

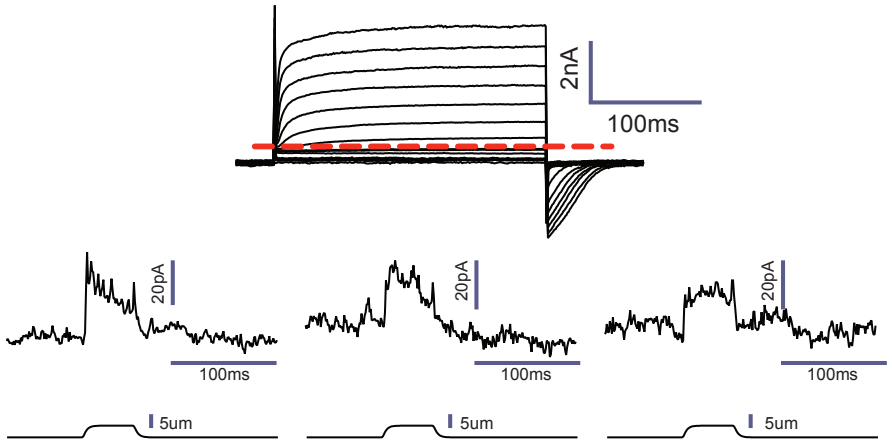

Figure 2. Positive effects of poking Sf9 cells expressing PChim. Top traces are the voltage-gated behavior of the cell under study, showing large expression of PChim channels. Cells is held at -80mV and stepped to positive voltages in 10mV steps. Red line marks the 0pA level. Below are three examples of poking stimulation on that same cell holding the voltage at 0mV. Only the few positive effects are shown, the majority of the trials resulted in no effect of poking.

2.2.2. Voltage-gated sodium channel Nav 1.7

Using HEK293 cells stably expressing full-length human Nav1.7 channel, (a gift from Bruce Bean's lab), I performed a similar battery of studies as in the previous section: hypo-osmotic swelling, whole-cell poking, and also excised-patch inflation.

Hypo-osmotic swelling experiments were performed as before, except that cells were held at -100mV to remove inactivation, and stepped to depolarized voltages (from -65mV until -15mV) in steps of 5mV. Sodium channels inactivate quickly after opening, which prevents tail current study. I therefore used the peak current achieved at each depolarization for current-voltage plots. Swelling

by means of hypo-osmotic shock did not have a significant effect; an example is seen in figure 3. Although there is variation and a small shift (less than 5mV between extreme traces), it did not follow a specific pattern or correlation with swelling, but rather represented a degree of typical variation that I observed in most cells, independent of stimulation.

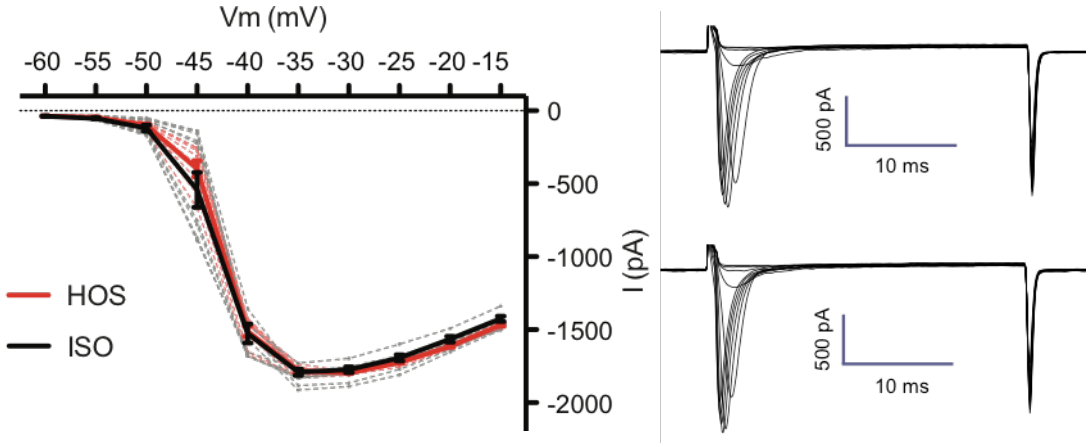

Figure 3. Effect of swelling by hypo-osmotic shock in HEK293 stably expressing human Nav1.7 channel. Left panel corresponds to 12 current-voltage (IV) curves in iso-osmotic solution (ISO, grey punctuated lines) and 8 IV curves in hypo-osmotic solution (HOS red punctuated lines). The average current +/- SEM at each voltage for each condition is indicated with solid red (HOS) or black (ISO) line. Right panels show examples of ISO (top) and HOS (bottom) currents from which the IV plot was constructed.

Figure 4 shows the effects of poking the same stable HEK293 cell line expressing Nav1.7. The inactivation of sodium currents is very fast, normally within 5ms of activation, which is faster than the delivery of the stroke by the poking device. It is therefore not useful to hold the membrane at certain voltages

and poke to observe increased activation; most of the channels would be inactive before the poking stimulation is delivered. I therefore studied the effect of poking on the voltage activation curve. Cells were held at -100mV and depolarized from -60mV to -15mV, and a poking step was applied simultaneously during the depolarization. I repeated the measurement several times, displacing the poking step relative to the voltage step to identify any potential shift in the voltage-activation curve or other parameter. I performed several depolarizations with and without poking stimulation to compare any potential shift in the IV curves, though no effect was observed; an example is shown in the figure.

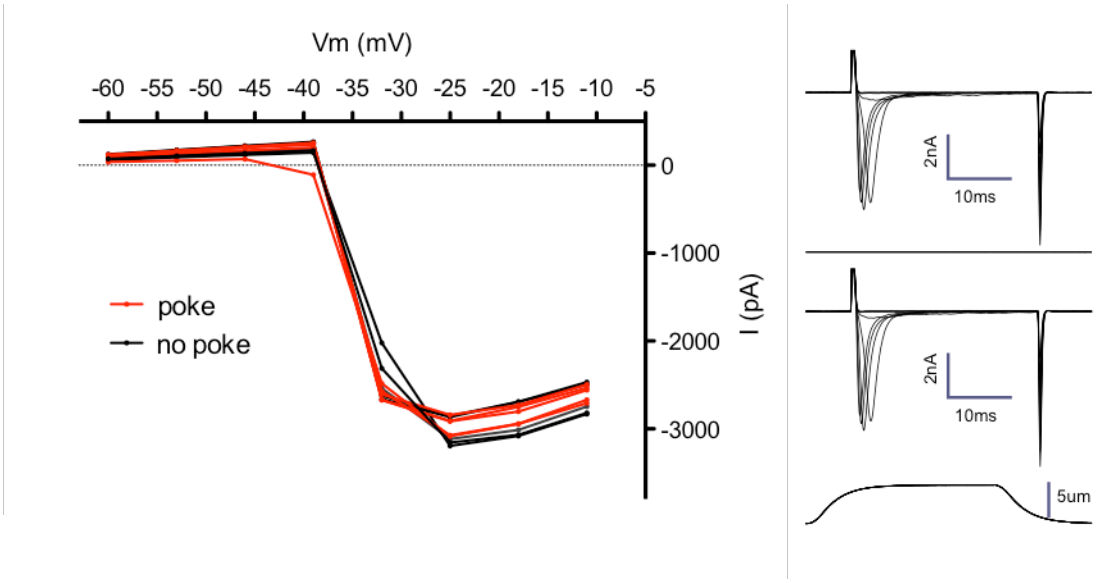

Figure 4. Effect of poking on the activity of human Nav1.7 channel. IV plots shows 3 curves in the absence of poking (black) and 4 in the presence of poking stimulation (red). Examples of traces of each are shown in the right panel. Top trace was done in the absence of poking step, lower trace shows a 5um poking step delivered for each of the depolarization.

Lastly, I studied the effect of pressurizing an excised patch of membrane. Current levels were small; I achieved only three successful experiments. The poor signal-to-noise at this current level makes the interpretation very difficult, but no effect was observed on the current-voltage curve of Nav1.7 in the absence or presence of an average of 15mmHg applied to the patch of membrane (figure 5). In summary, no effect was observed in either the conductance or the voltage-activation curve with any protocol.

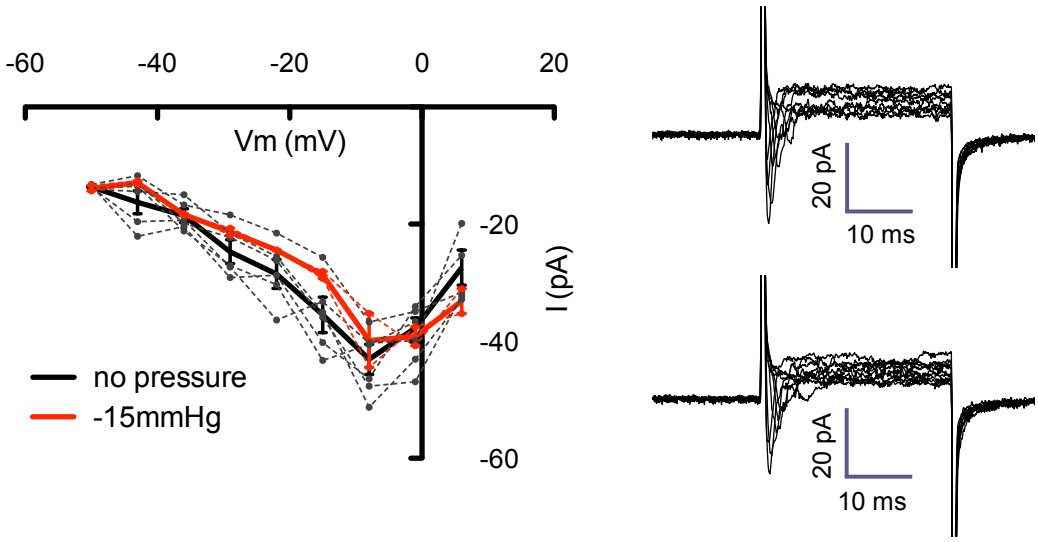

Figure 5. Effect of applying pressure to an isolated patch of membrane expressing human Nav 1.7. The left panel shows the current-voltage curves from the peak currents of multiple traces obtained alternating no pressure and -15mmHg. The thick lines are the averages of each +/- SEM. The left panels contain two example traces, in the absence of pressure (top) and in the presence of pressure (bottom).

2.2.3. Voltage-gated calcium channels

I co-expressed the 3 best-studied functional subunits (*alpha*, *beta* and *alpha2delta*) by means of co-transfecting the relevant constructs, following protocols from Diane Lipscombe's lab. I focused on 2 types of channels: Cav1.2 and Cav1.3, using similar methods as described above: pressurized excised patches, whole-cell swelling and poking. Additionally I made use of the fact that there are reliable calcium-binding dyes to add another methodology: whole-cell stretching.

Both channels expressed well and exhibited the expected voltage-activation curves (figure 6, A). Cav1.3 is the more left-shifted one, with a midpoint of activation around -40mV; Cav1.2, with a midpoint around -10mV, requires far stronger depolarization. However, it should be noted that the presence and stoichiometry of auxiliary subunits can modify the midpoint of activation[53]. Given that in these experiments there is no control over the ratio of auxiliary subunits per cell, this could explain some of the observed variability in values. It is also readily evident from the traces that the currents do not inactivate in their traditional manner. This is due to the usage of barium as carrier ion, rather than calcium. Barium, a divalent cation for which calcium channel conductances are often higher than that of calcium, is a far more physiologically inert ion that is often used as carrier in calcium channel experiments. Barium current through calcium channels inactivates noticeably slower than calcium current (figure 1.6, B).

A

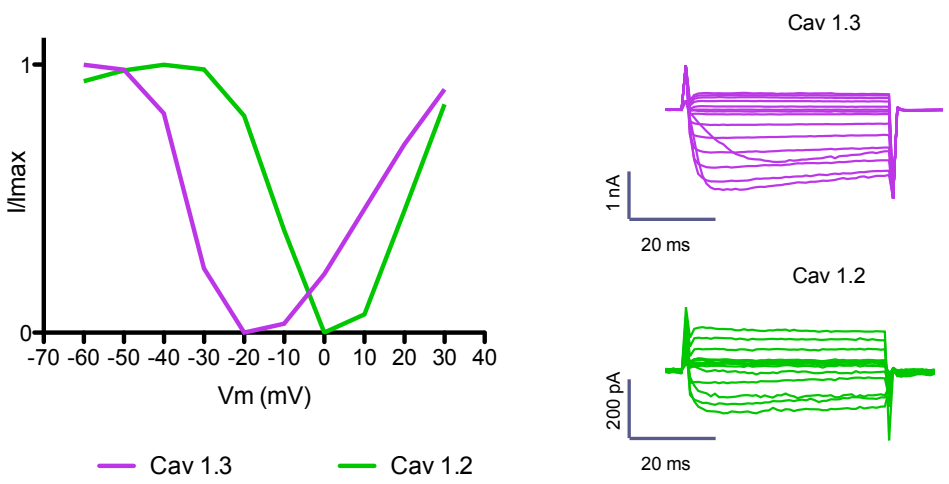

B

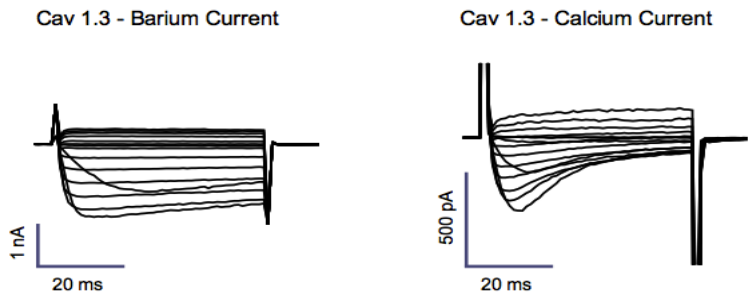

Figure 6. Expression of calcium channels in HEK cells. A) Left panel shows the current-voltage curves of whole cell recordings of Cav1.2 and 1.3 co-expressed with auxiliary subunits and using Barium as carrier ion. Right panels shows example traces of both types of channel. B) The effect of changing the carrier ion in the inactivation rate of Cav1.3 are shown. Barium currents inactivate much slower (left) than calcium currents (right).

Figure 7 shows the response of Cav1.3 to swelling by hypo-osmotic stimulation. Cells are held at -100mV to remove inactivation, and then stepped to -30mV in 10mV intervals. Current-voltage (IV) curves are constructed from the peak current at each depolarization step. The IV curves in the left panel show the transition in channel opening at every voltage from the initial condition at normal volume (ISO-osmotic bath, black), to the swollen state (Hypo-OSmotic bath, red), and finally to the reversed state when returned back to iso-osmotic bath (Back in ISO, blue). Example trace and images at each condition are shown in the right panels. Notice how, prior to stimulation, the -60mV trace (highlighted in pink in the figure) is that of a completely closed channel, no inward barium current is observed. During the stimulation the -60mV trace shows maximal barium current: in this condition channel is maximally open at this voltage. Upon returning the cells to the iso-osmotic condition, the -60mV trace goes back to a closed, non-conductive state. The process is reversible. I observed similar results in all of 9 independent trials. Similar results were obtained using calcium as carrier ion (figure 7, B).

Figure 7 (next page). A) Effect of swelling on Cav1.3, barium as carrier. Left panel shows the current-voltage curves as mean +/- SEM of at least 2 traces in three conditions: iso-osmotic bath (ISO, black), hypo-osmotic bath (HOS, red), and upon returning to iso-osmotic bath (Back in ISO, blue). A -10mV shift between conditions is observed. Right panels show the corresponding traces and images for the three conditions: top, ISO; middle, HOS; bottom, back in ISO. The trace corresponding to the depolarization to -60mV is colored in pink to highlight the transition from closed channel to fully open channel before and after swelling. B) Replica experiment conducted using calcium instead of barium as carrier ion. Notice the typical faster inactivation times in the traces. Also, voltage steps were 7mV apart to obtain better resolution of the closed-open transition.

A

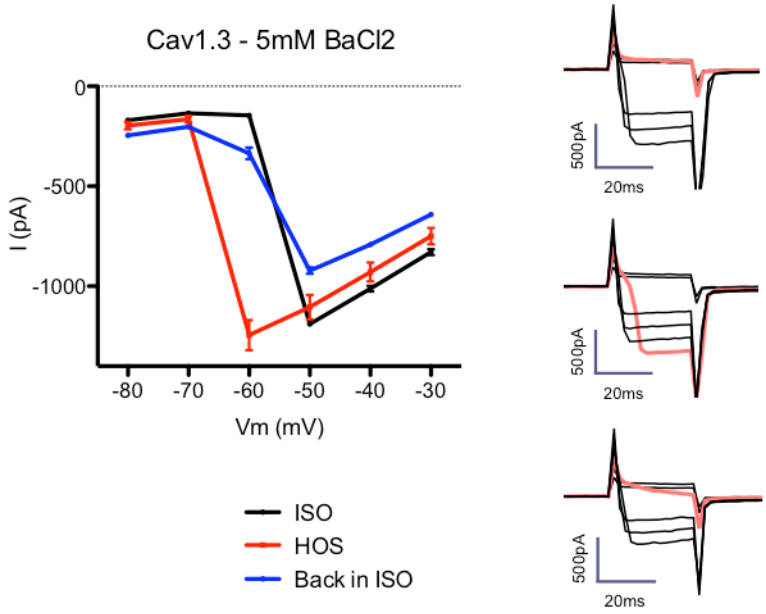
Cav1.3 - 5mM BaCl2
0
-500
-1000
I (pA)
-80
-70
-60
-50
-40
-30
Vm (mV)
ISO
HOS
Back in ISO
500pA
20ms
500pA
20ms
500pA
20ms

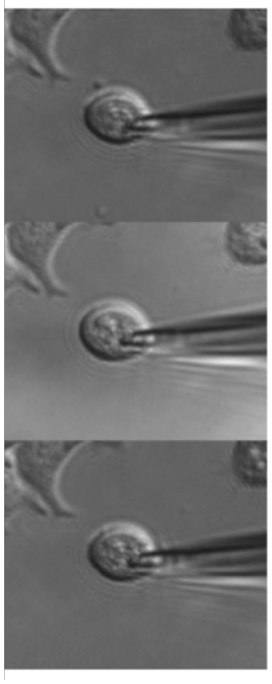

B

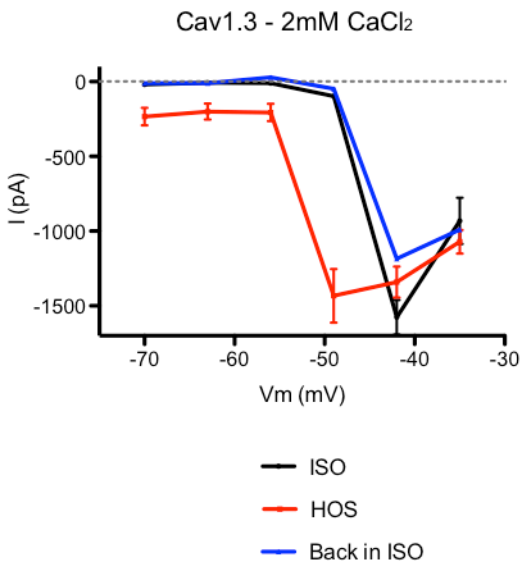
Cav1.3 - 2mM CaCl2
0
-500
-1000
-1500
I (pA)
-70
-60
-50
-40
-30
Vm (mV)
ISO
HOS
Back in ISO
500pA
20ms
500pA
20ms
500pA
20ms

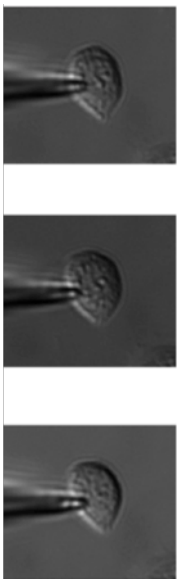

Cav1.2 exhibited a similar behavior; figure 8 shows examples using barium and calcium as carrier ions. The protocol was performed as described above, only adjusting the test voltages to match the channel's more right-shifted activation curve.

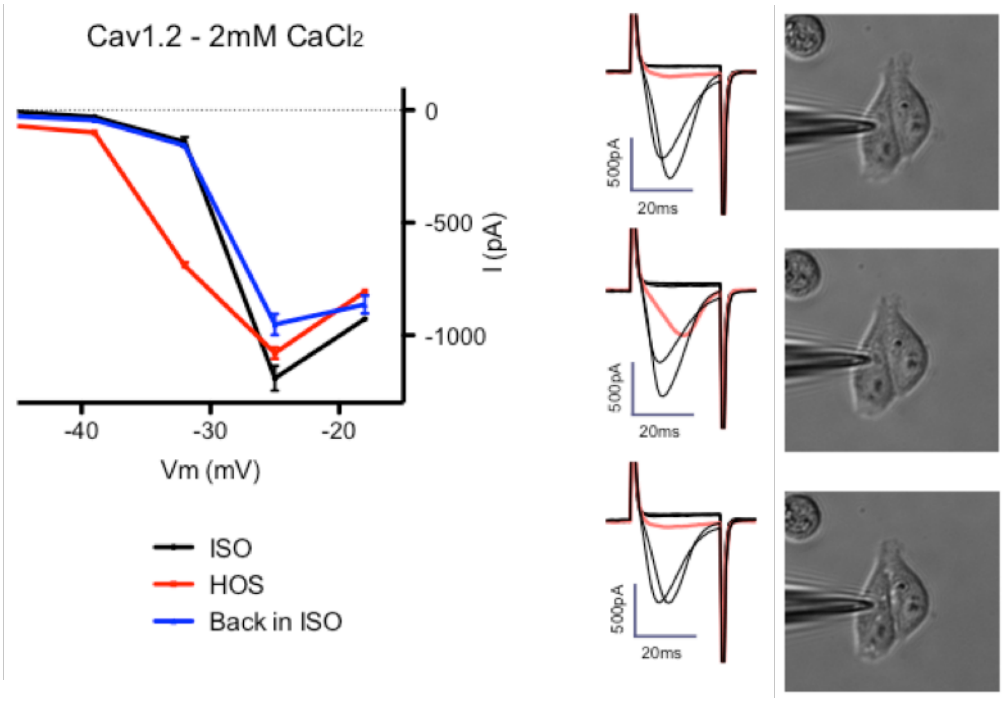

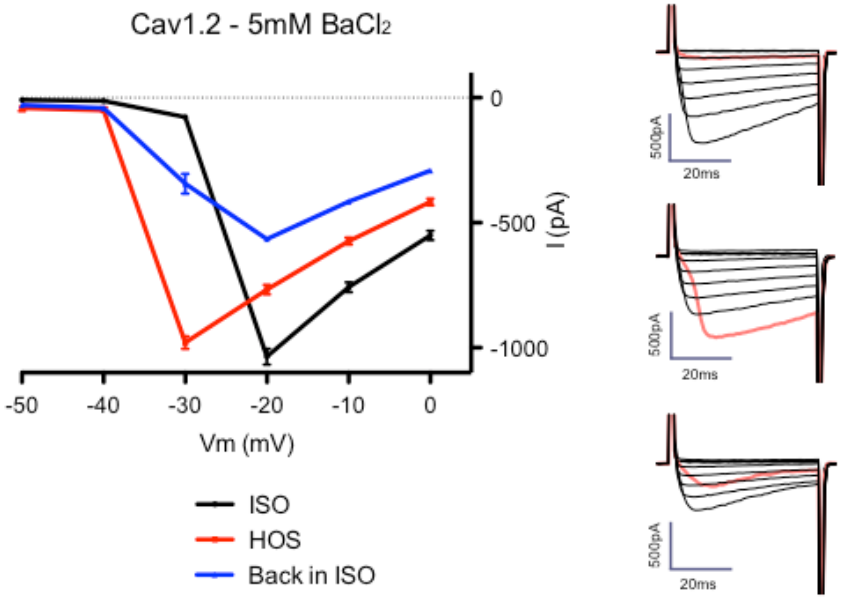

Figure 8. Effect of swelling Cav 1.2 using calcium (this page) and barium (next page) as carrier ions. Conditions and color coding is similar to last figure.

As mentioned multiple times throughout this manuscript, there are multiple drawbacks to the hypo-osmotic swelling as an experiment to assess tension-gated ion channels. One of them is the chemical nature of the stimulation: swelling is caused by water uptake, which modifies the local concentration of solutes, potentially leading to other changes. Therefore, in an attempt to isolate tension gated ion channel activity from potential chemical stimulation as a result of water uptake, I decided to attempt cell swelling without hypo-osmotic shock. I made used of the pressure clamp that delivers controlled pressure through the patch pipette to inflate the cells under whole-cell mode. In this experiment, the positive pressure applied through the pipette in whole-cell mode injects the cell with pipette solution (made to match intracellular electrolytes), causing cells to swell immediately. Cells were placed constantly in iso-osmotic bath solution, and positive pressure was applied through the recording pipette, and monitored visually for swelling. When possible, cells were returned to the original state by removing pressure. I succeeded only once, with a cell expressing Cav1.3. The results are qualitatively similar to those obtained by hypo-osmotic swelling (figure 9).

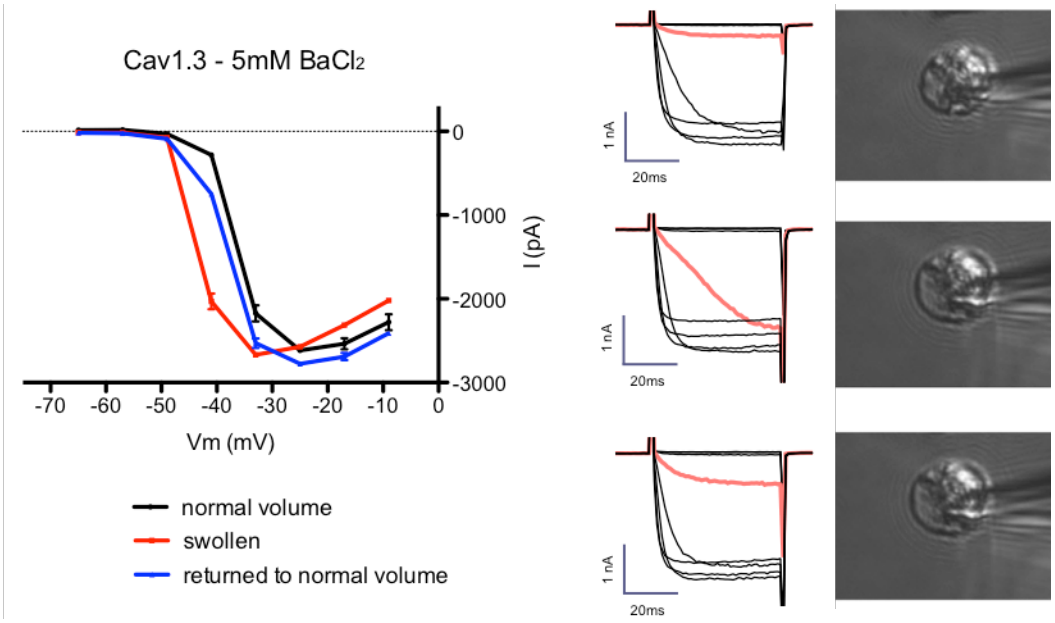

Figure 9. Effect of swelling on Cav1.3, using whole-cell inflation instead of hypo-osmotic shock. Left panel shows the current-voltage curves as mean +/- SEM of at least 2 traces in three conditions: before applying positive pressure (normal volume, black), during application of positive pressure (swollen, red), and after removing positive pressure (returned to normal volume, blue). Right panels show the corresponding traces and images for the three conditions: top, normal volume; middle, swollen; bottom, returned to normal volume. The trace corresponding to the depolarization to -41mV is colored in pink to highlight the transition from closed channel to fully open channel before and after swelling. Voltage steps were 8mV apart.

Patch inflation was unsuccessful due to the low density of channels in the membrane.

Direct poking of the cells expressing Cav1.3 did not exhibit any major activity under electrophysiological monitoring. Several poking protocols were used to circumvent the inactivation characteristics of calcium channels. No poking protocol produced either an increase in current or a shift in the voltage-activation curve (data not shown).

Lastly, a different kind of experiment was performed: cells were grown on an elastic silicone sheet ('membrane') coated with collagen and loaded with Fura-2, a ratiometric calcium dye. Membranes were then placed in a home-built stretcher device and uni-axially stretched while monitoring Fura-2 fluorescence. Using unlabelled cells observed under brightfield illumination I calibrated the device (figure 10). In the experiment shown, after 12 subsequent rounds of stretch and refocusing the field of view experiences a 30-40% stretch in the X-axis. Each round consist of ~3-4 seconds of stretch and an additional variable time needed to re-focus after the cells have moved. This 'dark' period lasts from 5 to 15 seconds, depending on how much the field of view has changed. In subsequent experiments, I varied the intensity and frequency of stretch periods as a compromise between strain and stimulation time. For the standard procedure, I started by acquiring a set of baseline images before stretching, and then applied the stimulation.

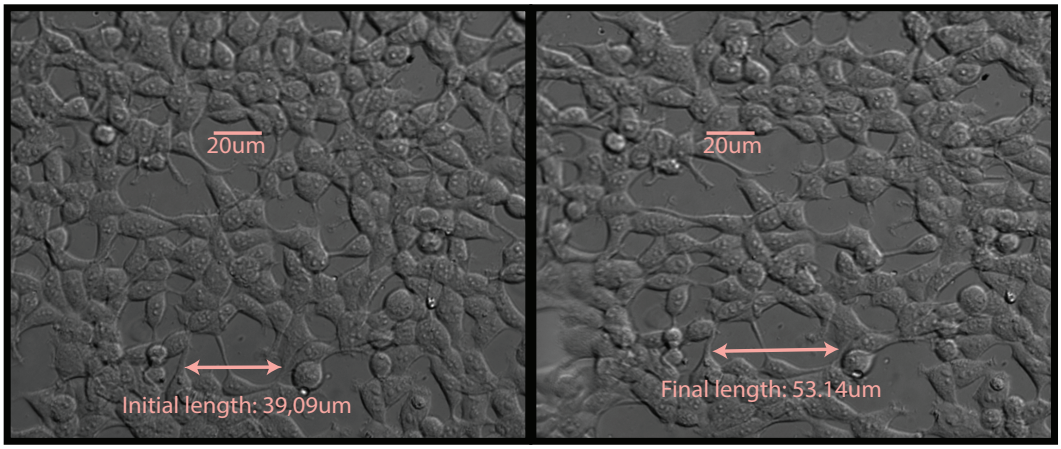

Figure 10. HEK293 cells stretched using a home-built device under DIC illumination. After 12 rounds of stretching and re-focusing, ~10-20 seconds each, a 35% uni-axial stretch is achieved.

HEK293 control cells (mock-transfected) loaded with Fura-2 exhibited minimal responses to the procedure. Figure 11 shows the results of 8 control membranes subjected to the treatment.

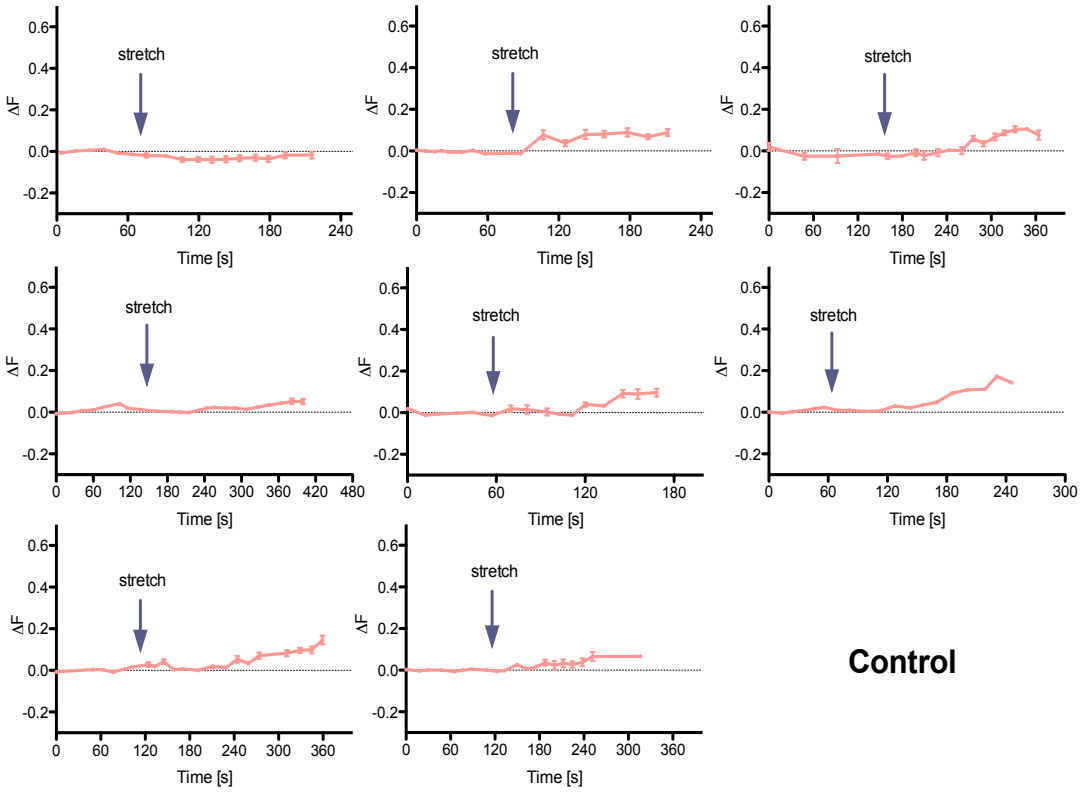

Figure 11. Effect of stretching control HEK293 cells loaded with Fura-2. Relative change in fluorescence is depicted as a function of time. Each panel corresponds to an independent experiment. Initiation of stretch periods is indicated with an arrow. The curve is the result of the average +/- SEM fluorescence change of several cells in the same field of view.

Cells transfected with Cav1.3 and auxiliary subunits showed an array of responses. Figure 12 shows a sequence of images taken from a time-lapse movie of a stretching experiment of HEK293 cells expressing Cav1.3. During this experiment, a baseline was acquired, cells were then stretched up to 32%, and then relaxed to an intermediate position (23% stretch) to study whether the increases in fluorescence are reversible. When the cells and setup allow it, as in the case shown, I then also performed a second stretching step, having previously added a saturating concentration of nimodipine to the bath solution. Nimodipine is a gating modifier that blocks L-type channel activity. This important step allows me to distinguish cells that are effectively showing a response to stretch due to channel opening from cells that are irreversibly damaged or ruptured and simply collapsed their membranes. A quantification of the process is shown in the figure.

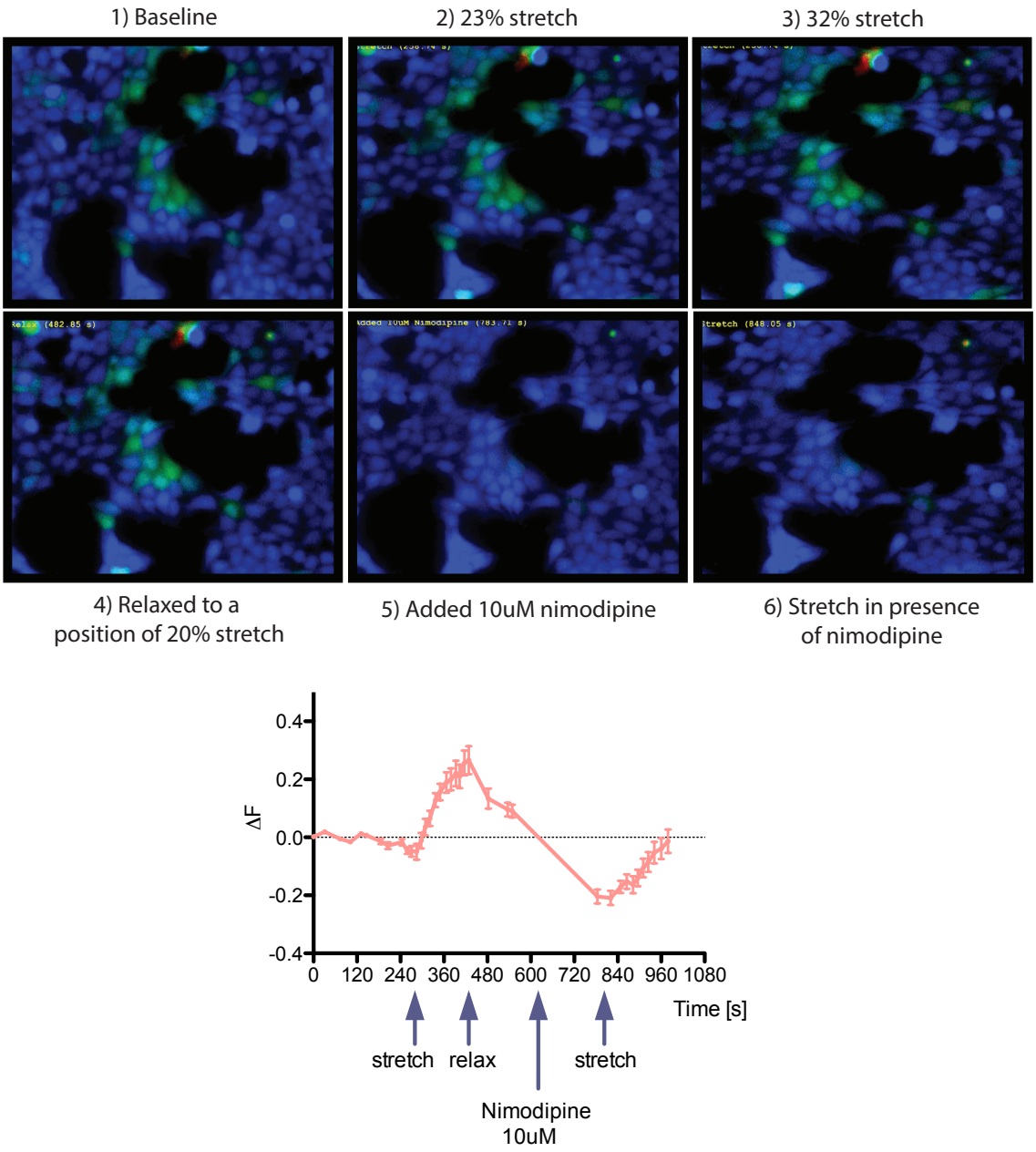

Figure 12. Sequential images of a stretch experiment using HEK293 cells expressing Cav1.3 and auxiliary subunits. Color coding is standard for ratiometric imaging: warmer color indicates higher calcium uptake. In this experiment cells were stretched, relaxed, added Nimodipine, and then stretched again. The bottom panel shows the quantification as the temporal evolution of the change in fluorescence of the groups of cells that exhibit initial fluorescence higher than the background.

A total of 12 independent experiments with Cav1.3 transfected HEK293 cells were conducted. The responses were modest, when observed. 5 out of the 12 membranes studied showed no responses at all, 2 out of the 12 showed completely irreversible responses (not diminishing when returned to the more relaxed state). The 5 membranes that showed a positive and reversible response had similar behavior to the one shown in figure 12.

The protocol can certainly be modified and parameters can be adjusted to achieve a more reproducible stretch stimulus between trials. However, the lack salient responses redirected my focus towards other goals.

Cav1.2 was not studied using whole cell stretch. Its current-activation curve lies much further to the right than that of Cav1.3. The resting voltage for most cells lies between -40mV and below, indicating that even if the stretch stimulation induces a left shift in the activation, it would still likely not be enough to cause substantial fluorescence changes in un-clamped cells.

2.3. Discussion

These studies, together with previous data from Daniel Schmidt, have clearly demonstrated the mechanosensitivity of certain voltage-gated potassium channels[3]. Because of their low-threshold range, it is mostly evident in comparisons of gating in different mechanical states of the membrane, such as gigaseal patch versus whole cell recording. However, the fact that certain mechanosensitivity can be observed in whole-cell experiments such as swelling indicates that these channels' mechanosensitivity can potentially be exploited by cells in physiological settings. A report by Delmas et al[62] showed that a distinct mechanosensitive current carried by potassium is found in high-threshold DRGs, and through toxin assays they attributed it to Kv1.1 oligomers. The involvement of Kv1.1 in modulating allodynia and other mechanical parameters is made clear in their study by the use of toxins and Kv1.1 -/- mutant mice. However, the direct implication of Kv1.1 in transducing the mechanical stimulation is less clear. Their heterologous expression data on HEK cells shows a very modest activity of Kv channels in response to poking, which contrasts with the large effects observed endogenously in DRGs, which they attribute to the same channel. Moreover, I was unable to robustly reproduce some of this data. Regardless, a physiological role for mechanosensitivity of Kv channels remains an interesting possibility.

My other explorations into mechanosensitivity of 6TM ion channels resulted in less exciting possibilities. Nav1.7 did not exhibit any mechanosensitive behavior. As is the case with these types of experiments, negative results do not exclude the possibility of other assays and/or other

conditions bringing out different behavior. However, in my general screening, Nav1.7 did not stand out as a potential candidate. It is worth mentioning that other groups have reported mechanosensitive activity of other Nav channels. Farrugia and colleagues report that pressurizing a membrane patch heterologously expressing Nav1.5 increases its maximal current and produces a leftward shift in its voltage-activation curve[63]. Morris and colleagues have used sodium-sensitive dyes and whole-cell stretching to show that HEK293 cells expressing Nav1.6 show an increase in cytoplasmic sodium levels after 50% stretch, a condition the authors liken to pathological trauma[64]. However, sodium levels do not decrease after release of stimulation, questioning the physiological relevance of the finding. Altogether, it is still likely that certain Nav channels will exhibit mechanosensitive behavior in specific cellular conditions.

L-type calcium channels Cav1.2 and Cav1.3 exhibit a clear response in hypo-osmotic shock in my experiments; but no other assay resulted in potential leads. Having experimented extensively with multiple forms of mechanosensation assays I have developed a personal perspective on their relative value, and place relatively less weight on the results of hypo-osmotic swelling if not supported by results on other more direct assays. As mentioned explicitly throughout this manuscript, multiple parallel signaling cascades activate simultaneously during swelling, which for heavily modulated channels like Cav's, allows for a myriad other mechanisms of activation other than membrane tension. In my view, the poking assay and the results of pressurized excised patches are better indications of a channels' response to mechanical stimulation. But as is the case for Nav channels, other groups have reported

interesting findings for mechanosensitive behavior or Cav channels. Farrugia and colleagues report an increase maximum current of Cav 1.2 channels expressed in HEK293 cells when subjected to shear stress, another form of mechanical stimulation[50]. Cav2.2, a neuronal calcium channel also expressed in Merkel cells, was reported to respond to stretch protocols both under whole-cell inflation and patch inflation[49]. As mentioned above, my results do not exclude the possibility of Cav 1.2 and 1.3 or other Cav channels being mechanosensitive, but perhaps other conditions would be better suited to study that possibility.

3. Identification of Novel Molecules Involved in Mechanosensation

3.1. Introduction

An interesting observation that our lab and multiple others came across is that certain dissociated cells, as well as multiple immortalized cell lines, exhibit some form of mechanosensitivity[5,21]. Multiple techniques have shown this over the years, perhaps the most conspicuous has been the 'poking' assay. Interestingly, only a fraction of these currents has been molecularly characterized. The recent identification of a structurally unique family of mechanosensory ion channels, the Piezos[21], and the plethora of mechanosensory processes to which they have since been associated[7,65,29,8,32,34], certainly filled in some of those gaps.

Piezos are present in most eukaryotes (with the notable exception of yeasts[21]) where they mediate light-touch sensation, nociception, vascular endothelial development, and cell migration, to name just a few. In their canonical forms, they inactivate quickly following stimulation with a time constant of less than 20ms and in a voltage-dependent manner[21,34]. Loss of function by knockout of either member of the Piezo family is unviable[32,7], but gain of function mutations can also result in severe defects: mutations in the human PIEZO1 gene that slow inactivation have recently been associated with hereditary xerocytosis, a disorder of ionic imbalance in red blood cells[34,66,67]. These results highlight the importance of a tight regulation in expression and kinetics of mechanosensory ion channels.

Interestingly, multiple cell lines exhibit a variety of undescribed stretch-activated currents that differ from Piezos in their kinetics. Dorsal root ganglia cells display three types of mechanosensory ionic currents when directly stimulated with a probe: rapidly-, intermediate-, and slow-inactivating currents[21]. Piezo2 only accounts for the rapidly-inactivating responses, with slow- and intermediate- inactivating conductances yet uncharacterized. Other cultured cell lines like C2C12 also express a form of slow-inactivating mechanosensory current, also not yet characterized. Understanding the components of slow-inactivating mechanosensory responses would not only aid in completing the landscape of mechanosensory ion channels and molecules but also provide insight into the fine-tuning of cellular responses to diverse stimuli.

In this chapter I describe the results of my own survey of mechanosensitivity across a variety of cell lines in the quest to identify slow-inactivating mechanosensory ion channels. I performed multiple screens in parallel; they will be described independently in sections 3.2.1 (mechanosensitive currents in cancer cell lines) and 3.2.2 (mechanosensitive currents in stem cells).

3.2.Results

3.2.1. Mechanosensitive currents in cancer cell lines

For the initial screening, a broad panel of several immortalized human cell lines derived from cancer patients was obtained as a gift from the Tavazoie lab. I chose the poking assay as the preferred screening method, because albeit not high-throughput, it reveals the presence of mechanosensitive conductances and offers information about their inactivation kinetics. For each cell line I recorded their endogenous voltage-gated activity and their mechanically-stimulated activity using standard voltage-clamp techniques and the poking probe (figure 13). The figure shows two breast cancer cell lines, MDAMB231, derived from a non-invasive cancer, and MCF7, derived from an invasive one. Voltage is held at -80mV and stepped towards more positive values in increments of 20mV. In MDAMB231 cells endogenous voltage gated activity is modest, but clearly visible is a very fast voltage-gated inward current resembling typical sodium currents in the beginning of the trace and voltage-gated potassium currents. Midway through the voltage protocol a step of mechanical stimulation was applied. The poking currents appear symmetrical at positive and negative voltages, and do not inactivate rapidly. MCF7 shows a different electrical profile. There are no inward currents and the overall voltage gated channel activity is smaller than the previous cell line. The mechanosensitive currents are not symmetrical with voltage, they inactivate much more rapidly at hyperpolarized voltages than at positive ones.

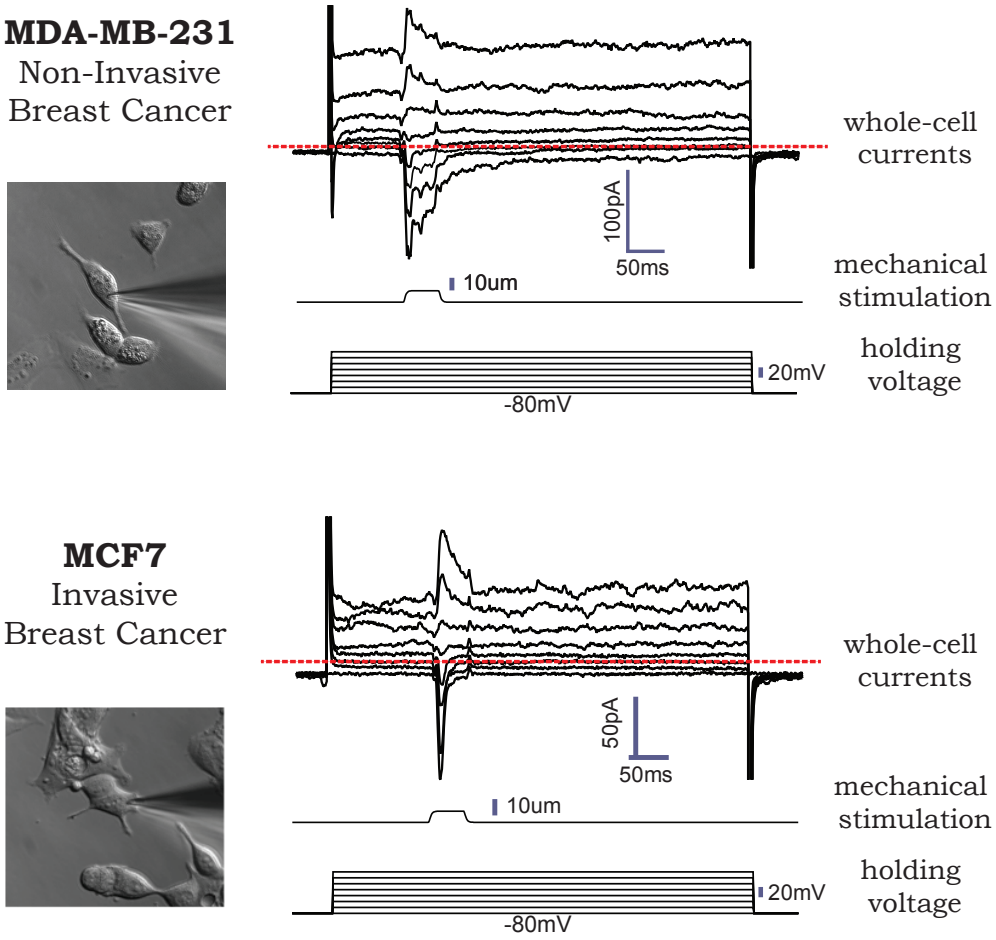

Figure 13. Examination of voltage-gated and mechanically-gated currents in different cancer cell lines. TOP: MDA-MB-231, a non-invasive breast cancer cell line. Left panel shows a brightfield image showing the cell's morphology. On the right panel an example experiment is shown. Top right: the current recorded in response to the stimulation. Middle right: the poking protocol is shown. A 10um step is applied ~150msec after each depolarizing step. Bottom right: The voltage protocol is shown. Cells are held at -80mV and stepped sequentially to positive voltages up to +40mV in 20mV steps. BOTTOM: MCF7, an invasive breast cancer cell line. Same protocol is performed.

This protocol and variations of it were performed for an average of 10 cells for each cell line under study. If the mechanosensitive (MS) current showed no striking kinetic differences at positive and negative voltages, I focused on clamping the voltage at -80mV continuously and increased the poking depth in increments of 0.5um to evaluate the maximum MS current achieved. A total of 8 different cancer cell lines were examined; examples of the mechanosensitive currents encountered are shown in figure 14.

To my surprise, all of the cell lines with the exception of HCT116 showed some form of endogenous mechanosensitivity. The amplitude of the evoked MS currents, as well as the frequency of their appearance within a same cell type varied wildly. To illustrate this point, in SKOV3, an ovarian cancer cell line, only about 50% of the cells studied (18/34) showed mechanosensory currents, but some of those currents were as large as 1.5nA over a very tight baseline.

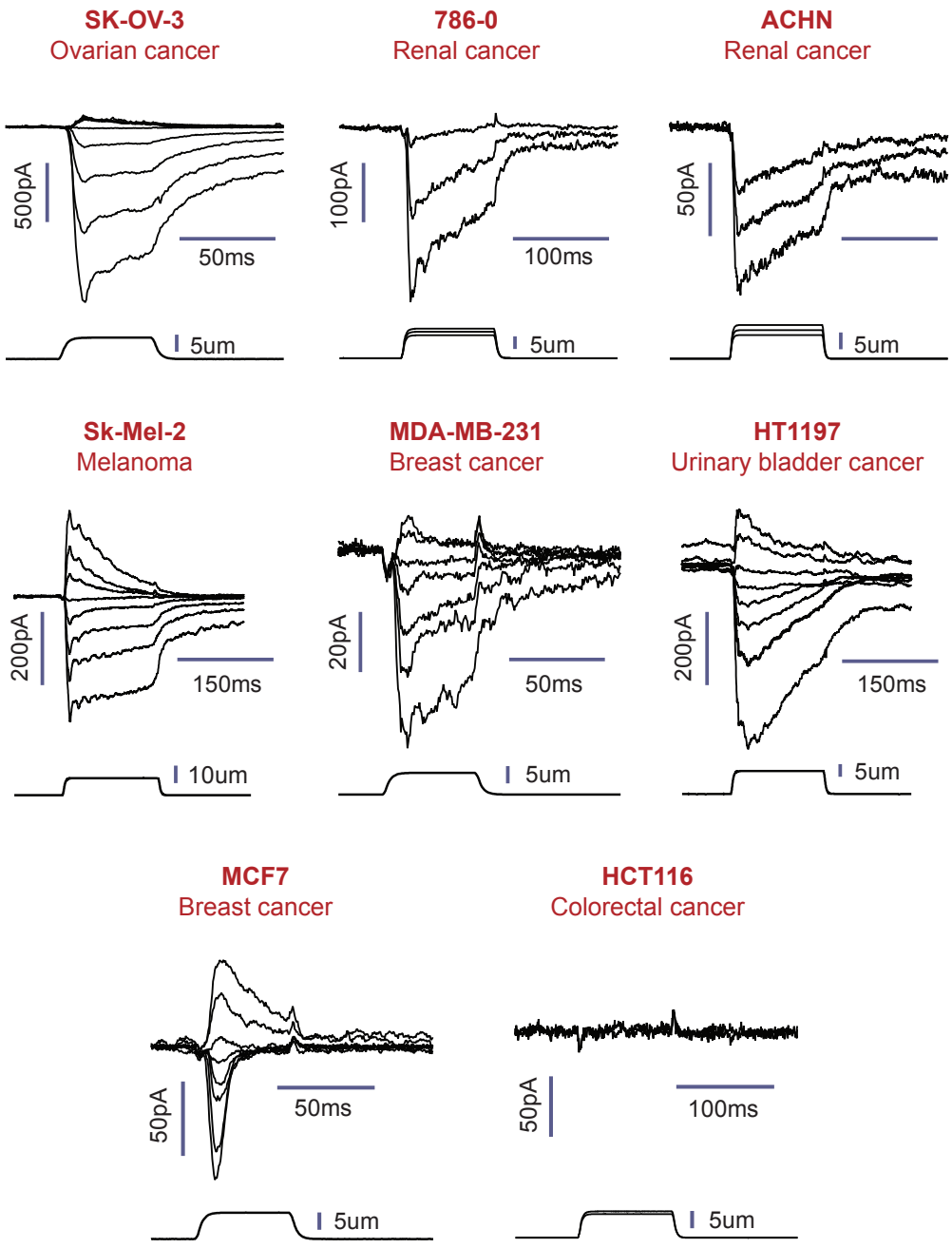

Figure 14. Examples of the eight cancer cell lines examined. Cells are either held at -80mV and poked to increasing depths (786-O, ACHN, HCT116), or depolarized sequentially to multiple voltages and poked after each step (SKOV3, SKMel2, MDAMB231, HT1197, MCF7).

3.2.1.1. Quantifying the kinetics of slow-inactivating MS channels

Among scientists who study poking-evoked currents, the time constant from an exponential fit to channel closing is typically used as a standard metric[21,68]. Piezo currents in particular are reasonably well described by this value. The slow-inactivating currents that I encountered in cancer cell lines are, however, not. Typically I observe very slow rates of apparently multi-exponential decay often to a non-zero (i.e. non-inactivating) baseline. Moreover, perhaps because of the sustained nature of the current, oscillations that appear related to membrane-relaxation events often dominate. (My reason for attributing the oscillations to mechanical fluctuations of the membrane is that consecutive traces often show different oscillatory patterns of relaxation). In addition, these oscillations, sometimes in the order of tens of milliseconds, render the fitting of curves very inaccurate. In figure 15, top, we see a canonical Piezo1 current recorded in N2A cells, adequately fitted to a mono-exponential function with a time constant, tau, of around 15ms. The bottom panels show undescribed MS currents in C2C12 cells, also fitted by mono-exponentials with time constant values of 16ms. The similarity of these values reflects the initial fast-decay of both currents. However, the current in C2C12 reaches a plateau distinct from 0, implying a fraction of the current remains active during the stimulation, whereas Piezo1 current in N2A cells disappears completely within the stimulation period. Here lies the property I wish to understand – mechanically activated currents with large non-inactivating components. To quantify this property I define the percentage of slow-inactivating current as the fraction of current that remains active 50ms past the beginning of the stimulation. Canonical Piezo currents

consistently show values under 20%, whereas all of the slow-inactivating currents that I studied show values above 50%.

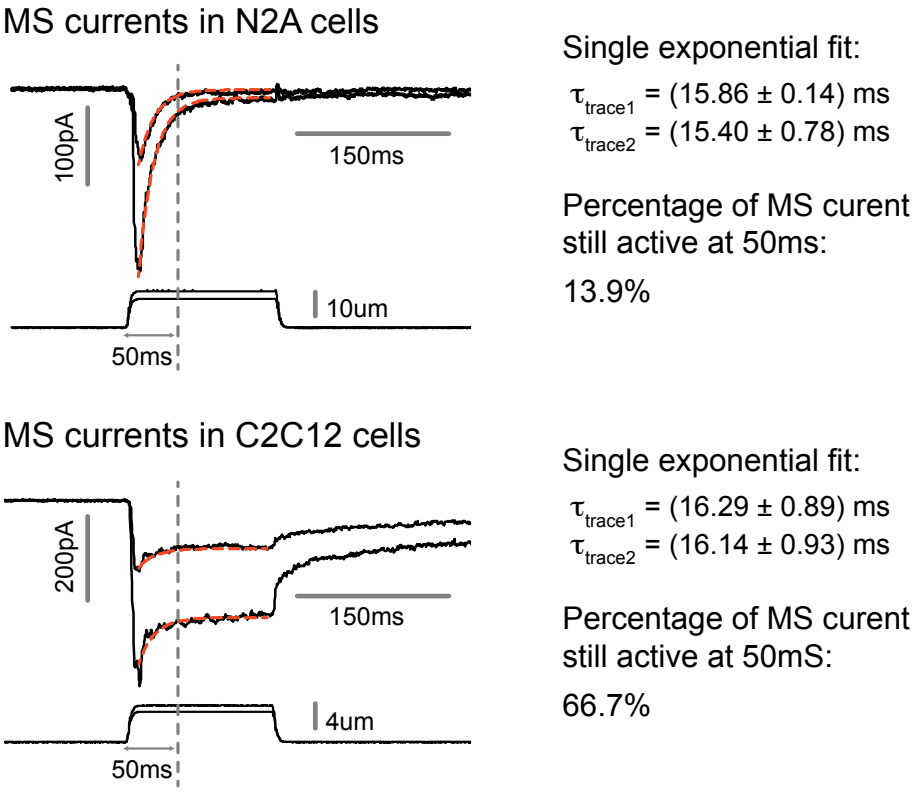

Figure 15. Quantification of the slow-inactivating component of slow mechanosensitive currents. Shown are poking recordings from Piezo1 in N2A cells and an unknown channel in C2C12 cells. Both currents can be fit to mono-exponential curves with similar time constant values. However, C2C12 currents are distinctive in that following an initial fast-inactivation, a large percentage of the current remains active throughout the stimulation. To quantify this parameter I chose to quantify the percentage of MS current that remains active at 50ms.

Figure 16 summarizes the MS currents found in all cancer cells studied. Under the same conditions, only HCT116 cells showed negligible endogenous MS currents. MCF7 cells showed rather large but fast-inactivating currents, very similar to canonical Piezo currents[69]. All other cell lines showed small to large slow-inactivating MS currents, with a percentage of slow-inactivating current of generally more than 50%.

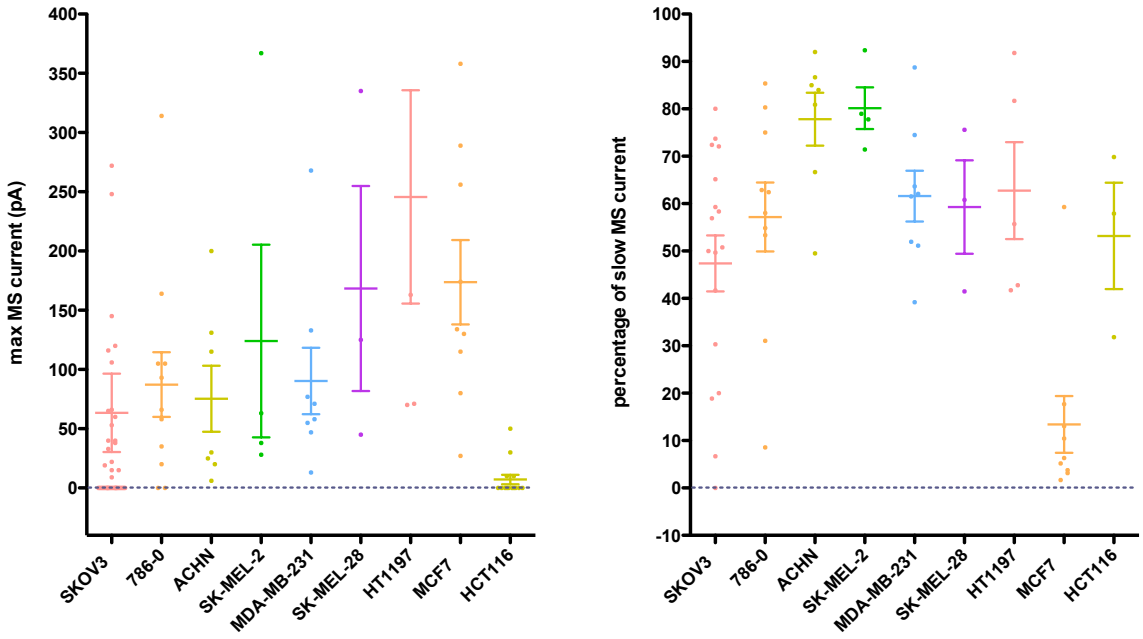

Figure 16. Poking currents in cancer cell lines. Left: each column contains all the recordings made per cell line. Average and SEM currents is shown. Right: percentage of slow current per cell line. Each dot represents the value for each cell studied; average and SEM are marked.

3.2.1.2. Generation of a list of candidate membrane proteins responsible for slow-inactivating currents in cancer cell lines

I performed a subtractive analysis to approach the identification of the undescribed slow-inactivating MS current. The basis was to compare the mRNA expression profile of cancer cell lines showing slow-inactivating currents to that of the cell line showing negligible MS current (HCT116), in order to obtain a list of candidates.

Because the mRNA expression profile (transcriptome) of most cancer cell lines has been extensively studied, I performed transcriptome comparisons from previously published data. I used publicly available microarray datasets from the NCI-60, a panel of 60 human cancer cell lines studied by the National Cancer Institute at the National Institute of Health. Three cell lines from my screening were excluded for this comparison: HT1197, because it is not included in the microarray database, SKOV3, because its MS currents, although rather large at times, only appeared in about half the cells examined, and MCF7, because it did not display slow-inactivating MS currents. In the NCI-60 database each probe of the microarray corresponds to one transcript of a gene. There are 54,000 total probes. Using standard bioinformatic techniques and Matlab I performed a statistical analysis using t-tests for each probe comparing the group of slow-inactivating MS current cell lines with HCT116. I defined as a candidate gene as any with 2-fold higher expression in slow-inactivating cell lines with a p value of 0.05 or less. These thresholds were chosen semi-arbitrarily: a p-value of less than 0.05 is a standard statistical threshold, and a fold change of 2 or more is a conservative threshold considering that the cell lines expressing slow-inactivating currents do so by at least 3 times as much as the control. The election

of conservative thresholds stems from the fact that for an initial screening, a larger set of candidates is preferable, and any false positives can be discarded in further steps. Ultimately, ~1100 candidate genes were identified to possess a global 2 fold change up-regulation with a 0.05 or smaller p-value.

Because ion channels are necessarily composed of membrane proteins, I then retrieved from *ensemble* the list of all membrane proteins in the human genome. I ran all those sequences through a hydrophobicity prediction software (TransMembrane Hidden Markov Model, TMHMM) and selected all membrane proteins spanning the membrane twice or more, a characteristic shared by all know eukaryotic ion channels. This resulted in the final list of candidate proteins, containing 113 candidates. Of all those candidates, some were very clearly not expressed in the plasma membrane according to published evidence. I prioritized the list, focusing first on those genes with unknown or poorly described function and localization.

3.2.1.3. Study of Piezo1 and Piezo2 expression in cancer cell lines

A first question to address is to determine whether Piezo1 or 2 is expressed in those cell lines and therefore could be responsible for the slow-inactivating MS responses. I addressed that question in multiple ways, although ultimately the results were inconclusive.

1) Transcriptome analysis reveals that Piezo2 is not significantly expressed in any of the cell lines, immediately excluding it from my list of candidates. For Piezo1, a bioinformatic analysis using the same parameters as the ones above shows that Piezo1 has significantly higher expression in the MCF7 cell line than in any of the slow-inactivating cell lines. MCF7 is the cell line that exhibits the

fast-inactivating, piezo-like current. This cell line, however, does not have twice as much general MS current as all other cell lines. This suggests a preliminary model in which there are two independent mechanosensitive channels at play, Piezo1 forming a fast-inactivating conductance and an unknown channel forming a slow-inactivating conductance.

2) I attempted knockdown of Piezo1 in two cell lines: MCF7 and SKOV3. Unfortunately, both attempts failed for different reasons. MCF7 cells were unresponsive to siRNA treatment; the mRNA levels of Piezo1 did not decrease using any combination of siRNAs targeting Piezo1. SKOV3 cells, on the other hand, deteriorated quickly after the transfection treatment, rendering them unsuitable for further knockdown studies. I discarded the idea of trying Crispr on them as most cancer cell lines contain an unusually high chromosomal complement and are relatively difficult to transfect.

3) A final approach was to investigate whether there is a cellular environment in cells with slow-inactivating currents that could potentially modify the kinetics of Piezo1, making its rate of inactivation significantly slower. For this purpose I transfected Piezo1 into C2C12 cells, a mouse myoblast cell line sthat shows robust slow-inactivating MS currents and is easy to transfect with high efficiency. When Piezo1 is transfected into C2C12 cells, the resulting current is fast-inactivating and showing the standard Piezo1 kinetics, indicating that the cellular environment within C2C12 cells is perfectly capable of exhibiting a fast-inactivating MS current.

The results of these experiments did not exclude the possibility of Piezo1 being the pore-forming subunit of the slow-inactivating channel, but did support

the hypothesis that a different and unknown conductance might still be present. I therefore decided to move forward with the screening.

3.2.1.4. Screening of candidate membrane proteins

The ultimate goal is to test the candidate membrane proteins to identify the molecules involved in the slow-inactivating mechanosensitive current. To that end, two different approaches are often used: *loss of function* (LoF) screening, typically consisting in knocking down RNA transcripts of individual candidates from a cell line with a high signal; and *gain of function* (GoF), consisting of the heterologous expression of candidates in a cell line with no background signal. I will briefly discuss the reasoning behind choosing the latter. Knockdown studies were clearly to be hindered by multiple factors. As mentioned, some of the cancer cell lines are not easy transfection targets. Additionally, the expected results of any knockdown studies aspire to an 80-90% reduction in the property under study, at best. In the case of some of the cell lines in my screen in which approximately 50% of the cells express fairly large (over 50pA) MS currents, the number of cells that would be necessary to study in order to achieve significant differences would be high. In *gain of function* screening, the riskiest assumption is that there is only one gene product necessary and sufficient for the generation of the desired phenotype. On the other hand, the biggest advantage of a *gain of function* screen is arguably the speed. If the host cell line for testing has sufficiently low background signal, the testing of a few cells per construct is a good enough initial screen and can be performed at a speed of 2-3 constructs a day. There are multiple examples of single-gene product ion channels that express beautifully in the absence of accessory subunits, and this screening

method can proceed at a fast enough pace that I decided to move forward in that direction.

I obtained cDNA for each candidate from various publicly available sources and subcloned them into a bicistronic GFP vector, a strategy that allows me to identify unequivocally the transfected cells through gain of fluorescence. For heterologous expression I chose *Chinese Hamster Ovarian* (CHO) cells, an easy-to-transfect expression system with the lowest levels of endogenous mechanosensitive currents detected thus far. The lack of MS currents in CHO cells does not stem, however, from an impossibility of the cells to produce such currents, as CHO cells are perfectly capable of expressing normal Piezo currents and other MS channels such as TRAAK[26].

I transfected naive CHO cells with each construct and studied the cells 24-48 hours after transfection. I used electrophysiological recordings and mechanical stimulation, similar methods as described throughout this chapter, and studied an average of 4 cells per construct. The results of the first 40 candidates screened are shown in figure 17. None of the candidates exhibited MS currents with a statistical difference from currents in control CHO cells. However, Two clones, LHFP and TSPAN4, did exhibit a slow-inactivating MS current, but not in a robust manner, as only a small fraction of the tested cells exhibited any MS current at all.

After screening the first 40 constructs with no significant positive hits, I focused my efforts on a different approach that showed more promising results, which will be detailed in the next chapter.

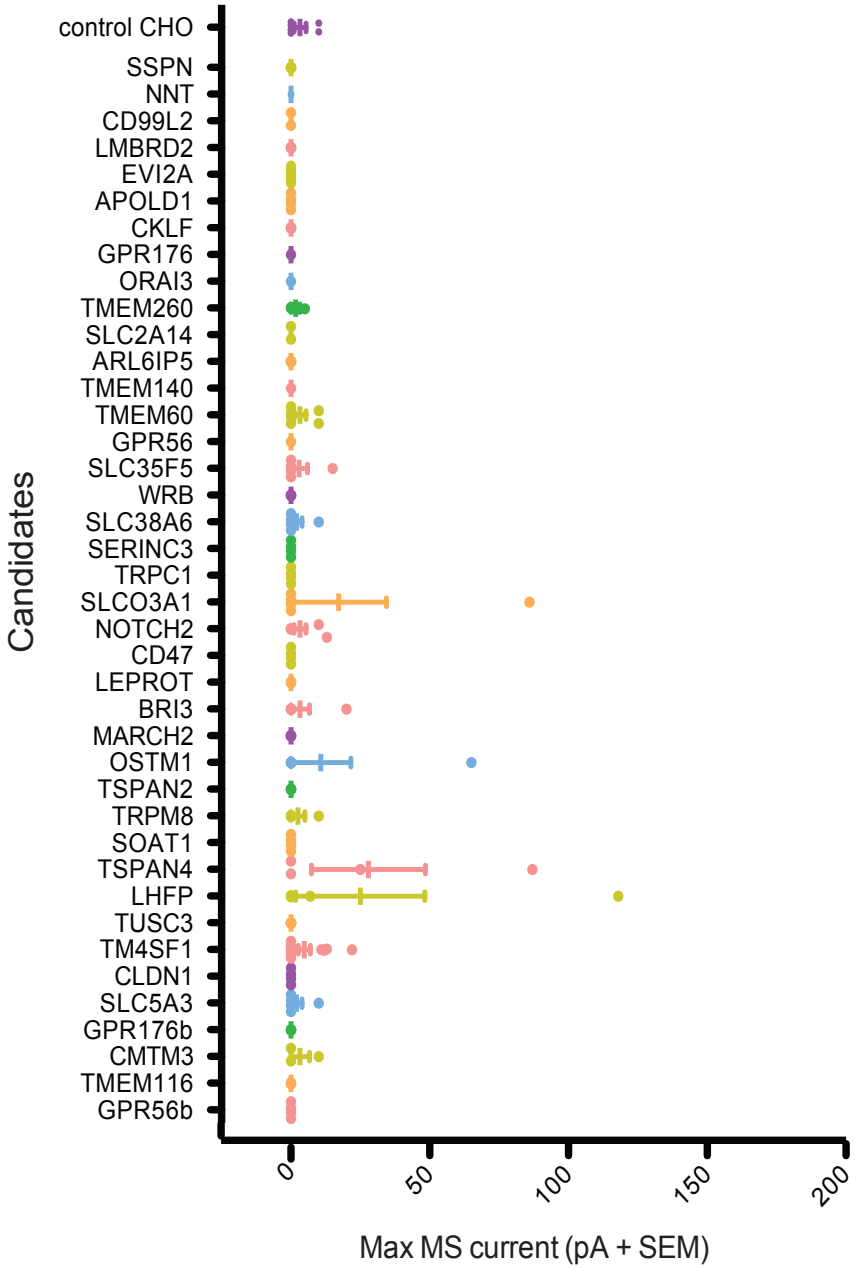

Figure 17. Gain of function screen of candidate molecules in CHO cells. CHO cells were transfected with constructs containing each candidate molecule. Constructs were marked with a bicistronic GFP cassette and transfection was assessed by fluorescent identification of transfected cells. Using unpaired t-tests between each candidate and control CHO cells, no candidates showed a significantly increased response.

3.2.2. Mechanosensitive currents in embryonic stem cells

The original scope of the project was to screen a diversity of human and mouse cell lines in an unbiased manner. That is, I did not focus on cells that would have an obvious natural role in mechanosensation. Among the cell lines that I decided to test for mechanosensitive currents were mouse and human embryonic stem cells. Aside from their potential medical relevance, stem cells possess the versatile ability to differentiate into a variety of distinct cell types. I sought to take advantage of this possibility by studying the evolution of mechanosensitive currents throughout several differentiations.

3.2.2.1. Human Embryonic Stem Cells do not exhibit mechanosensitive currents

In collaboration with Gist Croft, from the Brivanlou laboratory at the Rockefeller University, human embryonic stem cells were differentiated into layer VI cortical neurons. This process takes ~40-90 days in vitro during which stem cells are first exposed to drugs that block non-neuronal fates (neural induction), turning into forebrain neuroepithelial cells. Afterwards, the neocortical neurogenesis program is executed turning cells into neuronal progenitors that then give rise through maturation and synaptogenesis to fully mature, post-mitotic cortical neurons[70,71]. Using both voltage and current clamp in combination with mechanical stimulation, I studied the transition in its electrical and mechanosensitive aspects (figure 18).

Figure 18 (next page). Evolution of voltage-gated current, poking-evoked currents and morphology of human embryonic stem cells in their path to become neurons from the 6thcortical layer. Three stages were studied: human embryonic stem cells, neuroepithelial cells, and cortical layer VI neurons. For all three stages the voltage-gated currents are shown in the top traces (in steps from -80mV to +40mV), the poking-evoked currents and protocol are shown in the middle traces, and a brightfield image of cells at each stage is shown too. Additionally, for the cortical layer VI neuron, a current clamp experiment is shown, where current is clamped showing a resting potential of -65mV, and upon current injection multiple action potentials in sequence can be observed.

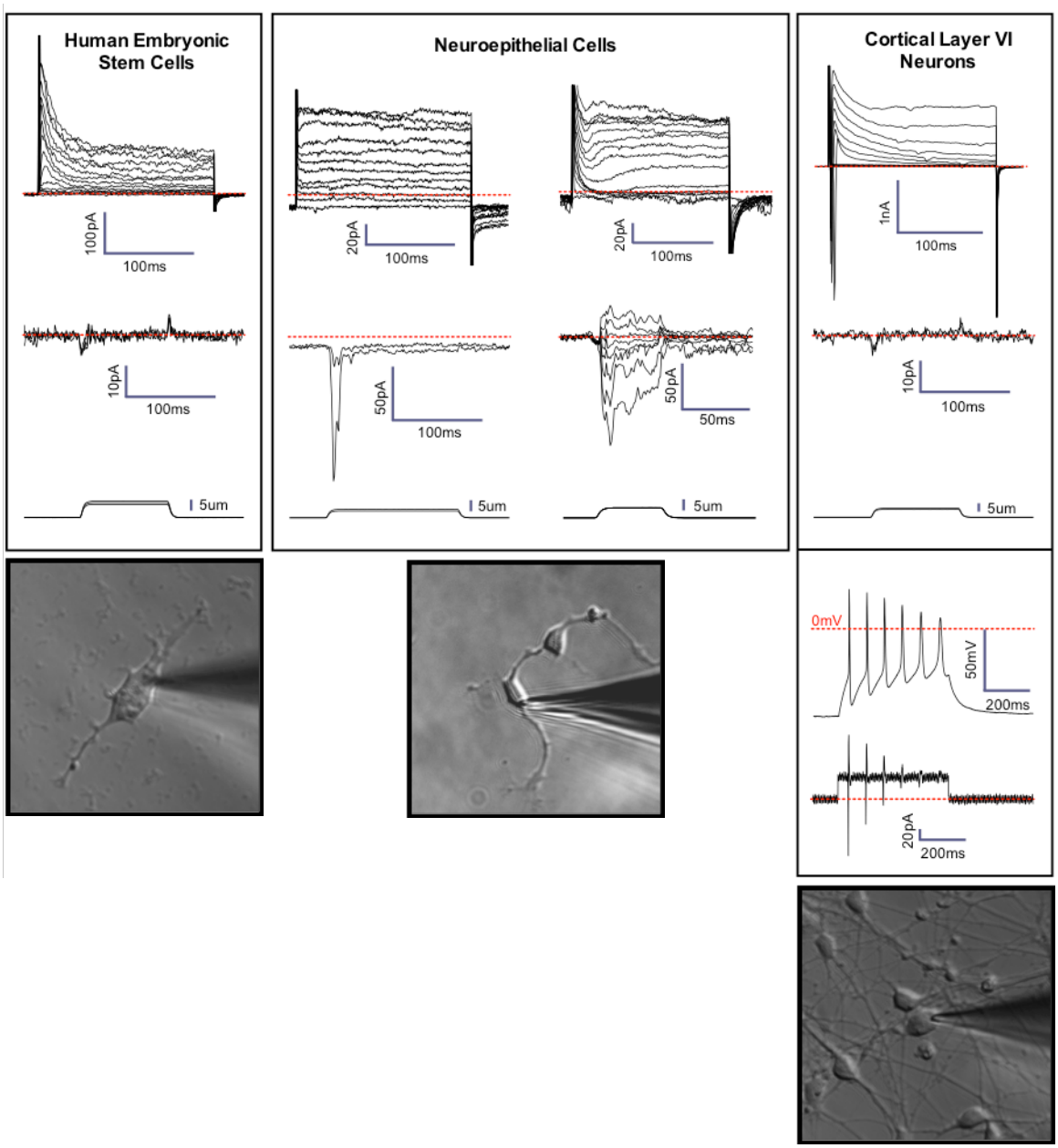
Human Embryonic Stem Cells
100pA
100ms
10pA
100ms
5um
Neuroepithelial Cells
20pA
100ms
20pA
100ms
50pA
100ms
50pA
50ms
5um
5um
Cortical Layer VI Neurons
1nA
100ms
10pA
100ms
5um
0mV
50mV
200ms
20pA
200ms

Human embryonic stem cells exhibited small voltage-gated potassium currents but did not exhibit prominent mechanosensitive current. Of the 14 cells analyzed, only 2 exhibited small (under 30pA) responses to poking, while the remaining 12 exhibited no currents at all. In contrast, neuroepithelial cells exhibited a variety of responses. Six of the 12 cells neuroepithelial cells studied showed some form of MS currents. Interestingly, of those 6 positive cells, half showed a fast-inactivating MS response, and the other half a slow-inactivating one. Heterogeneity is a known feature of neuroepithelial cells, a naturally plural stage where we can find anything from neuroepithelial stock cells, radial glial, or even progenitor neurons. Lastly, cortical neurons from layer VI did not exhibit any type of MS behavior. In this stage I found mostly fully mature post-mitotic neurons, but also some progenitor cells. Neurons were clearly mature and fully functional, exhibiting large voltage gated sodium and potassium currents. Neurons were also capable of firing normal action potentials and even some of them did so in a typical train burst. But, again, none of these exhibited mechanically-evoked responses. It should be noted that cells at the neuronal stage could only be stimulated in their cell bodies, as their processes are beyond the size range accessible to the poking probe.

Although the presence of MS currents in neuroepithelial cells is certainly interesting, they were not consistent and uniform enough to be a good lead for cloning attempts. I therefore analyzed another differentiation path.

3.2.2.2. Mouse Embryonic Stem Cells exhibit large slow-inactivating MS currents

Mouse embryonic stem cells can be robustly differentiated into motor neurons *in vitro*[72,73]. This differentiation takes seven days, during which cells undergo several defined stages (figure 19). To initiate the differentiation, growth factors are removed from the media to which mouse embryonic stem cells are exposed which terminates their pluripotent stage and sends them to a state in which they are responsive to patterning signals. Retinoic acid (RA) is then applied, which induces differentiation into spinal nerve cells. Further addition of *sonic hedgehog* (Shh) at day 3 controls ventralization of nascent spinal neurons. Lastly, addition of *glial cell derived neurotrophic factor* (GDNF) turns on the host of motor neurons-specific genes, along with the characteristic Hb9 transcription factor.

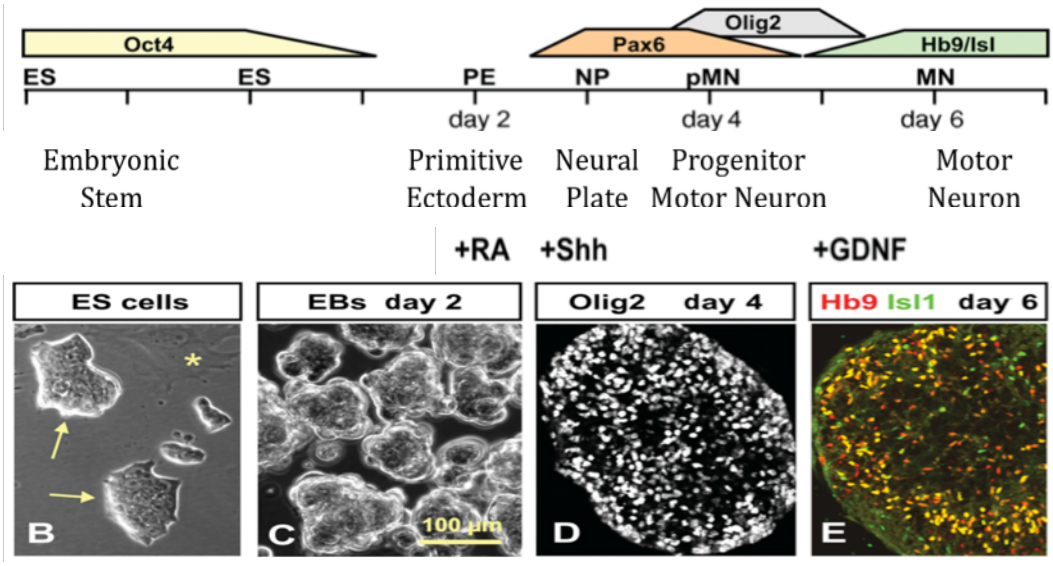

Figure 19. From Wichterle et al., 2008[73]. The scheme of differentiation of mES cells into motorneurons. A timeline is shown from Embryonic Stem (ES) cells into Motor Neurons (MN). On top of the timeline, specific transcription factors active at each stage are marked. The necessary supplements to facilitate the transition in vitro are shown below . Lower panels show images corresponding to 4 stages along the differentiation, stained using stage-specific antibodies.

To follow the differentiation we used an Hb9-GFP stem cell line, gift of the Wichterle lab, in which the motor neuron-specific promoter Hb9 drives GFP expression[72,73]. This system allows us to swiftly identify mature motor neurons and check the progress of the differentiation. We achieved 30-50% efficiency as assessed by GFP expression and morphological and functional characterization. We performed 3 independent differentiations and conducted the same studies and measurements on all three. These experiments were done in collaboration with Kouki Touhara, a graduate student in the MacKinnon Lab, who performed some of the tissue culture duties.

I studied the voltage-gated and mechanosensitive currents throughout each differentiation stage. Voltage-gated currents of mES cells were small and remained so throughout the first 4 stages studied. Interestingly, mouse embryonic stem cells (mES cells) exhibited the most robust and slow-inactivating mechanosensitive currents yet encountered (figure 20). Poking currents ranged from 0 to over 2100 pA over baseline, with an average value of (465 ± 112) pA. Because the MS currents could not be reliably fitted to mono- or bi- exponential curves, to quantify the slow-inactivating current I made use of a similar concept as in previous chapters: the percentage of slow-inactivating current active 75ms after the beginning of the stimulation. For this, I defined two quantities: the peak current, corresponding to the maximum MS current achieved at the beginning of the stimulation; and the slow current, corresponding to the MS current as measured 75ms into the poking step. The relative measurement of these quantities describes what percentage of the peak current is still active halfway through the stimulation. For mouse embryonic stem cells, the average percentage

of slow-inactivating current is (66.78 ± 4.37)%. A detailed study of this current reveals that it is non-selective for cations with high permeability to calcium ions (figure 20).

Figure 20 (next page). Mechanosensitive currents in mES cells. Top panel shows three example traces of poking-evoked currents in mouse embryonic stem cells. The cells were clamped at -80mV and poked at increasing depths. Currents are clearly slowly-inactivating or almost non-inactivating, with certain degree of variability between different cells. The bottom panel shows the reversal potential of the mechanically evoked currents of a mES cell using different ionic compositions in the recording solutions. For this experiment cells are depolarized to different voltages from -80mV to +40mV in steps of 10mV. The internal solution always contains KCl. The pink curve is done using NaCl in the external solution. The reversal potential sits at 3mV, indicating that both Na and K (and potentially Cl) are equally likely to travel through the pore. The purple trace corresponds to NaGluconate in the media. The removal of chloride in the bath solution situates the reversal potential for chloride at >+50mV. The fact that the current did not move its reversal potential in that direction at all indicates that chloride does not permeate the pore (the 9mV left shift can actually be accounted by the liquid junction potential generated when introducing gluconate, a much slower ion, into the bath solution). The blue curves is the shift in the absence of sodium. The reversal potential moves towards that of potassium, indicating a permeability for potassium (and none for NMDG). Finally, the green curve taken with calcium as only cation in the bath shifts to +14mV, closer to the reversal potential of calcium than to that of potassium, indicating a slightly higher permeability for calcium than for potassium. In summary, the pore is selective for cations with a slight preference for calcium.

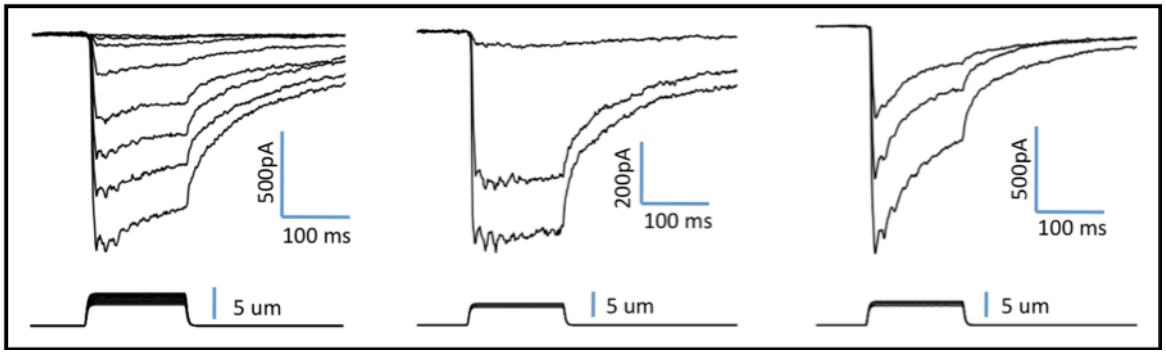
500pA
100 ms
5 um
200pA
100 ms
5 um
500pA
100 ms
5 um

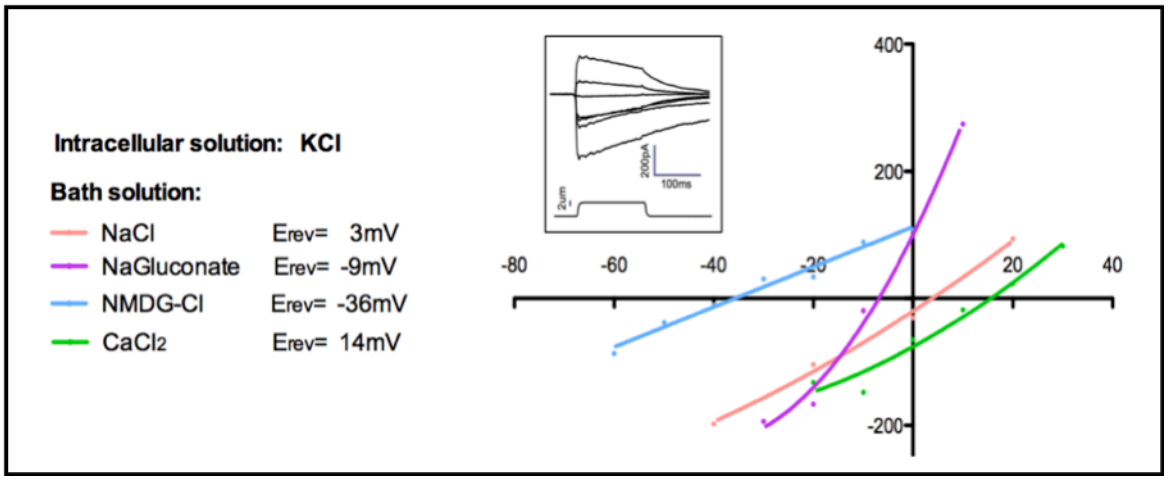
Intracellular solution: KCl
Bath solution:
NaCl Erev= 3mV
NaGluconate Erev= -9mV
NMDG-Cl Erev= -36mV
CaCl2 Erev= 14mV
400
200
-200
-80
-60
-40
-20
20
40

In an excised membrane patch, stimulation by pressure clamp elicits activity of single channels that correlates temporally with the stimulation (figure 21). An ensemble of multiple pressure-evoked recordings of single channels at the same voltage shows a macroscopic current whose kinetics mimics that of the whole cell poking currents. Amplitude histograms at multiple voltages allow me to estimate a single channel conductance of (24.7 ± 2.5) pS (figure 21).

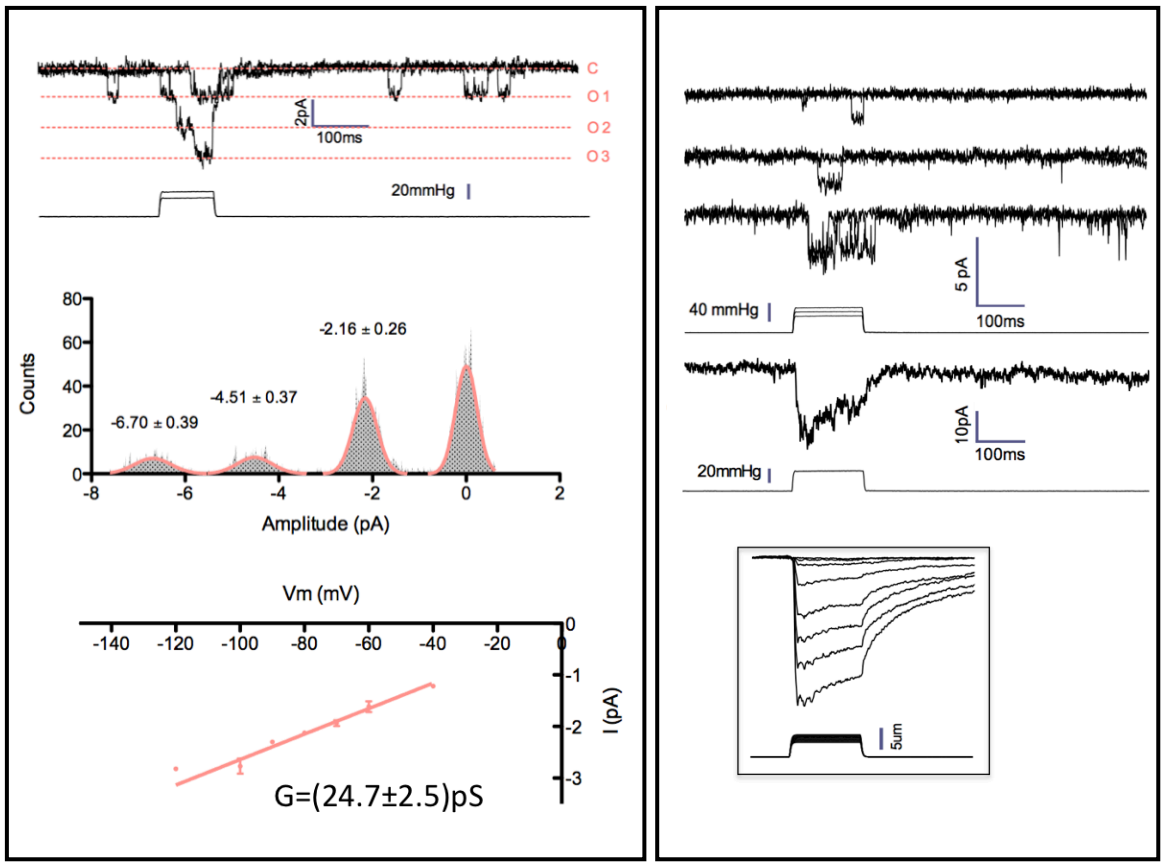

Figure 21. Single channel study of the MS channel in mES cells in outside-out excised membrane patches. Top left: membrane patch is held at -80mV and channel activity is evoked by pressure steps, the opening of 3 channels can be seen. Middle left: amplitude histograms of all 4 states (closed, open1, open2, open3). Bottom left: conductance estimation from amplitude histograms of multiple recordings at different voltages gives a value of ~25pS. Right panel shows multiple single channel recordings holding at -80mV and using pressure to evoke activity. The sum of those gives an apparent macroscopic current whose kinetics resembles that of the whole-cell poking currents (shown in an insert below the traces for comparison).

3.2.2.3. MS current in mES cells depends on the differentiation state of the cell

To study the evolution of this current after exiting the stem cell state, mouse embryonic stem (mES) cells were differentiated into motor neurons. Voltage-gated currents remain small during the initial steps of the differentiation, until approaching neuronal stage. Around day 5, voltage gated potassium currents become larger and some cells begin to exhibit small voltage gated sodium currents (Figure 22, top panels). This, along with low GFP expression, indicates the presence of immature motor neurons. By day 7, GFP expression increases in about 50% of the cells and GFP-positive cells acquire a typical neuronal profile and are able to fire action potentials. Morphologically, the differentiation progresses in a similar manner (figure 22, top images), with a rather non-differentiated appearance in the initial steps and the presence of neuronal processes as they approach days 5 to 7. Interestingly, mechanosensitive currents follow an opposite course of development than voltage-gated currents (figure 22, lower panels). Currents are large and slow-inactivating at the stem cell stage, and become increasingly smaller and faster-inactivating as differentiation progresses. By the time the neurons are mature, they do not exhibit mechanically-evoked currents. It should be noted that there is large heterogeneity throughout the process both between cells in similar stages of a differentiation and also between differentiations. Regardless, the trend towards diminishing and faster poking currents throughout the process is clear.

Figure 22 (next page). Morphology, voltage-gated and poking currents through differentiation of mES cells into motor neurons. 6 stages were studied and inspected under brightfield illumination (top images). Voltage gated currents were obtained by holding the cells at -80mV and depolarizing in steps from -80mV to +40mV (middle traces). Poking currents were obtained by holding at -80mV and poking at increasing depths (lower traces). Notice how voltage-gated currents are relatively small until day 5 and increase substantially by day 7 (notice the 10fold difference in scale). Poking currents are always heterogeneous but overall diminish and become faster as the differentiation progresses.

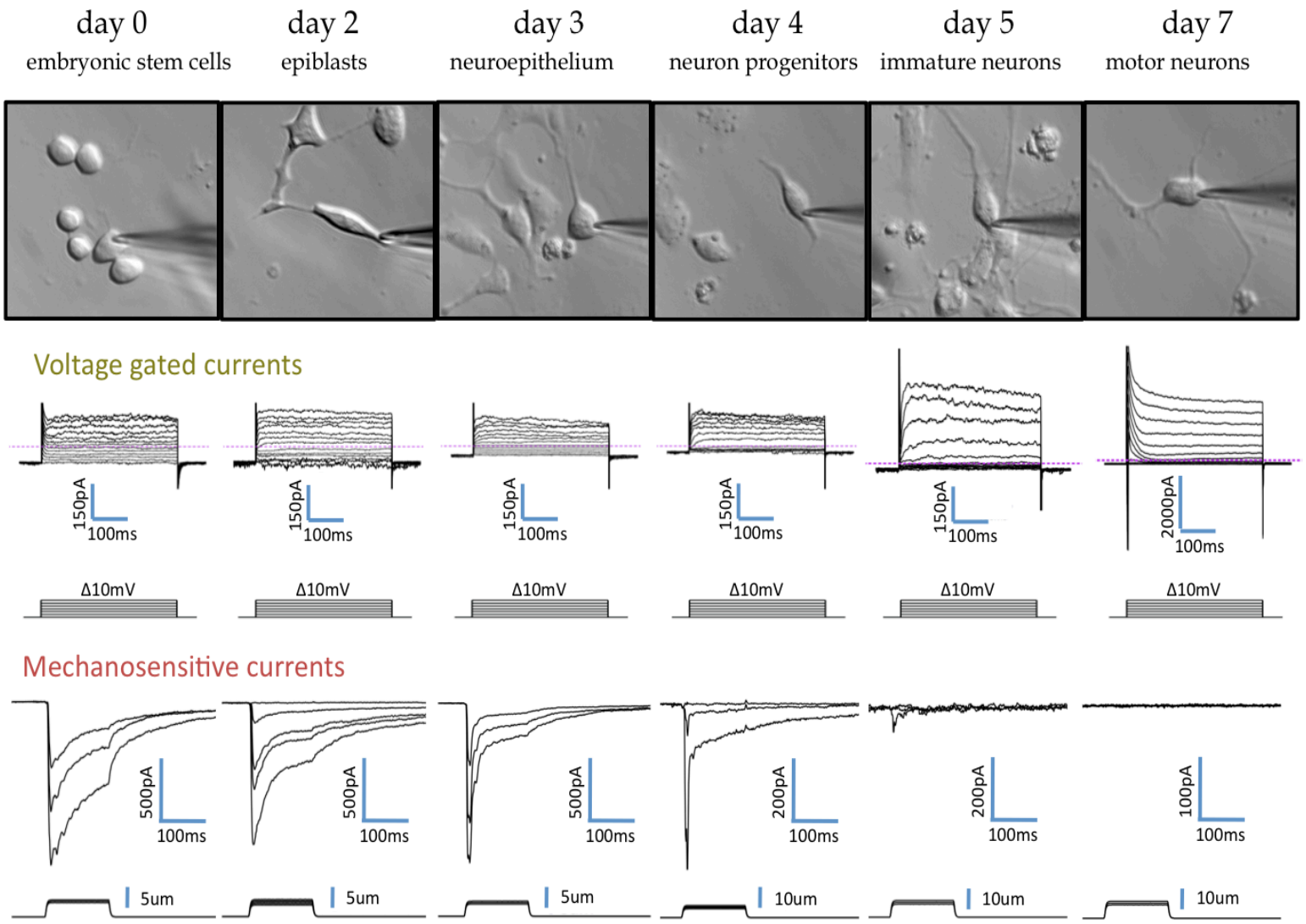
day 0
embryonic stem cells
day 2
epiblasts
day 3
neuroepithelium
day 4
neuron progenitors
day 5
immature neurons
day 7
motor neurons
Voltage gated currents
150pA
100ms
Δ10mV
2000pA
Mechanosensitive currents
500pA
200pA
100pA
5um
10um

A quantification of the MS currents throughout the differentiation is summarized in figure 23. Panel 2.12 shows the peak current at every stage, decreasing from (465 ± 112) pA on mES cells to (0.25 ± 0.25) pA in motor neurons. The bottom panel shows the percentage of slow-inactivating current during the process. For mES cells, values range from 25 to 100% with a mean value of 65%. By day 2, the percentage drops to 40% of the peak value, and keeps decreasing until day 7. Finally, there is also a decrease in the fraction of responsive cells, defined as any assayed cell that displayed a mechanosensitive response to stimulation. At the stem cell stage, 80% of the cells exhibit an MS response. The number drops monotonically towards a value statistically indistinguishable from zero on day 7.

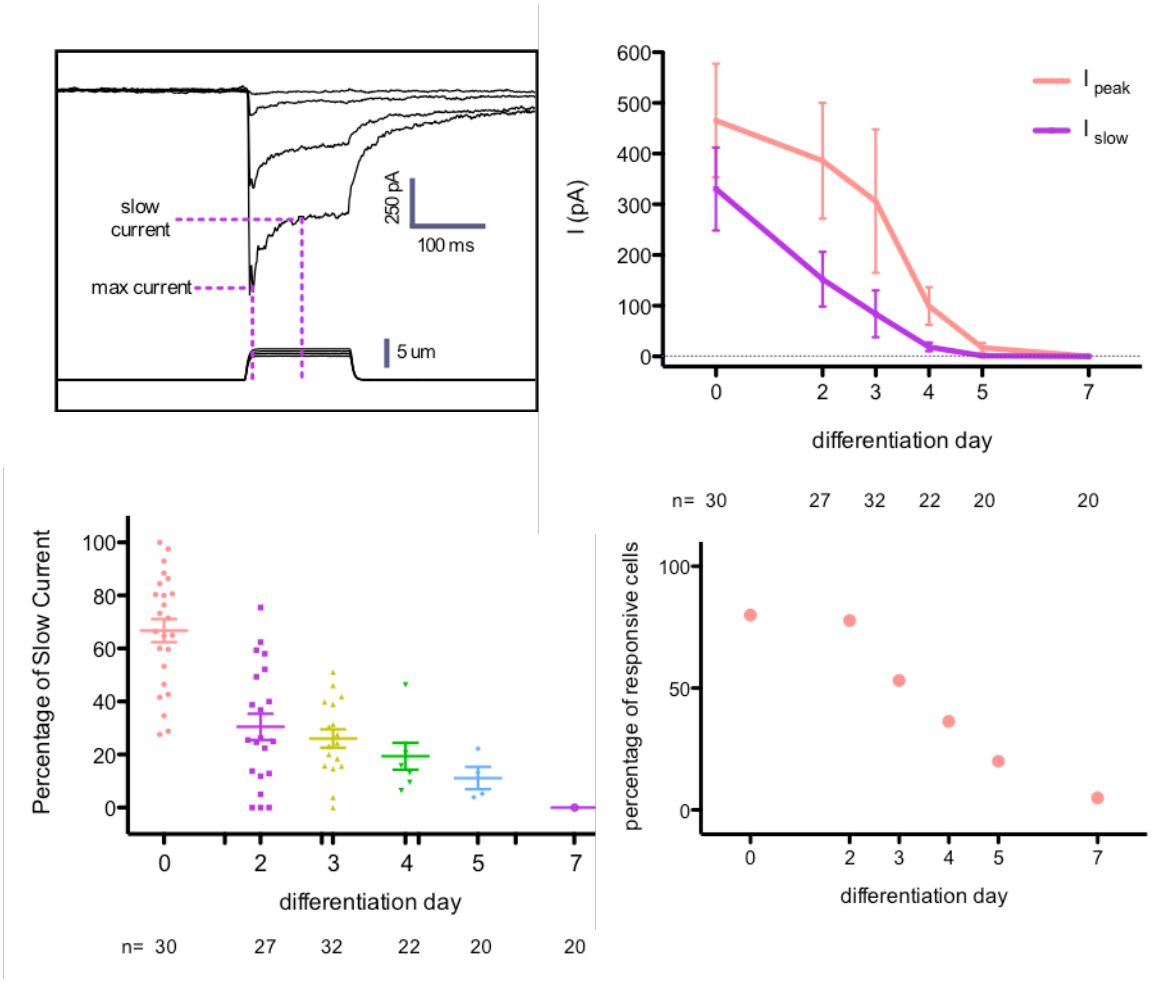

Figure 23. Quantification of poking currents throughout the differentiations. Top left panel details the quantification method used. A 'peak current' and a 'slow current' are defined to circumvent the inadequacy of using exponential fits. Right panel shows the evolution of the peak and slow current throughout the differentiations (3 independent differentiations were performed, data was pooled). Lower left panel shows the percentage of slow current in all stages. Below each dataset is the total number of cells assessed at each stage. Lower right panel shows the percentage of responsive cells at each stage. A responsive cell is any cell that shows a poking current.

3.2.2.4. Piezo1 forms the slow inactivating current of mES cells

As in previous chapters, I made use of transcriptome analysis to find the molecular components of the slow-inactivating current. I performed mRNA deep sequencing throughout the differentiation, and, using standard bioinformatic methods, selected as candidates those multi-pass membrane proteins whose expression profile correlates with that of the observed poking currents. The final list of candidates contained less than 150 molecules. Interestingly, Piezo1 was among those candidates in the list. I therefore decided to do a *gain of function* and a *loss of function* screening in parallel. I will discuss first the role of Piezo1; later in this chapter I will explore the contribution of other membrane proteins.

As mentioned above, the results from the deep sequencing revealed that expression of the Piezo1 gene correlates with that of the fast component of the MS current in mES cells (figure 24).

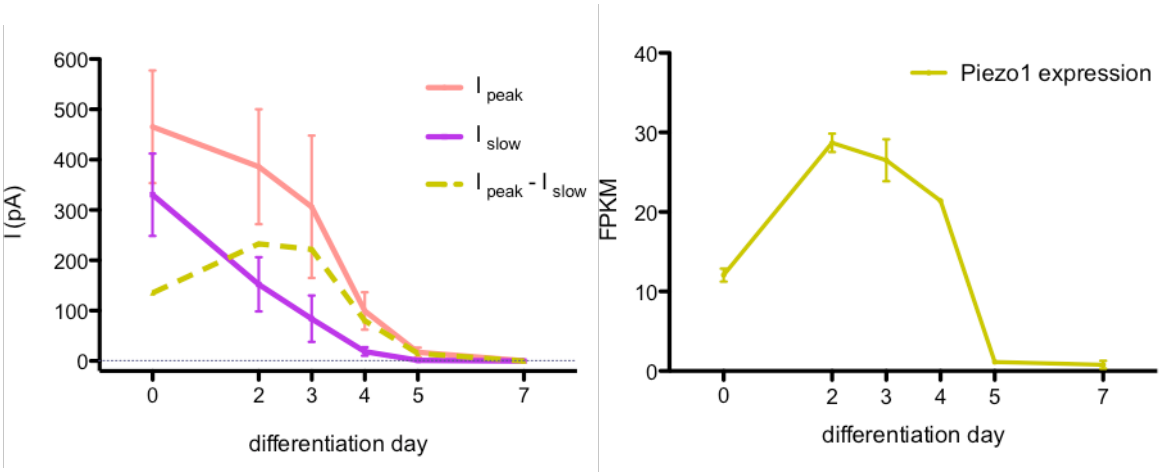

Figure 24. Fast and slow MS currents throughout the differentiation (left) and Piezo1 expression (right). The fast component of the MS current through the differentiation, estimated by subtracting the slow-component from the peak MS current, evolves in parallel as Piezo1 expression. mRNA expression studies were done in triplicates, therefore the mRNA expression is the average and SEM of those values. FPKM: fraction per kilobase per million reads.

After unsuccessful attempts at knocking down Piezo1 using siRNA, I used Crispr/Cas9 technology to knock out the Piezo1 gene from mES cells[74]. To avoid confounding factors from off-target effects, I obtained two independent knock out cell lines using two different sgRNA sequences to guide Cas9 nuclease (figure 25). For both separate colonies the Piezo1 gene was knocked out by the introduction of an early stop codon generated by a frame-shift mutation, the result of a double strand break by Cas9 early in the Piezo1 gene (figure 25). Study of the mechanosensitive behavior of these cells revealed that the entirety of the MS current is absent. These effects are unlikely to be due to off-target effects of Cas9, as they were observed in both colonies generated using different guide RNAs, and therefore a complete different set of off-targets. Ultimately, this provides strong evidence that Piezo1 carries the mechanosensitive current in mouse embryonic stem cells (figure 25).

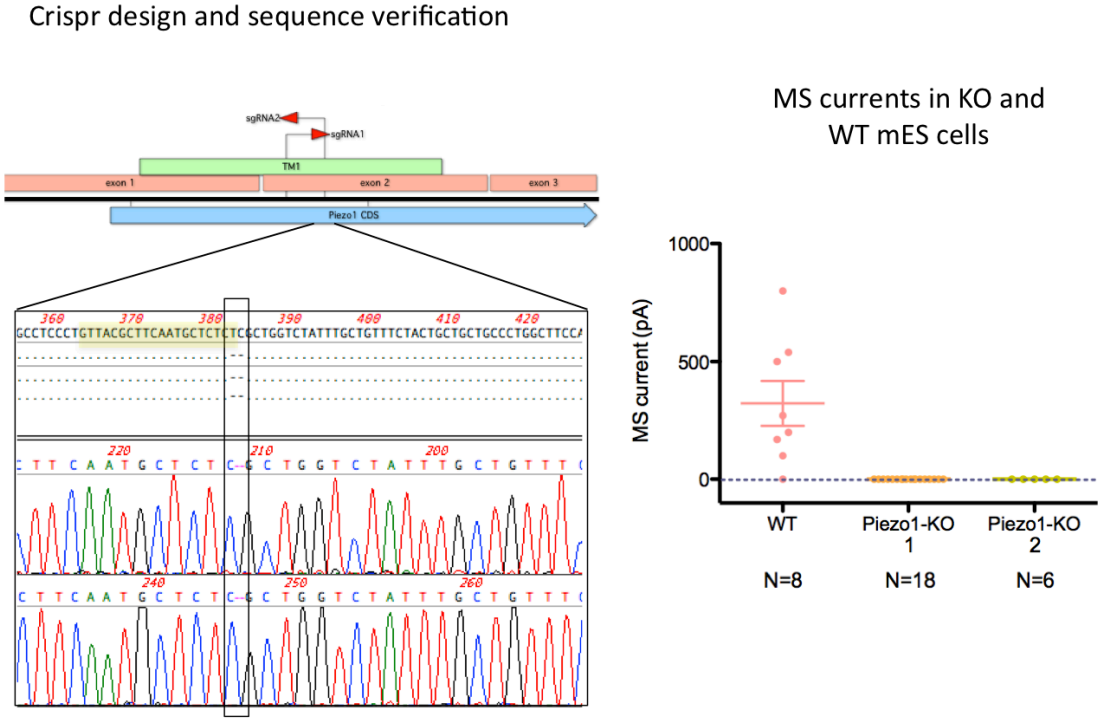

Figure 25. Knock out of Piezo1 in mES cells abolishes MS current. Left: a diagram of the beginning of the Piezo1 mRNA in mES cells is shown. The first 3 exons are shown, along with the coding sequence (CDS) and the first predicted transmembrane region. Two guide RNA sequences (sgRNAs) were chosen to generate a double strand break (DSB) in the beginning of the first TM region. Below the diagram, sequence reactions of a fragment of DNA extracted from the one of the modified colonies is shown. In yellow is marked the targeted sgRNA sequence, and boxed in black is marked the region with a two base-pair deletion that generates a frame-shift mutation, and an early stop codon shortly after. Only one sequence was obtained after sequencing with no background, indicating a homozygous mutation. Right: Piezo1 knock out colonies showed no mechanosensitive activity.

3.2.2.5. Heterologous expression of Piezo1 cDNA from mouse embryonic stem cells yields a fast inactivating MS current

Recent work reported that point mutations in the human PIEZO1 gene give rise to a version of the protein with slower inactivation rates[34,35]. To investigate whether the conspicuous kinetics of Piezo1 in mES cells is due to an intrinsic feature of the Piezo1 gene in these cells, I studied the sequence of Piezo1 cDNA from mES cells. I generated a mouse ES cell cDNA library from total mRNA, and initially intended to clone the entire Piezo1 transcript using primers that cover the entire coding sequence of the gene. This procedure was successful for the Patapoutian lab to clone Piezo1 from mouse N2A cells[21]. I, however, was unable to retrieve the full-length cDNA under the same conditions. I attempted multiple mRNA extractions, cDNA library generation methods, combinations of primers, and PCR conditions. The failure to retrieve a full-length clone could be due to multiple factors, one is the fact that the Piezo1 mRNA is very long, and if its relative abundance is not as high in mES cells as it is in N2A it is possibly not well preserved during the library generation process. I therefore designed primers that cover multiple short and overlapping fragments of the gene. With this method I easily retrieved multiple fragments that cover the entire coding sequence of the Piezo1 gene. Direct sequence of the PCR fragments showed a single sequence of the mouse Piezo1 transcript that differs in 3 aminoacids from the sequence retrieved from mouse N2A cells. The mutations are G147R, I229V, and V1572M (figure 26).

The possibility existed that these modifications generate an intrinsically slower-inactivating channel. I therefore cloned the Piezo1 gene retrieved from

mES cells including all three mutations into a heterologous expression vector. I expressed both constructs, the Piezo1 from mES cells and the Piezo1 from N2A cells, in HEK293 cells and compared the inactivation kinetics using the poking assay. It is worth noting that for this experiment I used a HEK293 cell line in which I previously knocked out the Piezo1 gene by using Crispr/Cas9 technology, effectively depleting all endogenous signal. Both constructs yielded currents with similar inactivation kinetics (figure 26), excluding the point substitutions of the mES cells Piezo1 gene from accounting for the altered kinetics of Piezo1 in those cells.

In summary, these findings suggest that Piezo1 is responsible for the totality of the MS current in mES cells, rendering it the likely pore forming subunit of the complex responding to the poking stimulus.

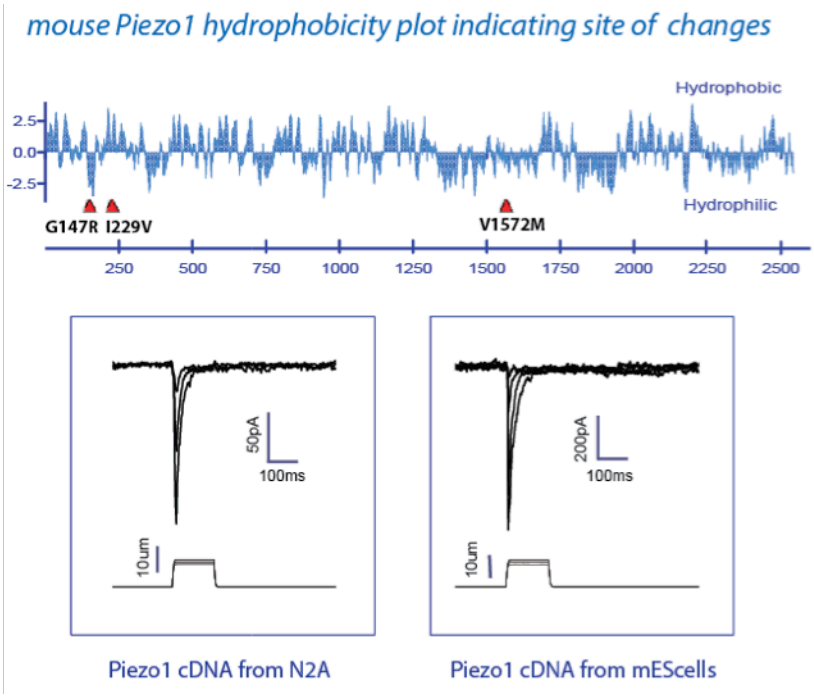

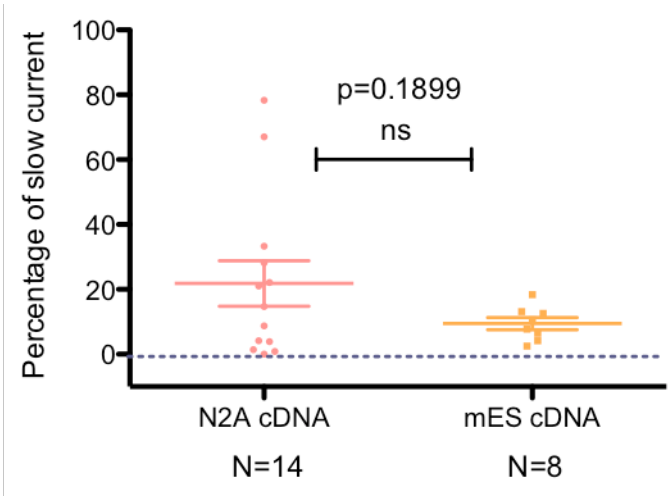

Figure 26. Piezo1 cDNA retrieved from mES cells differs in 3 positions from Piezo1 cDNA retrieved from N2A cells. Top: hydrophobicity plot of Piezo1 protein showing the positions where mutations were found. Middle: expression of both cDNAs, retrieved from N2A cells and retrieved from mES cells, in HEK293 cells shows no significant difference in the kinetics. Bottom: a quantification of the percentage of slow current from both constructs. No significant difference between both columns.

3.2.2.6. Gain of function screening of other candidate membrane proteins

In the previous sections of this chapter I described a large and slow-inactivating mechanosensitive current present in mouse embryonic stem cells elicited by direct poking of the cells. Through a *loss of function* screening I found that Piezo1 accounts for the totality of the MS current, rendering it the likely pore forming subunit of the complex responding to the poking stimulus. The knockout studies of Piezo1 were performed in parallel as a *gain of function* screening of other candidates; I will describe in the remaining sections some interesting results from those experiments.

For gain of function studies I pursued a similar method as described in the previous chapter. For each candidate, cDNA was obtained and subcloned into a mammalian expression vector for expression in CHO cells, chosen again for showing the smallest background endogenous response. It should be noted that the HEK293 cell line with a knockout of Piezo1 that I used in the previous section is a better expression system for *gain of function* studies, but I generated that cell line after these experiments were carried out. I then transfected each construct into CHO cells and studied the transfected cells' response to mechanosensitive stimulation using the 'poking' assay. Figure 27 shows the results of the screening for the first 14 candidates. Two proteins from this initial list elicited an interesting response; one of them, Plp2, with statistical significance when compared to the control CHO cells. The statistical significance of this result motivated me to study it further.

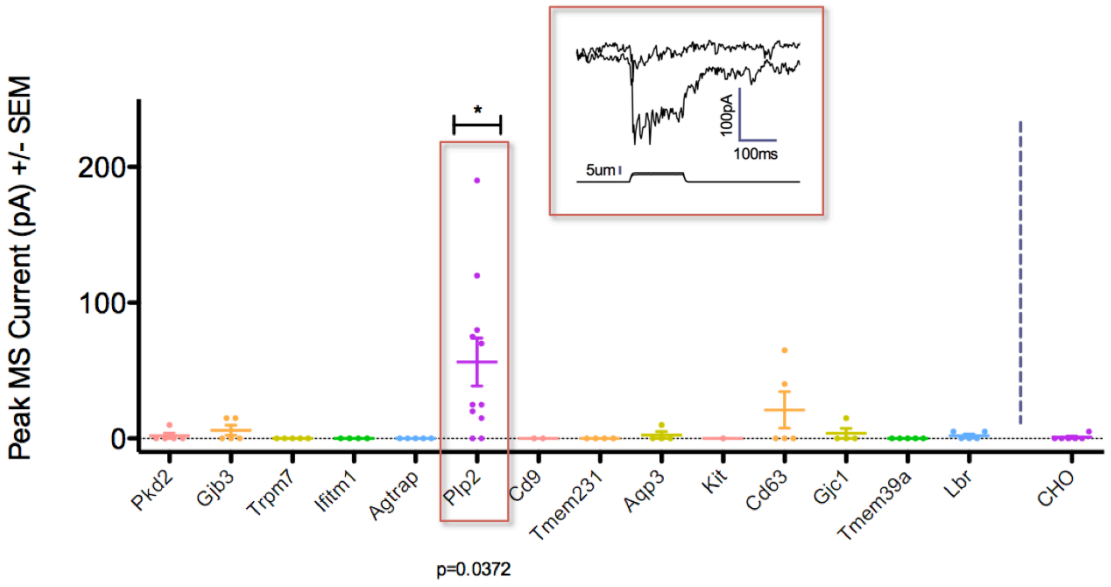

Figure 27. Screening by *gain of function* of other candidate membrane proteins. Candidate membrane proteins transfected in CHO cells and assessed by poking. Plp2 shows a significant difference with control CHO cells.

3.2.2.7. Heterologous expression of Plp2 induces a large and slow-inactivating MS current

Plp2 is a small membrane protein (17KDa) with 4 transmembrane domains and short connecting loops. Its role has been poorly studied, but it has been loosely linked to the chemotaxis response[75] and has been proposed to multimerize and form an ion channel[76]. Localization studies place it in the endoplasmic reticulum, endosomes, and the plasma membrane[75,77]. Structurally, it is part of a family of proteins named 'MARVELs' that includes occludins, physins and gyrins, and has been proposed to play a role in membrane apposition events and vesicular traffic[78].

To validate the result from the screen in CHO cells, I expanded the heterologous studies into two other expression systems, HEK293 and HCT116 cells. HEK293 cells are a human embryonic kidney cell line that has been used extensively for heterologous expression of multiple ion channels, Piezo1 and 2 included. HCT116 is a human cancer cell line that showed relatively small background mechanosensitive signal in previous experiments. Expression of Plp2 in CHO, HEK293, and HCT116 cells induces a medium-to-large and slow-inactivating mechanosensitive response to poking that is statistically significant compared to control responses (figure 28). The mechanosensitivity of CHO, HEK293, and HCT116 cells increases by ~47, 5, and 16 times, respectively when expressing Plp2. Moreover, the currents elicited by expression of Plp2 are robustly slow-inactivating. A study into the inactivation behavior using similar analytical tools as throughout this chapter shows that the Plp2-induced currents fully recapitulate the slow-inactivating currents from mouse embryonic stem cells. A detailed study shows that in HEK cells, the expression system showing the largest Plp2-induced currents, the percentage of slow-inactivating currents of Plp2-induced currents is close to 70%, significantly slower from the percentage of endogenous MS currents of the same cells. Furthermore, because the endogenous currents are rather small, I heterologously expressed Piezo1 in HEK cells and compared the inactivation behavior of the Plp2-induced currents with that of heterologously expressed Piezo1 channel in the same host cells. The Piezo1 channel expressed in HEK cells yields mechanosensitive currents of larger amplitude than Plp2-induced currents, but they are significantly faster. In summary, Plp2-induced currents are significantly slower than Piezo1-induced currents and than endogenous MS currents (figure 29).

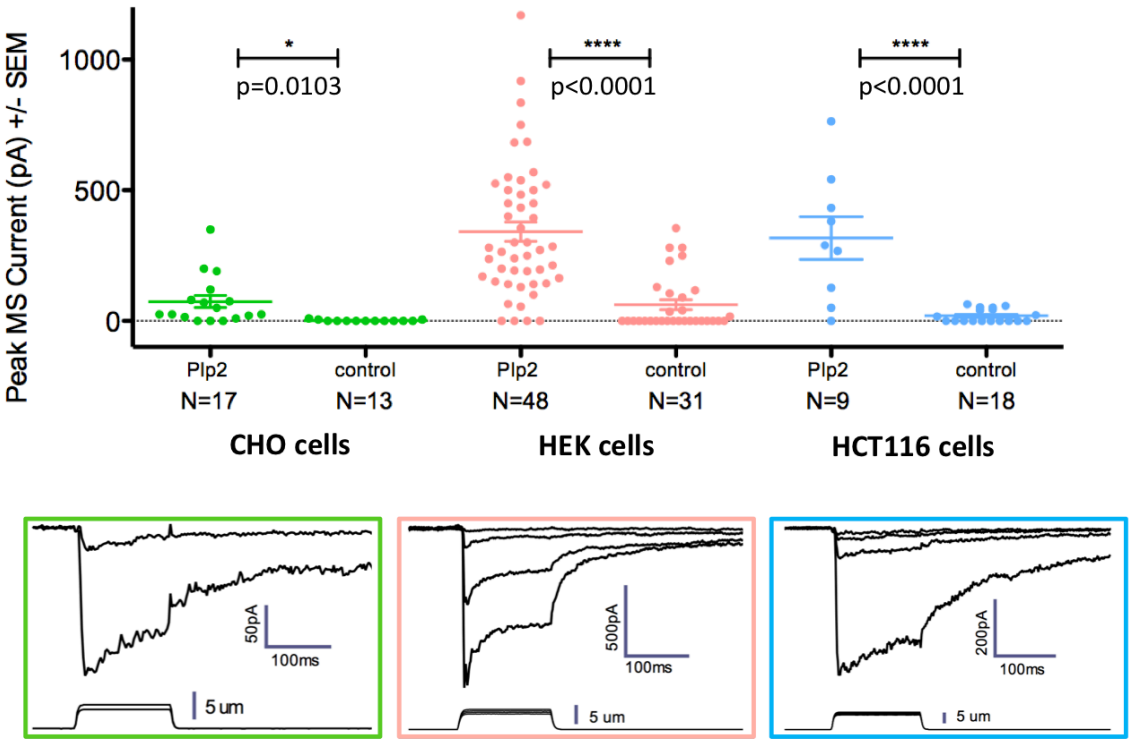

Figure 28. Plp2 induces a large and slow-inactivating poking current in mutliple heterologous expression systems. Plp2 was expressed in CHO, HEK293 and HCT116 cells and MS currents were assessed by poking. Top: maximum MS current evoked by Plp2 or endogenous in the three cells lines. Controls are either untransfected cells or cells transfected with an inert membrane protein. Bottom: examples of Plp2-evoked currents in all three systems.

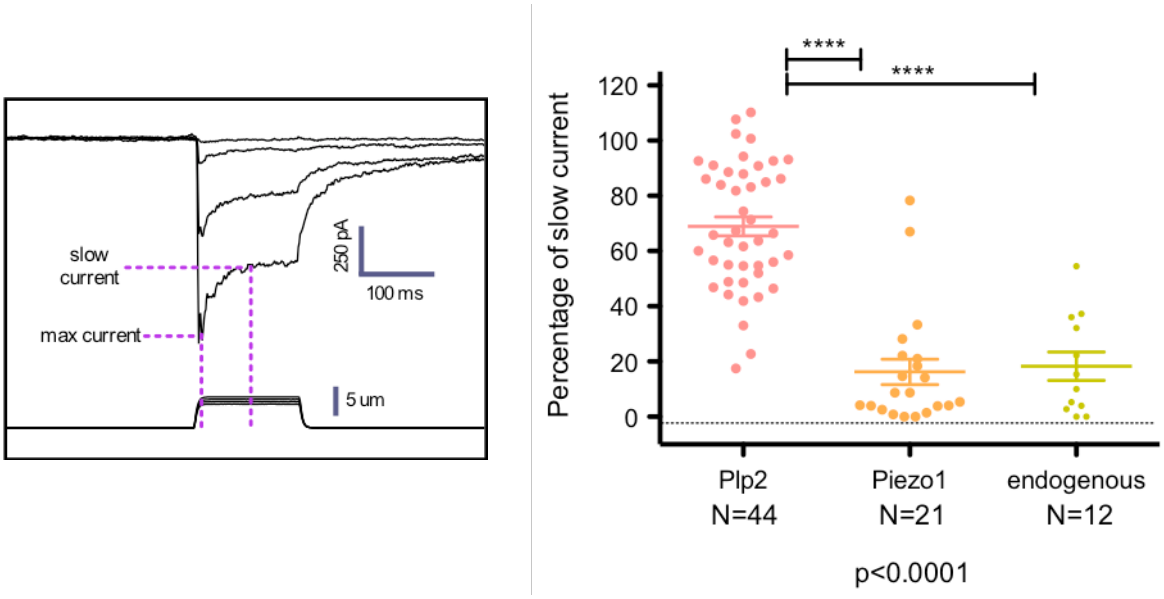

Figure 29. Inactivation behavior of Plp2-induced currents in HEK cells, compared with the endogenous currents and Piezo1-induced currents. Left: graphical visualization of the estimation of percentage of slow current as the fraction of current that remains active half-way through the poking step. Right: desensitization behavior of 3 types of poking currents were studied, HEK cells expressing Plp2 (pink), HEK cells expressing Piezo1 (orange), and endogenous MS currents in control HEK cells. Plp2-induced currents are significantly slower than either of the other.

Ion selectivity analysis of the Plp2-induced poking current shows that it is non-selective for cations (figure 30). Single channel analysis in a pressurized excised patch shows activity of channels that temporally correlates with the stimulation (figure 30). An ensemble of individual recordings shows a macroscopic current similar in behavior to that of the whole cell poking currents (figure 30). Conductance estimation by amplitude histograms gives a value of (24.93 ± 2.23) pS.

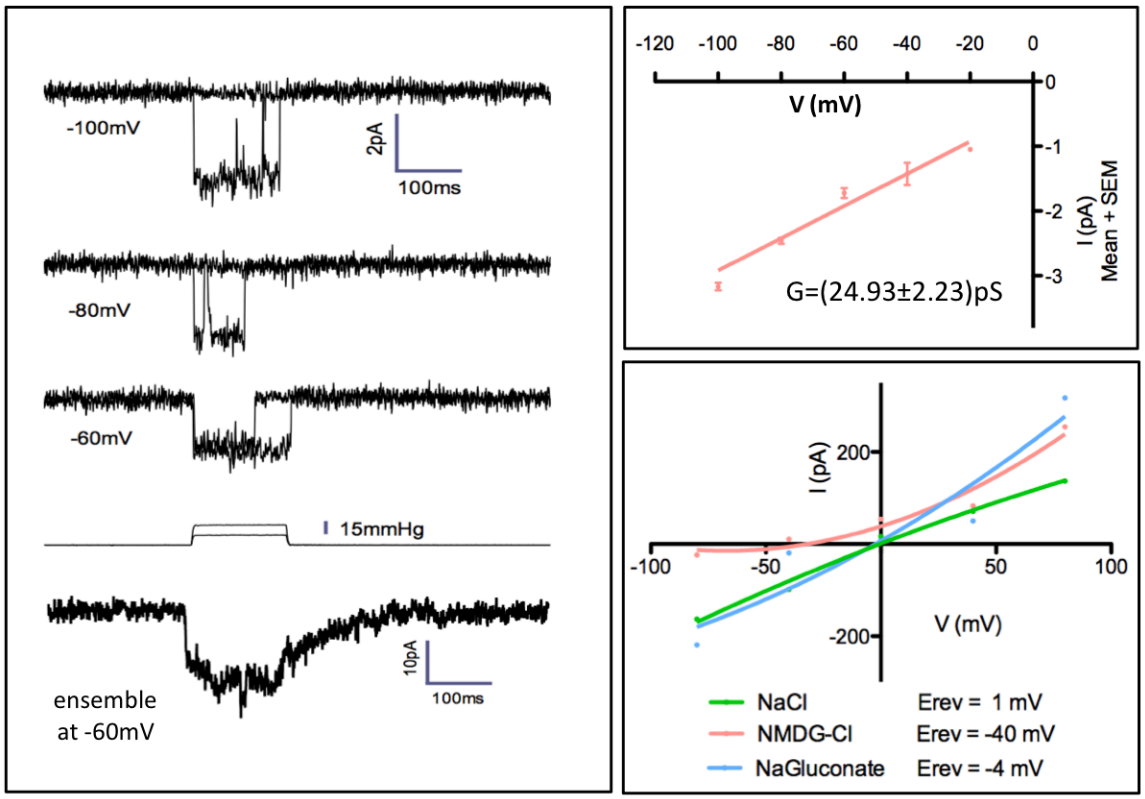

Figure 30. Selectivity and single channel analysis of Plp2-induced MS currents in HEK293 cells. Left: single channel activity evoked by pressurizing an outside-out patch of membrane expressing Plp2. Recordings at different voltages are shown. The bottom trace is an ensemble of multiple recordings at -60mV showing an apparent macroscopic current that resembles that of the whole-cell poking currents. Right, top: single channel conductance estimation from amplitude histograms at multiple voltages shows a conductance of ~25pS. Right, bottom: Selectivity studies in whole-cell mode changing bath solution (similar protocol and reasoning as used before) shows that Plp2-induced currents are cation-selective.

3.2.2.8. Knock out of Piezo1 from HEK293 cells abolishes the MS current induced by Plp2

The ion selectivity and conductance of the Plp2-induced current are highly reminiscent of those of the Piezo1 channel[21,28]. This observation, in addition to the results of the *loss of function* screening of the previous sections, motivated me to posit the possibility of Piezo1 being the pore forming subunit underlying the Plp2-induced MS currents.

To address this hypothesis Crispr technology was used to knock out PIEZO1 from HEK 293 cells. Using a similar strategy as before, I chose to minimize confounding results from off-target effects by obtaining independent knockout colonies using two different sgRNAs (figure 31). Sequence analysis of the clones confirmed homozygous IN-DEL mutations that generated early stop codons in the PIEZO1 gene for both colonies. I then heterologously expressed Plp2 in these cells and obtained no MS current, indicating that the Plp2-induced mechanosensitive current in HEK cells is indeed dependent on PIEZO1 expression (figure 31). As a control, I expressed Piezo1 in the same knockout cells, to verify that the lack of activity of Plp2 is not due to an inability of the knockout cells to express the MS current. Piezo1 expressed to normal levels in the knockout cells, therefore the lack of Plp2-induced currents can be entirely attributed to the knockout of the PIEZO1 gene.

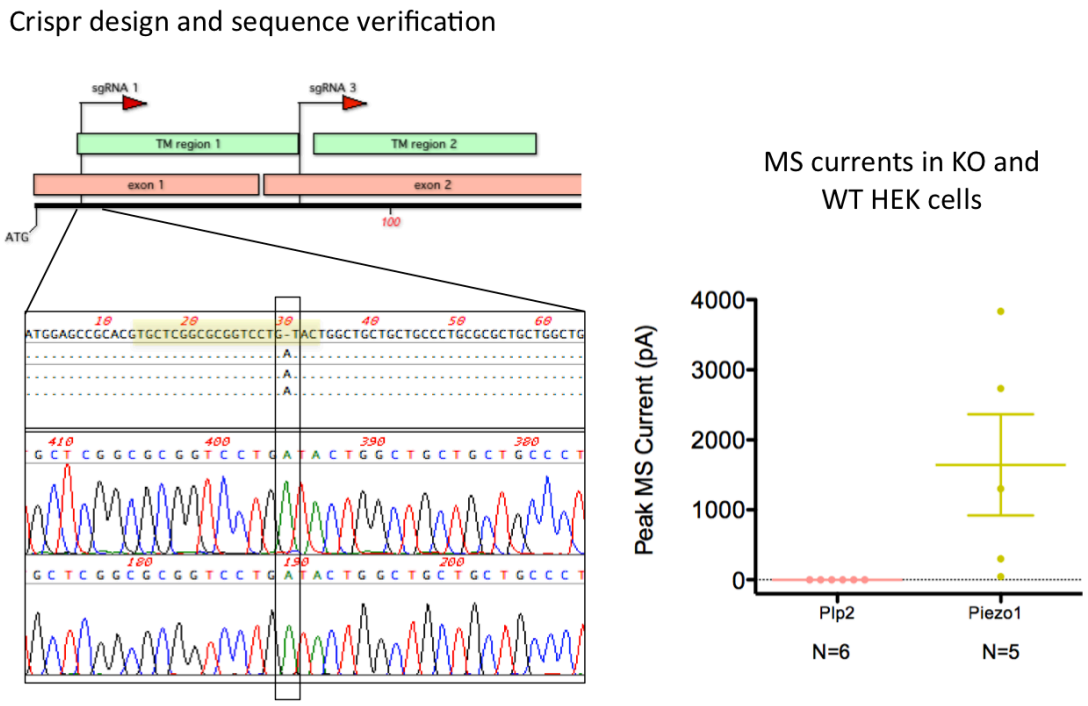

Figure 31. Knock out of PIEZO1 in HEK293 cells abolishes Plp2-induced MS currents. Left: a diagram of the beginning of the PIEZO1 mRNA in HEK cells is shown. The first 2 exons and 2 predicted transmembrane regions are marked. Two guide RNA sequences (sgRNAs) were chosen to generate a double strand break (DSB) in the beginning and end of the first TM region. Below the diagram are sequence reactions of a fragment of DNA extracted from one of the modified colonies. In yellow is marked the targeted sgRNA sequence, and boxed in black is marked the region with a one base-pair insertion that generates a frame-shift mutation, and an early stop codon shortly after. Only one sequence was obtained after sequencing with no background, indicating a homozygous mutation. Right: Plp2 transfected into PIEZO1 knock out cells showed no mechanosensitive activity. Piezo1 transfected into the same knock out cells shows large mechanosensitive currents, indicating that the cells are perfectly capable of expressing normal MS currents.

3.2.2.9. Plp2 does not form a functional ion channel in a cell-free reconstitution system

An early report on Plp2 function pointed to a possible role as ion channel[76]. To explore this possibility I decided to purify Plp2 protein and reconstitute it in a minimal system to perform cell-free electrophysiological recordings with the ability to perform mechanical stimulation. I expressed a GFP fusion tagged mouse Plp2 protein in Sf9 cells, a cell line derived from the insect *Spodoptera frugiperda* that is commonly use as a high-yield protein expression system. Using standard methods for membrane proteins I extracted Plp2 using a gentle detergent and ran it through a preparative size exclusion Superdex200 column. The protein eluted at 13.8 mL as a single peak with a small shoulder (figure 32). The purified protein eluted at a volume consistent with a monomer. To study its multimeric state I performed crosslinking on the purified protein using glutaraldehide in various concentrations from 0 to 2%. The resulting protein gel shows that Plp2 does not change its migration properties with increasing crosslinker, running always as a single band around 17kDa, the expected size of the monomer (figure 32). Finally, to study the possibility of Plp2 forming an ion channel in a cell-free system, I reconstituted the protein in soybean lipid extract removing all detergent, using different protein:lipid ratios. The resulting proteoliposomes were deposited onto glass coverslips where, through a previously described dehydration-rehydration process[26], formed unilamellar blisters that readily form gigaseal patches with a glass recording electrode and are therefore suitable for pressurized-patch recordings. I did not observe any consistent voltage-gated or pressure-induced channel activity when Plp2 was reconstituted using this method (figure 32).

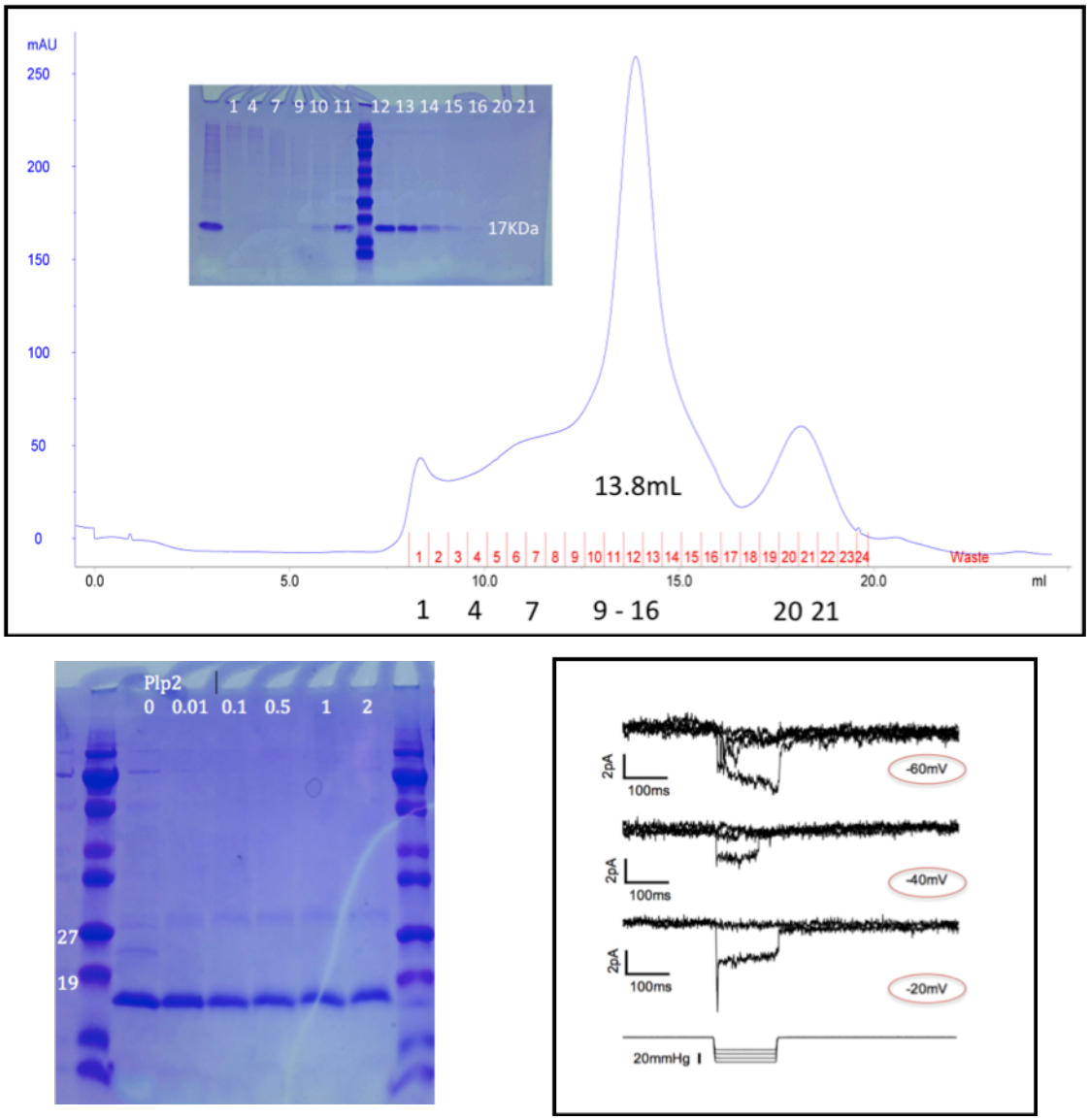

Figure 32. Mouse Plp2 purification from Sf9 cells. Top: Elution profile from a Superdex200 size exclusion column. Insert: SDS-PAGE gel of selected fractions (column input in the first lane). Fractions 11 to 14 were pooled for reconstitution. Bottom left: crosslinking study of Plp2. Glutaraldehyde from 0 to 2% was used, no multimerization evidence was found. Bottom right: examples of the very few channel-like behavior in cell-free reconstitution of Plp2, stimulated by pressure applied through the patch pipette. Most trials showed no channel behavior. The ones shown, at first sight appear channel-like, but show no consistency in conductance at different voltages, and are also sporadically seen in control protein-free vesicles.

3.2.2.10. Plp2 as a modulator of Piezo1

With no evidence for Plp2 acting as its own ion channel I decided to examine its potential modulation of Piezo1 currents. To explore this possibility, I co-expressed mouse Plp2 with mouse Piezo1 in HEK293 cells (containing a knockout of the endogenous PIEZO1) and compared the resulting poking currents with those from expression of mouse Piezo1 alone. I found that co-expression of Plp2 significantly slowed down the inactivation of Piezo1 (figure 33). Plp2 co-expression also increased the amplitude of the poking currents, but that effect is not statistically significant.

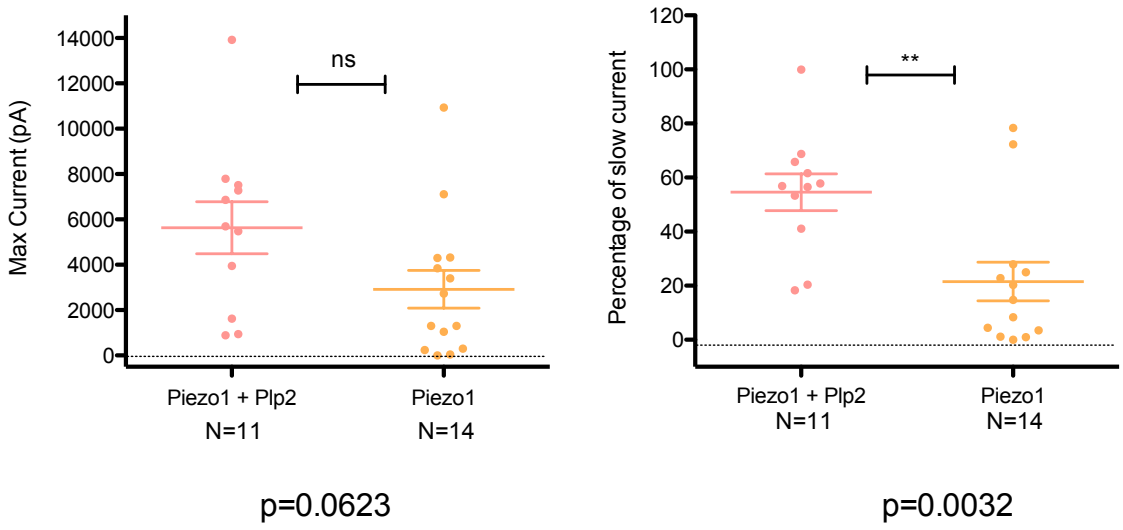

Figure 33. Co-expression of Plp2 and Piezo1 in HEK293 KO for PIEZO1. Left: maximum MS current achieved in cells tranfected with either Piezo1 + Plp2 (pink) or Piezo1 alone (orange). Right: percentage of slow current for those conditions. Plp2 slows down MS currents when co-expressed with Piezo1, with statistical significance.

Interestingly, the same experiment using CHO cells instead of HEK gives different results. In CHO cells, co-expression of Plp2 and Piezo1 significantly increases the overall MS currents, but does not produce statistically slower inactivating kinetics (figure 34). It should be noted that because both Plp2 and Piezo1 constructs were tagged with a GFP protein it is impossible to assess in these experiments the relative levels of expression of both proteins. Co-expression is generally accepted as an efficient method to deliver multiple DNA fragments to the same cell, as it is a generally observed that competent cells who accept DNA, do so from all the DNA sources available, resulting in an effective co-transfection method. However, it does not imply that both DNAs should be transcribed, and their products translated and processed with similar efficiencies, even when driven by the same promoter.

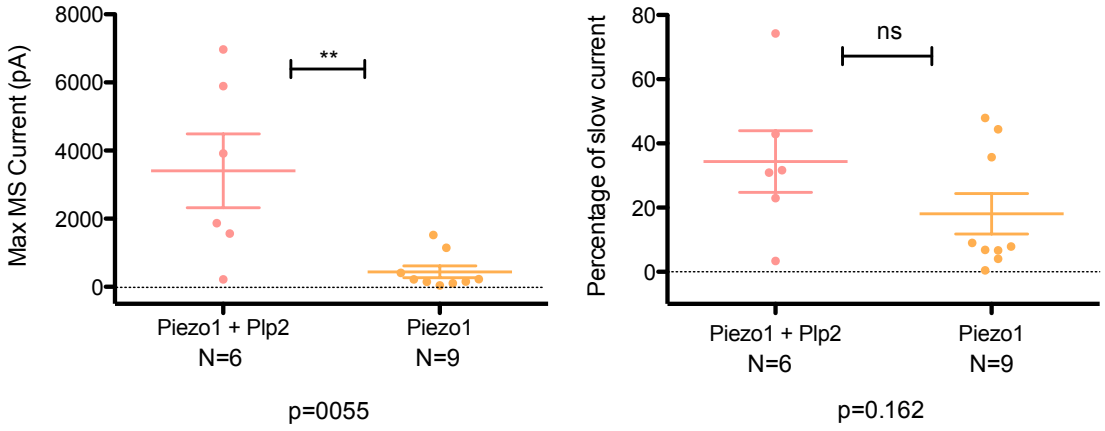

Figure 34. Co-expression of Plp2 and Piezo1 in CHO cells. Left: maximum MS current achieved in cells tranfected with either Piezo1 + Plp2 (pink) or Piezo1 alone (orange). Co-expression increases the overall maximum current significantly. Right: percentage of slow current for those conditions, no statistical significance.

3.2.2.11. Plp2 knockdown in mouse embryonic stem cells does not affect the mechanosensitive currents

A natural next step into this investigation was to knock out Plp2 from mouse embryonic stem cells and study the effect of that manipulation. Knock out was however inaccessible: the mouse Plp2 gene is very short, as is the protein, and the Cas9/Crispr potential targets in the initial region of the gene are of very low quality, meaning that the efficiency of double strand break would be very low, and the off-target effects a significant problem. As an alternative I decided to use lentiviral shRNA delivery to knock down the mRNA. I selected 2 sequences that, when introduced collectively, reached an almost complete abolishment of Plp2 mRNA levels (>99% reduction in Plp2 transcript after viral transduction). Cells were infected with the virus and then kept under Puromycin selection for 3-5 days to guarantee the study of a uniform population of knocked-down cells. I used scrambled shRNA as a negative control, submitting the control cells to the same infection and selection method. Neither the amplitude nor the desensitization kinetics of the poking currents differed in knocked down and control cells (figure 35). Aside from the lack of effect of the treatment, it should be immediately apparent that the values of slow-inactivation percentage for these cells are somewhat smaller than those provided for wild type mouse embryonic stem cells earlier in this chapter. Variability is a feature of mouse embryonic stem cells; I have found that different batches and different passage numbers can give different poking currents with no obvious rationale or correlation to any measurable factor. But in the particular case of the lentiviral infection, it is also entirely possibly that the infection and selection treatment posses challenges to the cells that generate a different homeostatic stage that

could affect gene expression. Regardless, the result is clear, complete Plp2 knockdown bears no effect on poking currents.

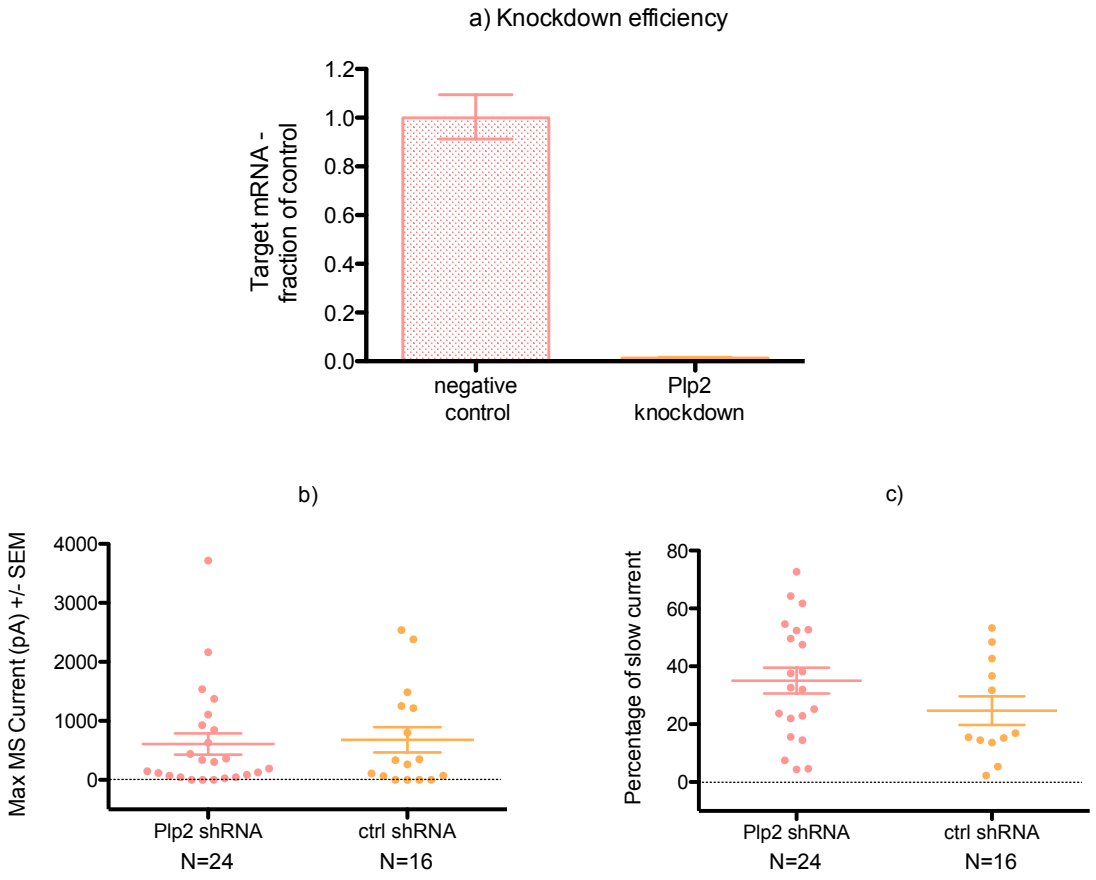

Figure 35. Knockdown of Plp2 in mouse embryonic stem cells does not affect MS currents. A) Knockdown efficiency assessed by a quantitative PCR of the mRNA levels of Plp2 in knockdown and control cells. B) Maximum MS current shows no difference between conditions. C) Percentage of slow current shows no statistically significant difference between conditions.

3.2.2.12. Study of Plp2 involvement in Piezo1 behavior

Summarizing all the result thus far, there is a clear effect of the expression of Plp2 on Piezo1 behavior, but there is no insight as to how that effect could be exerted. Having discarded the possibility of Plp2 forming an independent conductance by itself, the data supports a modulatory role of Plp2 on Piezo1. I then conducted an inquiry into some of the multiple possible ways in which Plp2 could modify Piezo1 behavior.

Retracing the ontology of a protein, the first potential effect of a modulator of Piezo1 could be over the translation rate of the PIEZO1 gene into mRNA, therefore producing overall more protein. To investigate this possibility I performed a quantitative PCR (qPCR) of PIEZO1 in wild type HEK293 cells transfected with Plp2, and compared those values to the endogenous levels of PIEZO1. It is worth remembering that expression of Plp2 on wild type HEK cells exhibits a large increase (~5 fold) of poking currents, mediated by Piezo1 (figure 28). Figure 36 shows that the levels of PIEZO1 mRNA in cells transfected with Plp2 were ~1.5 higher than the control, though statistically not significant. This increase, even if it was significant, does not account for the 5-fold increase in mechanosensitive current levels. This indicates that the amplifier effect of Plp2 on PIEZO1 currents is unlikely to occur through a boost in expression levels of the PIEZO1 gene.

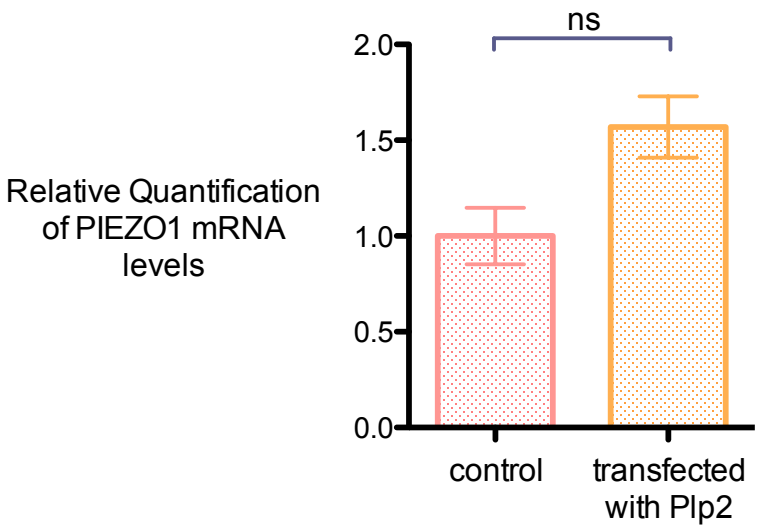

Figure 36. Transcriptional effect of Plp2 on PIEZO1 levels in HEK293 cells. HEK293 cells transfected with Plp2 increased the level of PIEZO1 mRNA by 1.5 fold, with no statistical significance.

To address how specific is the modulation of Plp2 on Piezo1 versus on other membrane proteins, I took advantage of the fact that HEK293 cells endogenously express a small amount of voltage gated (Kv) currents. I examined whether the expression of Plp2 increases the amplitude of the endogenous Kv currents as it does to the endogenous PIEZO1 currents. I found that Plp2 expression significantly increases the endogenous Kv currents by ~1.4 times, an increase that, however significant, does not match that of the endogenous PIEZO1 currents in the same cells (figure 37.a). Additionally, the increase in current level of both PIEZO1 and Kv channels could be due to an increased rate of extrusion of membrane vesicles onto the plasma membrane, modifying the total area of the cell. I therefore investigated whether Plp2 increases the overall

membrane area. A very good proxy for plasma membrane area is the cell's capacitance[61]. I measured the whole-cell capacitance of control and Plp2-expressing HEK293 cells and found no difference, indicating that Plp2 does not appear to act by increasing the membrane area of the cells (figure 37.b).

During the course of these studies I noticed that Plp2 seems to express at very high levels, as assessed by GFP expression of fusion constructs. Could Plp2 be expressed at such high levels as to modify biophysical properties of the membrane such as the elasticity? Given our ability to express and purify Plp2 protein in high yield, together with Daniel Firester, a rotation student in our lab, we addressed this question by reconstituting Plp2 into Giant Unilamellar Vesicles (GUVs) made of phosphatidylcholine (PC) and phosphatidic acid (PA) lipids in a 9:1 ratio. GUVs were investigated under brightfield microscopy while simultaneously suctioned by a non-adhesive pipette. The geometry of the portion of the GUV that enters the pipette (the 'meniscus') in addition with the measurement of the pressure applied to the pipette to suction the GUV allows us to estimate the elastic modulus of the membrane, which is the relation between the areal dilation and the tension in a linear range[79,80]. The values of this constant are similar for GUVs formed in the presence and absence of high levels of Plp2 protein, indicating that the lipid membrane's ability to dilate in response to tension is not influenced by expression of Plp2 (figure 37.c).

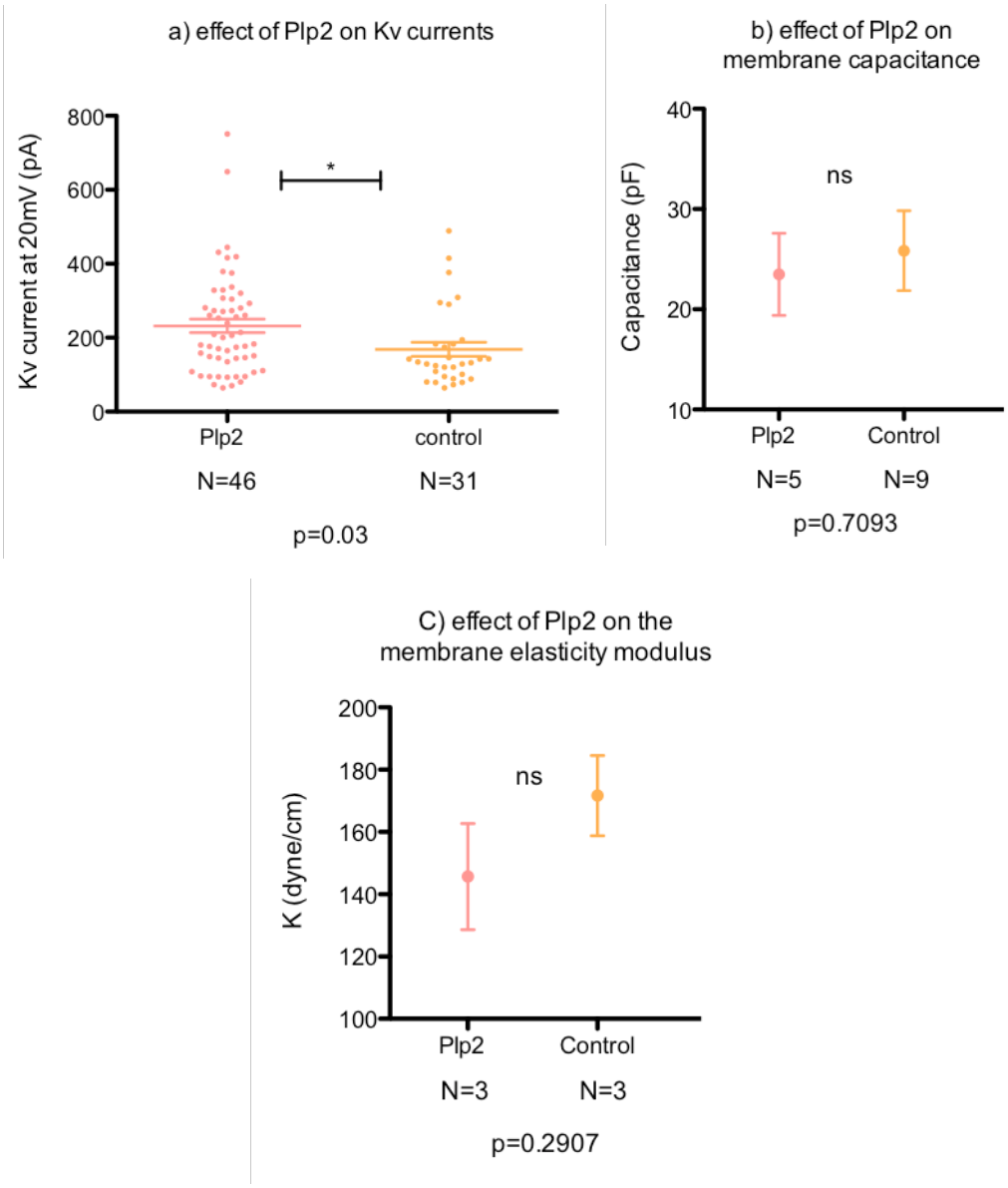

Figure 37. A) Effect of Plp2 on endogenous Kv currents. Kv current was assessed at 20mV HEK293 cells transfected with Plp2 or controls. B) Effect of Plp2 on the cells' membrane area estimated through their capacitance. Membrane capacitance was measured from HEK293 cells transfected with Plp2 or control. C) Effect of Plp2 on the membrane elasticity modulus of giant unilamellar vesicles constructed from PC:PA lipids. Vesicles were formed with a high content of Plp2 and in the absence of protein, and the vesicles ability to dilate in response to tension was estimated.

Another interesting avenue is to determine whether the expression of Plp2 modifies the activity of other mechanosensitive ion channels. Piezo2 and TRAAK are perhaps the two most conspicuous candidates for answering this question, as they both respond to poking stimulation in a very large, fast manner[26,21]. I therefore co-expressed Plp2 with the human TRAAK channel or the human PIEZO2 channel, and compared them to the recordings of the individual TRAAK or Piezo2 in the same cells. As host cells I used a HEK293 cell line knockout for PIEZO1, to abolish confounding effects from endogenous signals. Figure 38 shows the results: co-expression had no significant effect on maximum or slow-inactivating mechanosensitive current on either channel. Although the sample numbers are low, the lack of effect is readily evident.

From this series of experiments it would appear that Plp2 has a specific effect on Piezo1 in heterologous expression, but it cannot account for the slow-desensitization of Piezo1 in mouse embryonic stem cells by itself. I will briefly describe in the last section some other interesting results from the *gain of function* screening of mES cells membrane proteins that can perhaps offer some other possibilities.

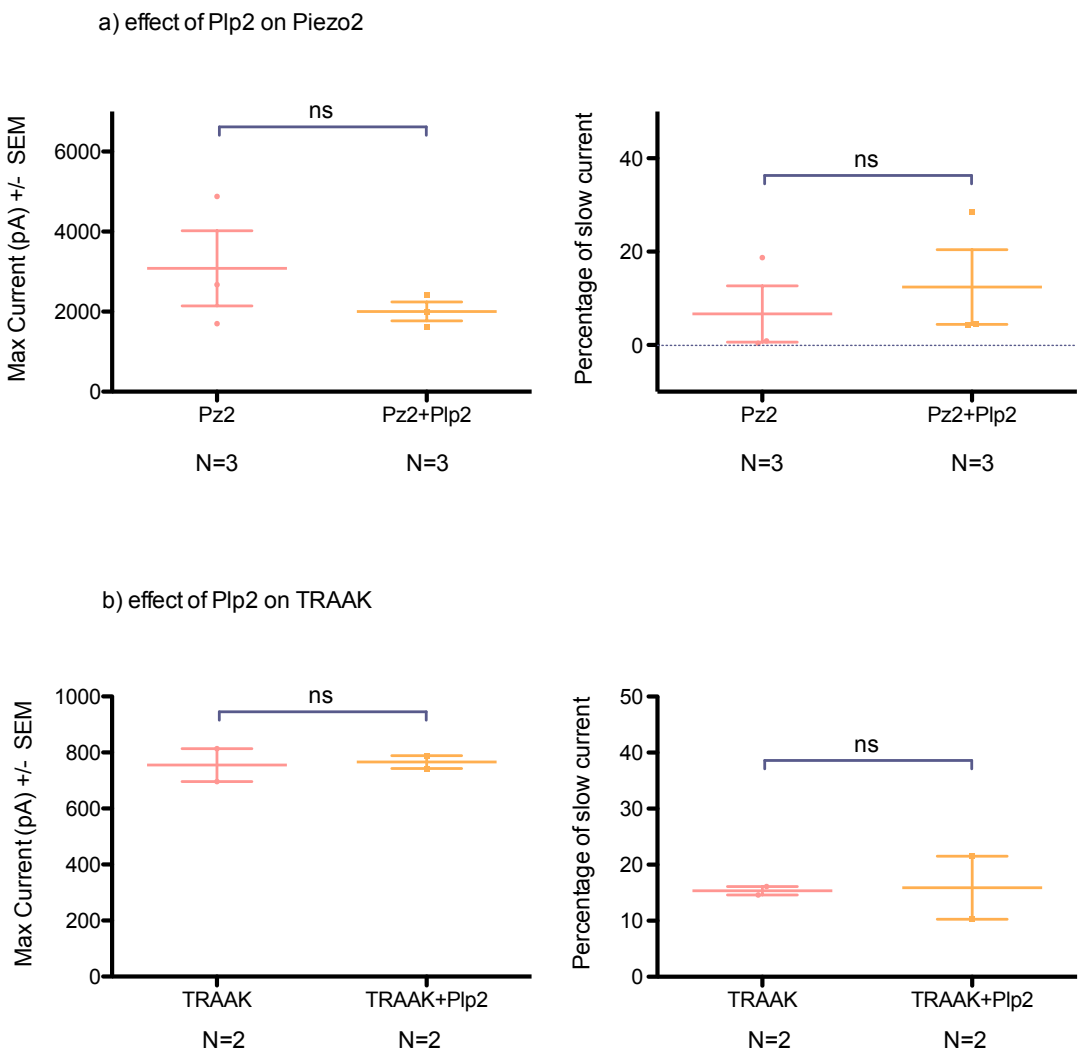

Figure 38. Effect of Plp2 on other mechanosensitive ion channels. A) Human PIEZO2 was expressed in HEK293 cells either alone or co-transfected with Plp2, maximum current and slow current were assessed. C) Similar experiment, transfecting HEK293 cells with either TRAAK alone or TRAAK + Plp2.

3.2.2.13. Cd63 expression in HEK cells induces a large and fast-inactivating MS current

In figure 2.15, the *gain of function* screening of a set of multipass membrane proteins of mouse embryonic stem cells, there is only one statistically significant hit: Plp2. But there is another protein, Cd63, whose expression in some CHO cells gives enough MS current to catch our attention. Cd63 is a four-pass membrane protein member of the tetraspanin (Tspan) family of proteins[81]. Localization reports place it as a surface antigen in the plasma membrane, in exosomes, and associated to lysosomal internal membranes[82,83]. Its function is ultimately unclear, but has multiple links to a host of biological processes such as cell adhesion, migration and spreading, intracellular vesicular processes, acting as surface receptor in signaling cascades, and platelet regulation[84]. In pathology, Cd63 has been the focus of extensive research as it has been shown to participate in the infective process by HIV-1 virus[85,86,83].

Expression of Cd63 in wild type HEK293 cells elicited a large and fast-inactivating mechanosensitive current, whose amplitude is 5.7 times larger than that of endogenous currents and whose kinetics are virtually indistinguishable from those of canonical Piezo1 (figure 39). These experiments were done in collaboration with Zhenwei Su, a postdoctoral associate in the MacKinnon lab.

Following a similar line of reasoning that guided the Plp2 experiments, we expressed Cd63 in HEK293 cells with knockout of endogenous PIEZO1 to assess whether the Cd63-induced poking current is also due to endogenous Piezo1 expression. Again, knockout of the endogenous Piezo1 gene abolished the Cd63-induced current, indicating once more that Piezo1 is the likely pore forming subunit of the mechanosensitive complex.

Because the poking currents observed in Cd63 expressing cells are fast-inactivating, I do not think this protein could account for the slow kinetics of Piezo1 in mouse embryonic stem cells. However, it does bring attention to the possibility of a multiplicity of ways of regulation of mechanosensitive ion channels that needs to be further investigated.

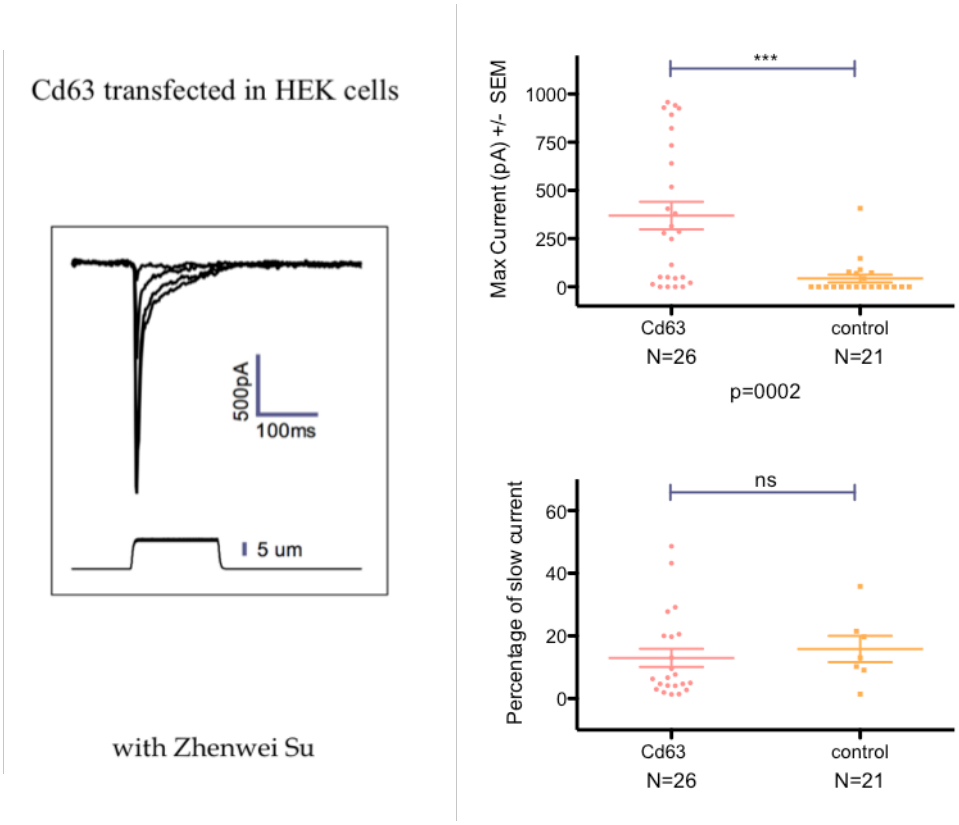

Figure 39. Effect of Cd63 on mechanosensitive currents in HEK293 cells. Cd63 transfected into HEK293 cells significantly increases the endogenous MS current (top right panel), and it looks identical to that of canonical Piezo1 currents in those cells (bottom right panel and trace).

3.3. Discussion

3.3.1. Modulation of Piezo1

One of the major contributions of this work is the determination that Piezo1 can indeed form a slow-inactivating current in physiological conditions. Having discarded the possibility of an intrinsically slower channel by sequence, we are left to assume that regulation of its kinetics can arise from either additional components (e.g. beta subunits) or from mechanical properties of the particular cellular environment, or a combination of both. We know yet very little about modulation of Piezo1 behavior. In a recent work, Bae et al demonstrated that the kinetics of human PIEZO1 can be regulated by pH[87]. Additionally, Sack's group observed that in certain conditions, a fast inactivating Piezo1 channel can be 'converted' into a slow one by repeated stimulation[68]. They postulate that Piezos could be located in confined arrays ('corrals') that can be disrupted through strenuous stimulations, and that the gating mechanism is somehow linked to these spatial arrays.

Regardless of the plausibility of the 'corral' model proposed by Sacks' group, it is conceivable that the membrane localization of ion channels can modify their behavior in multiple ways[88,89,90,91]. Channels could be positioned in membrane regions where cytoskeleton components or lipid composition favor certain kinetic behaviors[92,93,94]. Proteins like Plp2 could be aiding in the trafficking of Piezo1 towards certain regions of the cell, and therefore modifying its surface expression and localization. Alternatively, it is also possible that these proteins form direct associations with Piezo1 in the membrane, forming themselves part of the mechanotransducing complex. To shed light on the

potential mechanism of regulation of Piezo1 by small membrane proteins such as Plp2 it would be very relevant to obtain information about the associating partners of Piezo1 in a physiological environment. This would uncover whether fast-inactivating and slow-inactivating Piezo currents find themselves associating to different partners in the membrane, which could in turn help explain the difference in kinetics. I would like to emphasize the importance of assessing interaction partners in physiological contexts: as I mentioned before from data obtained by other groups and myself, there are multiple cell lines that exhibit a slow-inactivating mechanosensitive current that is attributable to Piezo1, such as mouse embryonic stem cells or mouse C2C12 cells. Interestingly, when transfected to overexpress Piezo1, these same cells exhibit large fast-inactivating currents. This change in kinetics could be understood in the context of a direct interaction between Piezo1 and other proteins or molecules in the cell, that exist at a natural ratio that is imbalanced when Piezo1 is overexpressed. For this reason, performing interaction studies of overexpressed Piezo1 can potentially miss natural interactions that exist at lower concentrations of the Piezo1 protein.

Further work should consider the current availability of fast gene-tagging techniques such as Crispr/Cas9 modification through homologous repair[74,95] as it opens the possibility of inserting tags in endogenous Piezo1 genes that can be used for pull-downs, super resolution imaging, and other necessary follow up experiments.

3.3.2. Natural variability in the Piezo currents reported by different groups

Expressing Piezo channels heterologously is a notably robust experiment. Most labs have had no trouble finding large mechanosensitive currents as the result of transfecting Piezo channels into a variety of host cells. However, a brief review of the Piezo literature shows some 'minor' differences between labs in their study of these currents. Let us take the case of the study of the inactivation kinetics of human PIEZO1 and its mutant forms that cause hereditary xerocytosis. These mutations were studied independently by the Sacks group[67] and the Patapoutian group[34]. Both groups report human PIEZO1 to have an inactivation constant of around 10ms. However, a M2225R mutant is reported to have an inactivation time constant around 35ms (Sacks group) or 13ms (Patapoutian group). Other mutants also show similar and rather large differences in both studies. These differences could be attributed to the slightly different bath solutions used by both groups, but they are accompanied by other interesting differences in other reports. For example, the Sacks group reports no endogenous mechanosensitivity in HEK293 cells[67] used as host cells. The Patapoutian group (personal communication) and our own experience indicate that at least the HEK293 strains we use have considerable endogenous activity. As another example, mouse Piezo1 inactivation constants in HEK293 cells have been consistently reported around (or below) 10ms by the Patapoutian group[21,28]. The Honoré group reports constants of around 40ms in COS and PCT cells[5].

Based off of my findings I would posit the possibility that there are unknown modulators of Piezo1 that exist at different levels in different host cell

lines and can influence the activity of these channels in ways that are still to be described.

3.3.3. Known modulators of Piezo currents

Despite the relative novelty of the discovery of Piezo proteins, a few proteins were already found to modify the behavior of Piezo both *in vivo* and *in vitro*.

One of the few described modulators of Piezo1 was identified through gene homology searches. The DEG/ENaC mechanosensory complex in worms contains a protein, MEC-2, whose mammalian counterpart is required for mechanosensation in ~40% of myelinated mechanosensory fibers[96,4,97]. This protein, named Stoml3 for Stomatin-like protein 3, is reported to tune up the threshold of sensitivity of Piezo2 currents in DRGs, such that its absence increases the threshold of activation of Piezo2 by an order of magnitude. The effect on Piezo2 is not specific: Piezo1 currents can too be increased and their thresholds lowered by expression of Stoml3. These results were reproduced in heterologous expression of Stoml3 with either Piezo1 or Piezo2 in HEK293 cells. Additionally, Stoml3 protein co-precipitates with Piezo1 or Piezo2 after heterologous expression in HEK293 cells, indicating some degree of association.

Another proposed modulator of Piezo1 currents is a protein known as PC2, for polycystin-2[5]. Overexpression of this protein reduced endogenous Piezo1 currents in PCT cells (proximal convolute tubule), and in overexpression experiments in COS cells. PC2 also co-precipitates with Piezo1 when overexpressed in COS cells.

These descriptions are yet incomplete, and as research progresses, we are likely to gain better understanding of the role of these proteins in modulating mechanosensation and fine-tuning the responses of Piezo proteins and perhaps other mechanosensory transducers.

3.3.4. Potential modulation of Piezo1 by MARVELs

Given that the complete knockdown of Plp2 in mES cells does not change Piezo1 current, it is unlikely that it will turn out to be a physiological partner of Piezo1 in those cells. However, its notably large effect on Piezo1 behavior brings the attention towards that family of proteins. As I mentioned before, Plp2 is a member of a superfamily of proteins known as MARVELs, for 'MAL-related vesicle trafficking and membrane link'[78], whose most notable members are occludin, physins, and gyrins. MAL protein, the founding member of the family, is found in polarized epithelial cells and behaves as an itinerant protein, traveling between Golgi cisterns, the plasma membrane, and endosomes continuously. Synaptophysin, synaptogyrin, and related proteins have a relatively obscure role but are known synaptic vesicle markers and have been implicated in transport processes. Occludin, another notable MARVEL protein, is the first transmembrane protein identified in tight junctions. Other MARVELs are found in tight junctions, transcellulin and marvelD3, all showing variable degrees of requirement for normal tight junction function[98,99,100].

Interestingly, there are multiple MARVEL proteins closely related to Plp2 that are expressed in mouse embryonic stem cells. Cmtm3, Cmtm4, Cmtm6 and Cmtm7, all named after 'CKLF-like MARVEL transmembrane domain containing

X', share 24~30% homology with Plp2 (with the exception of Cmtm7, which shares very little homology) and are expressed in mouse embryonic stem cells. Other than very obscure links between some of these proteins and functions such as 'cancer inhibiting', their physiological roles are entirely unknow[101,102,103,104]. It remains a possibility that some of these interact with or modify the activity of Piezo1 in mouse embryonic stem cells. The knockout of all of them is beyond the scope of this work, but it would be interesting to analyze whether a pull-down study of endogenous Piezo1 brings out 4TM proteins of the like.

In figure 2.12. I show that expression of the Piezo1 channel in mES cells temporally correlates with that of the fast component of the MS current in those cells. In fact, whereas total mechanosensitive current decreases during the course of the differentiation, Piezo1 expression actually peaks on an intermediate stage. In light of the knowledge that Piezo1 is responsible for the totality of the MS current in at least mES cells, we are now left to assume that there is another reason why the evolution of the MS current does not mimic that of the Piezo1 channel. One possibility is that there are other proteins, perhaps accessory subunits or components of the MS complex, which can both amplify and slow-down the kinetics of Piezo1 channel. I show in this work that Plp2 can in fact do both. And although Plp2 is not the protein that exerts that effect in mES cells, as proved by the knockdown of Plp2 in mES cells, it can certainly serve as an interesting proof of principle.

3.3.5. Are Piezo proteins mechanosensitive ion channels?

A very *out of the box* thinker might conclude that perhaps Plp2 and/or other proteins form the actually pore of a mechanotransducing complex, and Piezo proteins might actually be necessary to bring out or sensitize cells to mechanical stimulation (perhaps as tethers to the cytoskeleton or somehow aiding in the gating process). In fact, we have yet to see minimal reconstitution of purified Piezos to confirm their activity as mechanosensory ion channels. However, a few pieces of evidence strongly support the idea of Piezos themselves being mechanosensitive ion channels. In the first place, Piezo1 proteins have reportedly been shown to form MS conductances in every single cell line in which they have been expressed. Of course, we can always invoke a silent MS channel being present in all those cell lines, but the evidence does not stop there. A report by the Patapoutian group shows that the drosophila Piezo channel (dmPiezo) and the mammalian Piezo1 channel, when expressed in HEK293 cells heterologously, can both form a mechanosensory conductance[28]. Importantly, the two proteins form two different ion channels: mammalian Piezo1 forms a channel with a conductance of 29pS, whereas dmPiezo forms a channel with a conductance of 3.3pS. These results very strongly support the idea that the Piezo proteins actually form the pore, as it is highly unlikely that a protein that merely modulates the activity of an ion channel will have such an influence in its pore properties. It is therefore almost certain that Piezo proteins actually form the pore of the mechanosensory complex. Whether the ability to transduce mechanical stimulation resides in the same protein as well needs further experiments.

3.3.6. Notable results from the screening in cancer cell lines

Despite not having had significant hits in the initial screen in cancer cell lines, the two proteins that showed the highest responses when expressed in CHO cells bear certain relevance. LHFP (lipoma HMGIC fusion partner protein) is a fourpass transmembrane protein that is closely related to LHFPL5, also known as TMHS, or tetraspan membrane protein of hair cell stereocillia[105,106,107,108,18]. This protein is expressed in hair cells of the cochlea and has been proposed to be an integral component of the elusive hair cell mechanotransducing channel, as its deficiency causes deafness. This sensory loss is attributable to an almost complete loss of mechanotransducing currents in hair cells, indicating that TMHS' point of action is in the transduction machinery. Although the role of TMHS in mechanotransduction remains unclear, evidence suggests that TMHS regulates the surface expression of protocadherin PCDH15, a component of the tip links, and can physically associate with TMC1, another integral component of the mechanotransducer channel. Interestingly, a recent report shows that at least some of the effects of the knockout of TMHS could be due to a down regulation of surface expression of TMC1, as knockout of TMHS results in reduced TMC1 labeling in the stereocillia.

TSPAN4, the other interesting hit of the cancer cells screening, is also a 4TM protein member of the tetraspanin family, whose function and activity is entirely unknown. The Tspan family contains 33 members and is abundantly present in all cell types examined[109,110,111,112,113]. It has been proposed to form microdomains in the plasma membrane, sometimes referred to as 'tspan webs' or 'tetraspanin enriched microdomains, TEM', which interact with other membrane

components and cytoskeleton components such as integrins and claudins. Information on tetraspanin function shows a remarkably disperse set of phenomena. Evidence suggests tetraspanins can associate with receptors and influence receptor-binding signaling cascades. They are also linked to cell-adhesion processes, including adhesion to other cells or to pathogen. It is interesting to note that Cd63, the second hit from the stem cell screening, is also a member of the TSPAN family of proteins.

In summary, in the quest to find slow-inactivating mechanosensitive ion channels I encountered 4 interesting proteins: Plp2, Cd63, TSPAN4 and LHFP. All are 4TM membrane proteins somehow linked to either vesicle trafficking processes or membrane microdomains, suggesting an important potential regulation of Piezo1 currents by either the physical association to other membrane proteins or its membrane apposition.

4. Conclusions and Future Directions

Despite not having found the original source of modulation of Piezo1 currents in mouse embryonic stem cells, we found two proteins that distinctively modify the behavior of Piezo1 channels, *in vitro*. Whether this modulation is part of an in vivo system remains to be explored. Given the lack of data on *in vivo* interaction and/or modulation between Plp2 and Piezos, it remains a possibility that the results described are due to an aberrant effect of overexpressing Plp2. However, the fact that these effects seem particularly large and specific on Piezo1 activity does support the hypothesis that Piezo1 is susceptible to modulation by Plp2 as well as other similar proteins.

An immediate experiment that should be pursued is the assessment of interaction between Piezo1 and Plp2 or other related 4TM membrane proteins in an endogenous model. An example would be to use Crispr/Cas9 technology to insert a tag in the Piezo1 gene in mouse embryonic stem cells and perform co-immunoprecipitation studies without overexpressing any proteins. Further identification of precipitation partners through mass spectroscopy could shed light on potential novel partners of Piezo1 in vivo.

These results along with evidence from other groups bring attention to the organization of the cellular machinery of mechanosensitivity. It is foreseeable that for a sensory system highly dependent on positional cues, such as mechanosensation, the relative arrangement of channels, accessory proteins and lipids would be of particular relevance. The recent advent of multiple reports noting the superior complexity of mechanosensory processes and molecules[114,115,116], such as the case of the hearing transduction channel[106,108]„ or

the Piezo2-Stoml3 complex in DRG neurons[4], highlights the need for further investigating the roles of accessory subunits.

Lastly, it is a fact that there are likely other unknown mechanosensory ion channels. The Patapoutian group reported that only the fast-inactivating component of the mechanosensory currents in DRG neurons can be attributable to Piezo2[21]. Piezo1 is not supposedly expressed in those cells, so we are left to assume that there is still at least one novel source of slow- and/or intermediate-inactivating mechanosensitive currents present in DRGs. A most fascinating challenge in the field will be to identify the source of that current and unveil the mechanisms behind its behavior and function.

5. Methods

All poking experiments were performed using a probe drawn from borosilicate glass (Sutter Instruments) fire polished (MF-83, Narishige Co.) until sealed. The probe was mounted to piezo-driven actuator driven by a controller/amplifier (P-601/E-625; Physik Instrumente) controlled through Clampex software. After formation of a whole-cell seal by a different electrode, the probe was positioned at 60° to the cell ~2 μm away from the membrane.

All pressure applications through patch pipettes were performed with a high-speed pressure clamp (ALA Scientific) controlled through the Clampex software. Pressure application velocity was set to the maximum rate of 8.3 mmHg/msec.

HEK293 tsA201 cells were obtained from Sigma and maintained in DMEM (Gibco) supplemented with 10% Fetal Bovine Serum (Gibco) and 1% L-Glutamine (Gibco). CHO-K1 cells were obtained from ATCC and maintained in DMEM/F12 (Gibco) supplemented with 10% Fetal Bovine Serum (Gibco) and 1% L-Glutamine (Gibco).

5.1. Kv Paddle Chimaera

Kv Paddle Chimaera bacculovirus was used to infect Sf9 cells 1-2 days prior to recordings. The isoosmotic extracellular solution contained (mM): 100 NaCl, 10 KCl, 4 CaCl2, 5 MgCl2, 10 Glucose and 80 Sorbitol and MES-NaOH pH 6.4. The hypoosmotic extracellular solution lacked Sorbitol. The intracellular solution contained (mM): 85 KCl, 60 KF, 1 MgCl2, 5 EGTA, 10 Glucose and 20 HEPES-KOH pH 7.2. The grounding electrode was separated from the perfused chamber and connected through a salt bridge of low resistance. Perfusion was achieved

using a custom-built gravity perfusion system. Cells were patched in whole-cell mode while perfusing with isoosmotic solution.

For poking experiments Sf9 cells infected with Paddle Chimaera were patched in whole-cell mode with no perfusion. Extracellular and intracellular solutions same as for swelling (isoosmotic).

Electrodes were drawn from borosilicate patch glass (Sutter Instruments) and polished (MF-83, Narishige Co.) to a resistance of 0.8–1.5 MOhms. Analog signals were filtered (1 kHz) using the built-in 4-pole Bessel filter of an Axopatch 200B patch clamp amplifier (Molecular Devices) in patch-mode and digitized at 10 kHz (Digidata 1440A, Molecular Devices).

5.2. Nav1.7

HEK293 cells stably expressing full-length human Nav1.7 were obtained as a gift from Bruce Bean's laboratory. For electrophysiology recordings, the isoosmotic extracellular solution contained (mM): 100NaCl, 5KCl, 1MgCl2, 10Glucose, 10Hepes-Na, 100Mannitol (pH7.3, 320mOsm/kg). The hypoosmotic extracellular solution lacked mannitol (220mOsm/kg). The intracellular solution contained (mM): 160CsCl, 10EGTA, 1EDTA, 10Hepes-K (pH7.3, 310mOsm/kg). Cells were placed on isoosmotic solution and patched using standard whole-cell technique. Perfusion of hypo and isoosmotic solutions was achieved using a local microperfusion system (ALA Scientific).

For poking experiments isoosmotic extracellular and intracellular solutions were used.

Patch inflation was carried in the on-cell mode using isoosmotic bath solution. Electrodes were drawn from borosilicate patch glass (Sutter Instruments) and

polished (MF-83, Narishige Co.) to a resistance of 2.5-4 MOhms. Analog signals were filtered (1 kHz) using the built-in 4-pole Bessel filter of an Axopatch 200B patch clamp amplifier (Molecular Devices) in patch-mode and digitized at 10 kHz (Digidata 1440A, Molecular Devices).

5.3. Calcium channels

Constructs were obtained as a gift from Diane Lipscombe's lab. Mouse Cav1.2 (GenBank #AY728090) from brain tissue, rat Cav1.3 (GenBank #AF370009) from superior cervical ganglia, rat Cav$\alpha_2\delta$-1 (GenBank #AF286488) from superior cervical ganglia and rat Cavβ_3 (GenBank #M88751) from brain were all in pcDNA vectors for mammalian expression. Cav1.2 or Cav1.3 were co-transfected into HEK293 cells with Cavβ_3, Cav$\alpha_2\delta$-1 and a GFP-expressing plasmid in 1:1:1:0.1 molar ratio. Lipofectamine 2000 (Invitrogene) or FugeneHD (Promega) were used for transfection. Cells were studied 24 hours after transfection.

Swelling experiments: The isoosmotic extracellular solution contained (mM): 100NaCl, 5KCl, 1MgCl2, 10Glucose, 10Hepes-NaOH, 90Mannitol, 5BaCl2 or 2CaCl2 (pH7.3, 320-330mOsm/kg). The hypoosmotic extracellular solution lacked mannitol (220mOsm/kg). The intracellular solution contained (mM): 135CsCl, 10EGTA, 1EDTA, 10Hepes-KOH (pH7.3, 310mOsm/kg). Cells were placed on isoosmotic solution and patched using perforated patch technique, using 240ug/ml Amphotericin B in the intracellular solution to achieve whole cell access. Perfusion of hypo and isoosmotic solutions was achieved using a local microperfusion system (ALA Scientific).

Electrodes were drawn from borosilicate patch glass (Sutter Instruments) and polished (MF-83, Narishige Co.) to a resistance of 2.5-4 MOhms. Analog signals were filtered (1 kHz) using the built-in 4-pole Bessel filter of an Axopatch 200B patch clamp amplifier (Molecular Devices) in patch-mode and digitized at 10 kHz (Digidata 1440A, Molecular Devices).

Stretching experiments: stretcher was custom-built using a stage (Newport #9066COM), a 6-axis controller (Newport #8766NF) and 2 picomotor actuators (Newport #8301NF). Elastic membranes pre-coated with collagen were obtained from Flexcell Inc. and pre-cut to fit the stretcher stage. Cells were plated directly onto the pre-cut membranes and transfected with the relevant constructs 24-36 hours before imaging. The day of imaging, membranes were loaded onto the stage of the stretcher and clamped. Cells were then loaded with 2uM Fura-2 (Molecular Probes) for 20 minutes and washed with PBS, and placed in bath solution containing (mM): 100NaCl, 5KCl, 10Glucose, 10Hepes-Na, 1MgCl2, 2CaCl2, 100Mannitol (pH 7.3, 320mOsm/kg). Stretching was applied bi-axially using a home-built LabView interface. Stretching was done in consecutive intervals of 3-5 seconds followed each by 5-15 seconds of re-focusing. All imaging was performed with a Nikon Ti-E microscope. When indicated, 10uM Nimodipine (Sigma) was used to block calcium channel activity.

5.4. Cancer cell lines

All cell lines were obtained from the Tavazoie lab except from HT1197, obtained from ATCC, and C2C12, obtained from the Brivanlou lab. Cells were kept in the following media: MDAMB231 in DMEM, 10%FBS, 1%L-Glutamine, 1% Sodium Pyruvate, 1%PenStrep, 0.4%Fungizone. MCF7 in DMEM, 10%FBS, 1%L-

Glutamine, 1% Sodium Pyruvate, 1%PenStrep, 0.4%Fungizone, 0.01mg/ml Insulin. SKOV3 and HCT116 in McCoy's 5a, 10%FBS, 1%L-Glutamine, 1%PenStrep, 0.4%Fungizone. SKMEL2, SKMEL28, and ACHN in EMEM, 10%FBS, 1%L-Glutamine, 1%Pen Strep, 0.4%Fungizone. 786-O in RPMI, 10%FBS, 1%L-Glutamine, 1%PenStrep, 0.4%Fungizone. C2C12 in DMEM, 10%FBS, 1% L-Gln, 1%PenStrep.

Cells were dissociated and plated on tissue culture treated 35mm plastic petri dishes (Corning) 24-72 hours before electrophysiological studies.

Extracellular solution for electrophysiology experiments (mM): 150NaCl, 3KCl, 1MgCl2, 2.5CaCl2, 10Hepes-Na, 10Glucose (pH7.3, 310mOsm/kg). Intracellular solution (mM): 115KGluconate, 30KCl, 10NaCl, 10Hepes-K, 5EGTA, 1EDTA or 150KCl, 2MgCl2, 10Hepes-K, 5EGTA (pH7.3, 310mOsm/kg).

Electrodes were drawn from borosilicate patch glass (Sutter Instruments) and polished (MF-83, Narishige Co.) to a resistance of 2.5-4 MOhms. Analog signals were filtered (1 kHz) using the built-in 4-pole Bessel filter of an Axopatch 200B patch clamp amplifier (Molecular Devices) in patch-mode and digitized at 10 kHz (Digidata 1440A, Molecular Devices).

For transcriptome analysis the NCI-60 panel was used (NCBI DataSet Record GDS4296, Series GSE32474) in which multiple human cancer cell lines are analyzed by expression profiling by array (Affymetrix U133 Plus 2.0). *Ensembl* BioMart Data Base was used to retrieve a list of human membrane proteins. The Center for Biological Sequence Analysis Server (cbs.dtu.dk) was used to run a TransMembrane Hidden Markov Model (TMHMM) algorithm to obtain the number of predicted transmembrane domains.

cDNA of candidate membrane proteins was obtained from Harvard Medical School Plasmid Repository and Dharmacon. Each cDNA was cloned into pIRES-EGFP vector (Clontech) using In-Fusion cloning technique and reagents (Clontech). Transfection was performed using Lipofectamine 2000 (Invitrogen) or FugeneHD (Promega).

Electrophysiology screening of candidate membrane proteins expressed in CHO-K1 cells was performed using extracellular solution (mM): 150NaCl, 2MgCl2, 3KCl, 2CaCl2, 10HepesNa, 10Glucose (pH 7.4, 325mOsm/kg) and intracellular solution (mM): 150KCl, 10EGTA, 10Hepes, 2MgCl2 (pH 7.4, 310mOsm/kg).

5.5. Embryonic stem cells

5.5.1 Human embryonic stem cells

On the first day of the differnentiation, human embryonic stem cells (RUES2 hESC line) were passaged into N2B27 media[70] supplemented with 20uM Y27632 (RhoK inhibitor, Stem Cell Technologies), 10uM SB431542 (ALK inhibitor, Sigma) and 0.2uM LDN193189 (ALK inhibitor, Sigma). On day 2, 10uM retinoic acid (RI) 10uM was spiked into the cultures. Embryonic bodies (EBs) were collected on day 2 with serological pipet and resuspended in N2B27 media supplemented with SB and LDN but without RI. Cells were fed every two days for ~8 days. On day 10 cells' media was supplemented with brain-derived neurotrophic factor (BDNF, R&D Systems), ascorbic acid (AA, Sigma) and cAMP (Sigma) while removing SB and LDN. Cultures were fed every 2 days. On days 12-22 cultures require FGF pathway activation for efficient specification of cortical layers, therefore 5-50ug/ml FGF-8 (Life Technologies) and 20nG FGF-2 (Life

Technologies) were added to the feeding media. On days 25-40 insulin like growth factor (IGF1, R&D Systems) was supplemented to the media for supporting differentiation into layer VI cortical neurons and N2 and B27 concentrations were increased to 1x. For terminal differentiation, day 40 and onwards, media is switched to Neurobasal (Gibco) supplemented with L-Glutamine (Gibco), NS21 (Miltenyi), N2 (Gibco), BME (Sigma), E, BDNF (R&D Systems, cilliary neurotrophic factor (CNTF, R&D Systems), IGF1 (R&D Systems), db-cAMP (Sigma), glutamate (Gibco), laminin (Invitrogen) and fed every 4 days. Cells were dissociated and plated on poly-ornithine (Sigma) and laminin (Invitrogen) coated dishes for electrophysiological recordings on days 0 (human embryonic stem cells), 12-25 (neuroepithelial cells) and ~40 (cortical layer VI neurons).

For electrophysiology, cells were recorded using standard whole-cell patch techniques and extracellular solution (mM): 150NaCl, 3KCl, 1MgCl2, 2.5CaCl2, 10Hepes, 10Glucose (pH7.3, 320mOsm/kg); and intracellular solution (mM): 115KGluconate, 30KCl, 10NaCl, 10HepesNa, 5EGTA, 1EDTA, 4MgATP (pH7.4, 300mOsm/kg). Current clamp recordings were performed on the I-fast mode.

Electrodes were drawn from borosilicate patch glass (Sutter Instruments) and polished (MF-83, Narishige Co.) to a resistance of 2.5-4 MOhms. Analog signals were filtered (1 kHz) using the built-in 4-pole Bessel filter of an Axopatch 200B patch clamp amplifier (Molecular Devices) in patch-mode and digitized at 10 kHz (Digidata 1440A, Molecular Devices).

5.5.2. Mouse embryonic stem cells

Mouse embryonic stem cells (Hb9-GFP) were obtained from the Wichterle lab (Wichterle et al, Cell 2002). This cell line contains a GFP transgene driven by the Hb9 promoter, a motor neuron specific promoter. Cells were kept in serum-free 2i + LIF media[117]. Cells were passaged every 2-3 days. For electrophysiological recordings of mouse embryonic stem cells, cells were plated on 12mm poly-D-lysine coated coverslips (NeuVitro), pre-coated with Matrigel (Invitrogen). Cells were plated ~6 hours before recording. In general I observed that cells become very flat 24 hours after plating, which makes poking very difficult. I found that the best poking currents were observed ~4-10 hours after plating the cells. Because mouse embryonic stem cells normally grow forming tight associations called embryonic bodies that impede patch clamp procedures, in order to facilitate electrophysiological recordings, cells were dissociated to single-cell level using Accutase (Gibco) or Trypsin (Gibco) and plated at low density (2,000 to 25,000 cells per 12mm coverslip) in the presence of Rho-K inhibitor (Millipore), an inhibitor of apoptotic pathways that are triggered when cells are plated at low densities. For electrophysiological recordings of Day 5 and Day 7 cells, coverslips were coated with PDL and Laminin EHS.

For differentiating mouse embryonic stem cells into motor neurons we followed protocols by the Wichterle lab[73], but replacing Sonic Hedgehog by SAG (smoothened agonist). Apparition around day 5 of GFP-positive neurons signals a successful maturation of motor neurons. The differentiation was performed 3 times and each time electrophysiological recordings were carried. The results of all 3 differentiations were pooled together.

Electrophysiology: whole-cell recordings during the differentiation were performed using extracellular solution (mM): 150NaCl, 2MgCl2, 3KCl, 2CaCl2, 10HepesNa, 10Glucose (pH 7.4, 325mOsm/kg) and intracellular solution (mM): 150KCl, 10EGTA, 10Hepes, 1EDTA (pH 7.4, 310mOsm/kg). Electrodes were drawn from borosilicate patch glass (Sutter Instruments) and polished (MF-83, Narishige Co.) to a resistance of 3-6 MOhms. Analog signals were filtered (1 kHz) using the built-in 4-pole Bessel filter of an Axopatch 200B patch clamp amplifier (Molecular Devices) in patch-mode and digitized at 20 kHz (Digidata 1440A, Molecular Devices).

For single channel study of MS channel in mouse embryonic stem cells the following solutions were used (mM): Pipette: 150KCl, 10Hepes-Na, 10EGTA-Na (pH7.3, 310mOsm/kg). Bath: 150NaCl, 3KCl, 2CaCl2, 2MgCl2, 10Hepes-Na, 10Glucose (pH7.3, 310mOsm/kg). All recordings were done in excised outside-out mode. Analog signals were filtered (1 kHz) using the built-in 4-pole Bessel filter of an Axopatch 200B patch clamp amplifier (Molecular Devices) in patch-mode and digitized at 20 kHz (Digidata 1440A, Molecular Devices).

For ion selectivity study of MS channel in mouse embryonic stem cells the following solutions were used (mM): Intracellular; 150KCl, 10Hepes-Na, 10EGTA-Na (pH7.3, 310mOsm/kg). Extracellular NaCl; 150NaCl, 10Hepes-Na, 10Glucose (pH7.3, 310mOsm/kg). Extracellular NaGluconate; 152NaGluconate, 10Hepes-Na, 10Glucose (pH 7.3, 310mOsm/kg). Extracellular NMDG-Cl; 152NMDG-Cl, 10Hepes-K, 10Glucose (pH7.3, 310mOsm/kg). Extracellular CaCl2; 90CaCl2, 7.5Hepes-Na, 7.5Glucose (pH7.4, 310mOsm/kg).

Transcriptome analysis during the differentiation: total RNA was extracted at days 0 (mouse embryonic stem cells), 2, 3, 4, 5, and 7 (motor neurons) of each

differentiation using a Trizol/RNeasy hybrid protocol. Briefly, cells are homogeneized using a recommended volume of Trizol (Invitrogen), chloroform is added in the recommended volume and the mix is shook vigorously. After centrifugation to allow phase separation, the aqueous phase is kept and mixed with 70% ethanol 1:1. The protocol follows using an RNeasy column (QIAGEN) and following the manufacture's instructions. For days 5 and 7 a step was added previous RNA extraction: cells were sorted using a BDFACSAria Cell Sorter (BD) to isolate only the GFP-positive fraction, therefore enriching the sample in motor neurons. GFP-positive cells were sorted into Trizol LS (Invitrogen) and extraction of RNA proceeded as before.

High throughput RNA sequencing was done in triplicates except for days 5 and 7, which were done in duplicate. Each duplicate or triplicate sample was obtained from an independent differentiation. The RNA samples were first treated with DNase, then one library per sample was prepared using Illumina's TruSeq RNA Sample Prep Kit, where polyA-fragments were selected, followed by cDNA synthesis and ligation of amplification and sequencing adapters. Libraries were then individually barcoded and then pooled with 6 libraries per lane on an Illumina HiSeq 2500 instrument (Illumina). All samples were sequenced as single-read with read lengths of 50bp. For analysis of RNA-seq data, reads were uploaded to the Galaxy environment (usegalaxy.org) and were curated and trimmed according to the quality of the sequences using default options. Curated sequences were ran through Tophat for Illumina using a built-in reference genome mm10 (GRCm38/mm10) for mapping the reads to the mouse genome. Sequences were then ran through the Cufflinks package which assembles transcripts and estimates their abundances to obtain, for each sample,

a list of transcripts with their associated transcript counts. Transcript counts are obtained as FPKMs (fragments per kilobase of transcript per million mapped reads), a normalized quantification in which each transcript's FPKM is relatively proportional to the abundance of that particular transcript in the sample. Finally, Cufflinks (CuffDiff) was used to calculate differential expression of transcripts between samples. The list of differentially expressed transcripts between day 0 and day 7 was then filtered for multi-pass membrane proteins using similar procedures as described in the previous section (cancer cell lines).

Knockout of Piezo1 in mES cells using Crispr: px459 (Addgene) was used to express Cas9 and guide RNA sequence along with a Puromycin resistence cassette. Two guide RNA sequences were cloned separately to obtain 2 independent knock-out colonies. Sequences were ACGCTTCAATGCTCTCTCGC and AGAGAGCATTGAAGCGTAAC, both located in the beginning of the second exon of the mouse Piezo1 gene. hB9-GFP mES cells were then transfected with the pX459 vector using Lipofectamine 2000 (Invitrogen) and selected with 1uG/ml Puromycin for 1 day. Single colonies were isolated, expanded, and DNA was extracted using QuickExtract DNA Extraction solution (Epicentre). A 500bp region containing the Cas9 target was amplified by PCR using the following primers: CGTGTGCATCCACGTATGA and AGGTGTGCACTGAAGGAACC. Obtained fragment was then sequenced. Sequencing results showed that some colonies contained a mix of 2 sequences, indicating differential mutations in both alleles of the Piezo1 gene. However, 4 colonies showed a clear single sequence, indicating a homozygous mutation near the PAM sequence. I selected 2 colonies for further studies.

Cloning of Piezo1 cDNA from mouse embryonic stem cells: total RNA was extracted from mES cells using RNeasy kit (QIAGEN) and cDNA was made using Quantitect Reverse Kit (QIAGEN). The following primers were used in various combinations to obtain PCR fragments that cover the entire coding region of the mouse Piezo1 gene: TGCACTACTTCCACAGACCG, CAGGAAGATGAGCTTGGCGT, CTACTCCCTCTCACGTGTCCA, TCTACTG GCTGTTGCTGCC, CCAGCAACACAATGACCAGC, ATGGAGCCGCACGT GCTG, GATGCTGCCCCAGCCGTGGG, GGCCTGCCTCATCTGGACGG, AGC AGTTGGGCGACCTGGGC, TGCCCGCCCAGGCTGTGTGC, AGCCCAGCTC GTGCTGTGGG, CACGGTAGACGGGCTGACGC, CGGCGCTATGAGAACAA GCC, CGACCGTGCCCTCTACCTGC, GGAGTATACTAATGAGAAGC, AGG GACGCTGTGTCCCTACC, TACTGGATCTATGTGTGCGC, CATACCAGGTCA CACAGGTC, TCCTCCTGATGCTCAAGCAGAGG, CTAGGTCCAGCAGCC GGTCAG, CTCACTCCATCATGTTCGAGG. PCRs were done using Phusion HF (NEB) or Pfu Ultra II (Agilent). For some difficult reactions 5% DMSO was added to the PCR reaction. The Piezo1 construct from N2A cells was obtained from the Patapoutian lab. For whole cell poking of both constructs transfected into HEK293 cells the following solutions were used (mM): 150 KCl, 10 Hepes-NaOH, 10 EGTA-NaOH (pH 7.3, 310mOsm/kg; intracellular) and 150 NaCl, 3 KCl, 2 CaCl2, 2 MgCl2, 10 Hepes-NaOH, 10 Glucose (pH 7.3, 310mOsm/kg; extracellular).

Gain of function screening of candidate membrane proteins: cDNA of candidate membrane proteins was obtained from Harvard Medical School Plasmid Repository and Dharmacon. Each cDNA was cloned into pIRES-EGFP vector (Clontech) using In-Fusion cloning technique and reagents (Clontech).

Transfection was performed using Lipofectamine 2000 (invitrogen) or FugeneHD (Promega).

Electrophysiology screening of candidate membrane proteins expressed in CHO-K1 cells was performed in whole cell mode using extracellular solution (mM): 150NaCl, 2MgCl2, 3KCl, 2CaCl2, 10HepesNa, 10Glucose (pH 7.4, 325mOsm/kg) and intracellular solution (mM): 150KCl, 10EGTA, 10Hepes-Na, 1EDTA-Na (pH 7.4, 310mOsm/kg).

The cDNA sequence of the two relevant hits from the screening is:

Plp2:

ATGGCGGATTCTGAGCGTCTCTCGGCCCCCGGCTGCTGGTTAGCCTGCAC
CAGCTTCTCGCGCACCAAAAAGGGAATTCTCCTGTTTGCTGAGATTATAC
TGTGCCTGGTGATCTTGATTTGCTTCAGTGCATCTACAACATCGGCCTACT
CCTCCCTGTCGGTGATTGAGATGATCTGTGCTGCTGTCTTACTTGTCTTCTA
CACGTGTGACCTGCACTCCAAGATATCATTCATCAACTGGCCTTGGACTG
ACTTCTTCAGATCCCTCATAGCAACCATCCTGTACCTGATCACCTCCATTG
TTGTCCTTGTAGAAGGAAGAGGCAGCTCCAGAGTTGTCGCTGGGATACTG
GGCTTACTTGCTACGTTGCTCTTTGGCTACGATGCATACATCACCTTCCCT
CTAAAGCAGCAAAGACATACAGCAGCTCCCACTGACCCCACTGATGGCC
CGTGA

Cd63:

ATGGCGGTGGAAGGAGGAATGAAGTGTGTCAAGTTTTTGCTCTACGTTCT
CCTGCTGGCCTTCTGCGCCTGTGCAGTGGGATTGATCGCCATTGGTGTAGC
GGTTCAGGTTGTCTTGAAGCAGGCCATTACCCATGAGACTACTGCTGGCT
CGCTGTTGCCTGTGGTCATCATTGCAGTGGGTGCCTTCCTCTTCCTGGTGG
CCTTTGTGGGCTGCTGTGGGGCCTGCAAGGAGAACTACTGTCTCATGATT

ACATTTGCCATCTTCCTGTCTCTTATCATGCTTGTGGAGGTGGCTGTGGCC
ATTGCTGGCTATGTGTTTAGAGACCAGGTGAAGTCAGAGTTTAATAAAAG
CTTCCAGCAGCAGATGCAGAATTACCTTAAAGACAACAAAACAGCCACT
ATTTTGGACAAATTGCAGAAAGAAAATAACTGCTGTGGAGCTTCTAACTA
CACAGACTGGGAAAACATCCCCGGCATGGCCAAGGACAGAGTCCCCGAT
TCTTGCTGCATCAACATAACTGTGGGCTGTGGGAATGATTTCAAGGAATC
CACTATCCATACCCAGGGCTGCGTGGAGACTATAGCAATATGGCTAAGG
AAGAACATACTGCTGGTGGCTGCAGCGGCCCTGGGCATTGCTTTTGTGGA
GGTCTTGGGAATTATCTTCTCCTGCTGTCTGGTGAAGAGTATTCGAAGTGG
CTATGAAGTAATGTAG

Ion selectivity study of Plp2-induced currents in HEK293 cells were carried in the following solutions (mM): Intracellular; 150KCl, 10Hepes-Na, 10EGTA-Na (pH7.3, 310mOsm/kg). Extracellular NaCl; 150NaCl, 10Hepes-Na, 10Glucose (pH7.3, 310mOsm/kg). Extracellular NaGluconate; 152NaGluconate, 10Hepes-Na, 10Glucose (pH 7.3, 310mOsm/kg). Extracellular NMDG-Cl; 152NMDG-Cl, 10Hepes-K, 10Glucose (pH7.3, 310mOsm/kg).

Single channel study of Plp2-induced currents in HEK293 cells were carried in excised patches in outside-out configuration in the following solutions (mM): bath, 150NaCl, 5KCl, 1MgCl2, 10Hepes-Na, 10Glucose (pH7.4, 310mOsm/kg); pipette, 150KCl, 1EGTA-K, 0.5MgCl2, 10Hepes-K, 10Glucose (pH7.4, 305mOsm/kg). Analog signals were filtered (1 kHz) using the built-in 4-pole Bessel filter of an Axopatch 200B patch clamp amplifier (Molecular Devices) in patch-mode and digitized at 10 kHz (Digidata 1440A, Molecular Devices).

For knockout of human Piezo1 in HEK293 cells using Crispr: px459 (Addgene) was used to express Cas9 and guide RNA sequence along with a Puromycin

resistence cassette. Two guide RNA sequences were cloned separately to obtain 2 independent knockout colonies. Sequences were TGCTCGGCGCGGTCC TGTAC and CCGCTTCAGCGGACTCTCGC, located in the beginning of the first and second exons of the human Piezo1 gene. HEK293 cells were then transfected with the pX459 vector using Lipofectamine 2000 (Invitrogen) and selected with 5ug/ml Puromycin for 2 days. Single cells were isolated, expanded, and DNA was extracted using QuickExtract DNA Extraction solution (Epicentre). A 500bp region containing the Cas9 target was amplified by PCR using the following primers: AGAAAGATGGGTCAAAACCCCAG and AAAGCTGTACGAAT TTTGGCCC for exon 2 and GTCGCCTGAGCGAGCG and AGAGAAAAAGAGATTCGTGCTCC for exon 1. The obtained fragment was then sequenced. Sequencing results showed that some colonies contained a mix of 2 sequences, indicating differential mutations in both alleles of the Piezo1 gene. However, 2 colonies showed a clear single sequence, indicating a homozygous mutation near the PAM sequence.

Plp2 purification and reconstitution: Plp2 protein was obtained as a C-terminal PreScission protease-cleavable EGFP-10× His fusion protein from Sf9 cells. Plp2 protein was extracted from frozen Sf9 cells expressing the construct using 50mM Hepes-KOH, 150mM KCl, 60mM dodecyl-β-D-maltoside (Affymetrix), 0.1 mg/mL DNase 1, 1 μg/mL pepstatin, 1 μg/mL leupeptin, 1μg/mL aprotinin, 10 μg/mL soy trypsin inhibitor, 1 mM benzamidine, and 1 mM phenylmethysulfonyl fluoride (added immediately before use) at a ratio of 1 g cell pellet/4 mL lysis buffer. The soluble fraction (containing the solubilized membrane proteins) was washed using 50mM Hepes-KOH, 150mM KCl and 6mM dodecyl-β-D-maltoside. GFP-nanobody resin was added to the supernatant

(2 mL resin slurry/1 uG bound protein) and stirred gently for 2 h at 4C. PreScission protease (~1:50 wt:wt) was added to the elution and incubated overnight at 4C with gentle rocking. Supernatant containing the cleaved protein was collected and concentrated using a 10kDa molecular weight cutoff (MWCO). Concentrated protein was applied to a Superdex 200 column (GE Healthcare) equilibrated in size exclusion chromatography (SEC) buffer containing 20 mM Hepes-KOH, 150 mM KCl, 1 mM EDTA, 1mM dodecyl-β-D-maltopyranoside. Pure Plp2 from selected fractions was concentrated (10 kDa MWCO) to 1.5 mg/mL for reconstitution. Samples were analyzed by SDS/PAGE gels (Bio-Rad) and stained by Coomassie blue. Reconstitution of Plp2 into multi lamellar vesicles was performed following protocol in Brohawn, Su, and Mackinnon, PNAS 2014.

Crosslinking was performed using Glutaraldehide (Sigma-Aldrich) 0.01% to 2%, incubated with purified Plp2 for 15 minutes at room temperature. 1M Tris pH8 was added 1:10 and incubated 15 minutes at room temperature to stop the reaction.

Co-expression of Plp2 and Piezo1 in HEK293 cells was carried using Lipofectamine 2000 (Invitrogen) and various ratios of Plp2 to Piezo1 DNA, or individual constructs alone. HEK293 cells were previously knocked out for the endogenous Piezo1 gene as described above. Whole cell poking recordings were carried using the following solutions (mM): extracellular, 150 NaCl, 3 KCl, 2 CaCl2, 2 MgCl2, 10 Hepes-NaOH, 10 Glucose (pH 7.3, 310mOsm/kg); intracellular, 150 KCl, 10 Hepes-NaOH, 10 EGTA-NaOH (pH 7.3, 310mOsm/kg).

Knockdown of Plp2 in mouse embryonic stem cells: shRNA lentivirus was generated by cloning the relevant oligos into the pLKO.1 plasmid (Addgene #8453) using AgeI and EcoRI sites; and transfecting HEK293 cells with the pLKO.1 vector containing the shRNA sequences along with a packaging plasmid (Addgene #12259) and an envelope plasmid (Addgene #12268). Target sequences were CCATTGAAAGTGCTTATGGTA, CCTGGTGATCTTGATTTGCTT, CCTGTCGGTGATTGAGATGAT, CTCCAAGATATCATTCATCAA and CCTCATAGCAACCATCCTGTA. Scramble shRNA (Addgene #1864) was used as control. The media containing viral particles was collected 3 and 4 days after transfection. Mouse embryonic stem cells were infected with the viral particles and selected in 1uG/ml puromycin for 3 days. On the fourth day, total RNA was extracted using RNeasy Kit (QIAGEN) and 200ng of each sample were used to make a cDNA library using Quantitect Reverse Transcription Kit (QIAGEN). cDNA was diluted 1:5 and a real-time PCR (or qPCR) was set up for each sample testing the levels of mouse Plp2 and mouse GADPH enzyme. Real-time Taqman PCR assays for mouse Plp2 (assay ID: Mm02342686_g1) and mouse GADPH as control (assay ID: Mm99999915_g1) with a FAM reporter dye and universal TaqMan Master Mix II with UNG (cat#4440042) were purchased from Life Technologies. The reaction was ran in triplicates using 3uL cDNA per well in a QuantStudio 12K Flex instrument (Applied Biosystems). Analysis was done using the comparative Ct method (ΔΔCT), where ΔΔCT = ((CT (target gene) -CT (reference gene)) - (CT (calibrator) - CT (reference gene)). The target gene was mouse Plp2, the reference gene was mouse GAPDH and the calibrator was the control scrambled shRNA sequences condition.

Whole-cell poking was done 6 days after infection using solutions (mM): extracellular, 150 NaCl, 3 KCl, 2 CaCl2, 2 MgCl2, 10 Hepes-NaOH, 10 Glucose (pH 7.3, 310mOsm/kg); intracellular, 150 KCl, 10 Hepes-NaOH, 10 EGTA-NaOH (pH 7.3, 310mOsm/kg).

Transcriptional effect of Plp2 on PIEZO1 mRNA level in HEK293 cells: HEK293 cells were transfected with Plp2 or mock transfected using Lipofectamine 2000 (Invitrogen). 72 hours later RNA was extracted using RNeasy Kit (QIAGEN) and 200ng of each sample were used to make a cDNA library using Quantitect Reverse Transcription Kit (QIAGEN). cDNA was diluted 1:5 and a real-time PCR (or qPCR) was set up for each sample testing the levels of human Piezo1 and human GADPH enzyme. Real-time Taqman PCR assays for human Piezo1 (assay ID: Hs00207230_m1) and human GADPH as control (assay ID: Hs03929097_g1) with a FAM reporter dye and universal TaqMan Master Mix II with UNG (cat#4440042) were purchased from Life Technologies. The reaction was ran in triplicates using 3uL cDNA per well in a QuantStudio 12K Flex instrument (Applied Biosystems). Analysis was done using the comparative Ct method ($\Delta\Delta$CT), where $\Delta\Delta CT = ((CT\ (target\ gene) - CT\ (reference\ gene)) - (CT\ (calibrator) - CT\ (reference\ gene))$. The target gene was human Piezo1, the reference gene was human GAPDH and the calibrator was the control mock transfected condition.

Effect of Plp2 the membrane elasticity modulus: Plp2 was reconstituted into proteoliposomes according to the following procedure: pre-dried phosphatidylcholine (PC, Avanti Polar Lipids) and phosphatidic acid (PA, Avanti Polar Lipids) in a 9:1 ratio were redisolved in pentane and dried again. Reconstitution buffer was used to rehydrate, 20mg/ml final lipid concentration

used. Reconstitution buffer was 20mM Hepes-K pH7.4, 150mM KCl, 1mM EDTA-K, 5mM DTT. Lipid solution was sonicated, and DM was added until 10mM final concentration. Protein was added for a final 1:100 w/w protein to lipid ratio. Solution was dialized to remove detergent at 4C for 1 day against reconstitution buffer. Dialazed proteoliposomes were treated with activated BioBeads SM-2. Supernatant was frash frozen and stored at -80C until use. Plp2 was purified as above with a few modifications: cobalt resin (Clontech) was used instead of GFP-nanobody resin in order to retain the GFP epitope. To elute the protein from the cobalt resin, increasing amounts of imidazole pH8 were used (10mM, 30mM, 300mM). The procedure used for electroformation of GUVs closely mirrored that of Girard et al[118]: proteoliposomes in buffer (20mM Hepes-K, 150mM KCl, 1mM EDTA-K, 5mM DTT) were diluted into DDI water and deposited in 2 uL droplets on ITO coated glass slides (Sigma Aldrich). The slides were subsequently dried overnight over saturated NaCl solution. Electroformation chambers were prepared using FastWells (Sigma Aldrich) filled with electroformation buffer (400 mM sucrose, 2 mM Hepes-Tris), and were sealed from above with a second ITO glass slide. A sinusoidal AC field was applied to the chamber using a pulse generator in the following sequence: 20 V/m at 10Hz for 45 minutes; 36 V/m at 10 Hz for 90 minutes; 48 V/m at 4Hz for 60 minutes. Formed GUVs were diluted into slightly hypertonic KCl solution for examination under DIC microscopy. Measurement of elastic modulus was conducted using standard procedures[119]. A height adjustable monometer allowed for precise control of pressure inside an aspiration pipette with tip radius 1-10 uM. Pipettes under slightly negative pressure were brought into close

proximity to the GUV until the GUV became aspirated into the pipette. Varying pressure adjusted the length of cylindrical projection of the GUV into the pipette. Stills were captured after step changes in pressure for further image analysis. Image analysis was preformed using custom designed software in IgorPro (WaveMetrics). Briefly, the aspirated edge of the GUV was determined to subpixel resolution through iterative intensity profile fitting under convex continuity assumptions. The elastic modulus of the membrane was found by as described by Evan Evans[120], namely, as the ratio of membrane tension change to areal change.

Effect of Plp2 on TRAAK and Piezo2: HEK293 cells containing a knockout of Piezo1 were used as host cells. Lipofectamine 2000 (Invitrogen) was used for transfection. Human TRAAK with a C-terminal truncation and fused to GFP (Brohawn et al, Science 2012; Brohawn et al, PNAS 2014) was used. Full length human Piezo2 was obtained from (X). For whole cell poking recordings the following solutions were used (mM): extracellular, 150NaCl, 1CaCl2, 1MgCl2, 10Hepes-Na, 10Glucose (pH7.4, 325mOsm/kg); intracellular, 150KCl, 10EGTA, 1MgCl2, 10Hepes-Na, 10Glucose (pH7.4, 325mOsm/kg).

References

1. Corey, D. P. & Hudspeth, a J. Response latency of vertebrate hair cells. *Biophys. J.* **26,** 499–506 (1979).
2. Schmidt, D. & MacKinnon, R. Voltage-dependent K+ channel gating and voltage sensor toxin sensitivity depend on the mechanical state of the lipid membrane. *Proc. Natl. Acad. Sci. U. S. A.* **105,** 19276–81 (2008).
3. Schmidt, D., Del Mármol, J. & Mackinnon, R. Mechanistic basis for low threshold mechanosensitivity in voltage-dependent K+ channels. *Proc. Natl. Acad. Sci. U. S. A.* **109,** 10352–7 (2012).
4. Poole, K., Herget, R., Lapatsina, L., Ngo, H.-D. & Lewin, G. R. Tuning Piezo ion channels to detect molecular-scale movements relevant for fine touch. *Nat. Commun.* **5,** 3520 (2014).
5. Peyronnet, R. *et al.* Piezo1-dependent stretch-activated channels are inhibited by Polycystin-2 in renal tubular epithelial cells. *EMBO Rep.* **14,** 1143–8 (2013).
6. Bagriantsev, S. N., Gracheva, E. O. & Gallagher, P. G. Piezo Proteins: Regulators of Mechanosensation and Other Cellular Processes. *J. Biol. Chem.* **289,** 31673–31681 (2014).
7. Ranade, S. S. *et al.* Piezo2 is the major transducer of mechanical forces for touch sensation in mice. *Nature* (2014). doi:10.1038/nature13980
8. Kim, S. E., Coste, B., Chadha, A., Cook, B. & Patapoutian, A. The role of Drosophila Piezo in mechanical nociception. *Nature* **483,** 209–12 (2012).
9. Pathak, M. M. *et al.* Stretch-activated ion channel Piezo1 directs lineage choice in human neural stem cells. *Proc. Natl. Acad. Sci.* **111,** (2014).

10. Lumpkin, E. a, Marshall, K. L. & Nelson, A. M. The cell biology of touch. *J. Cell Biol.* **191,** 237–48 (2010).
11. Kung, C. A possible unifying principle for mechanosensation. *Nature* **436,** 647–54 (2005).
12. Sukharev, S. I., Blount, P., Martinac, B., Blattner, F. R. & Kung, C. A large-conductance mechanosensitive channel in E. coli encoded by mscL alone. *Nature* **368,** 265–268 (1994).
13. Penn, R. D. & Hagins, W. a. Kinetics of the photocurrent of retinal rods. *Biophys. J.* **12,** 1073–94 (1972).
14. Cruickshank, C. C., Minchin, R. F., Le Dain, A. C. & Martinac, B. Estimation of the pore size of the large-conductance mechanosensitive ion channel of Escherichia coli. *Biophys. J.* **73,** 1925–31 (1997).
15. Häse, C. C., Le Dain, A. C. & Martinac, B. Purification and functional reconstitution of the recombinant large mechanosensitive ion channel (MscL) of Escherichia coli. *Journal of Biological Chemistry* **270,** 18329–18334 (1995).
16. Bautista, D. M. & Lumpkin, E. a. Perspectives on: information and coding in mammalian sensory physiology: probing mammalian touch transduction. *J. Gen. Physiol.* **138,** 291–301 (2011).
17. Chalfie, M. Neurosensory mechanotransduction. *Nat. Rev. Mol. Cell Biol.* **10,** 44–52 (2009).
18. Ranade, S. S., Syeda, R. & Patapoutian, A. Mechanically activated ion channels. *Neuron* **87,** 1162–1179 (2015).
19. Bhattacharya, M. R. C. *et al.* Radial stretch reveals distinct populations of mechanosensitive mammalian somatosensory neurons. *Proc. Natl. Acad.*

Sci. U. S. A. **105,** 20015–20 (2008).

20. Pfister, B. J., Weihs, T. P., Betenbaugh, M. & Bao, G. An In Vitro Uniaxial Stretch Model for Axonal Injury. *Ann. Biomed. Eng.* **31,** 589–598 (2003).
21. Coste, B. *et al.* Piezo1 and Piezo2 are essential components of distinct mechanically activated cation channels. *Science* **330,** 55–60 (2010).
22. Sakmann, B. & Neher, E. Patch clamp techniques for studying ionic channels in excitable membranes. *Ann. Rev. Physiol.* **6,** 455–472 (1984).
23. Opsahl, L. R. & Webb, W. W. Lipid-glass adhesion in giga-sealed patch-clamped membranes. *Biophys J* **66,** 75–79 (1994).
24. Sukharev, S. I. Energetic and Spatial Parameters for Gating of the Bacterial Large Conductance Mechanosensitive Channel, MscL. *J. Gen. Physiol.* **113,** 525–39 (1999).
25. Yan, Z. *et al.* Drosophila NOMPC is a mechanotransduction channel subunit for gentle-touch sensation. *Nature* **493,** (2013).
26. Brohawn, S. G., Su, Z. & MacKinnon, R. Mechanosensitivity is mediated directly by the lipid membrane in TRAAK and TREK1 K+ channels. *Proc. Natl. Acad. Sci. U. S. A.* **111,** 3614–9 (2014).
27. Brohawn, S. G., del Mármol, J. & MacKinnon, R. Crystal structure of the human K2P TRAAK, a lipid- and mechano-sensitive K+ ion channel. *Science* **335,** 436–41 (2012).
28. Coste, B. *et al.* Piezo proteins are pore-forming subunits of mechanically activated channels. *Nature* (2012). doi:10.1038/nature10812
29. Woo, S.-H. *et al.* Piezo2 is required for Merkel-cell mechanotransduction. *Nature* **509,** 622–626 (2014).
30. Maksimovic, S. *et al.* Epidermal Merkel cells are mechanosensory cells that

tune mammalian touch receptors. *Nature* **509,** 617–621 (2014).

31. Li, J. *et al.* Piezo1 integration of vascular architecture with physiological force. *Nature* **515,** 279–282 (2014).
32. Ranade, S. S. *et al.* Piezo1, a mechanically activated ion channel, is required for vascular development in mice. *Proc. Natl. Acad. Sci. U. S. A.* **111,** 10347–52 (2014).
33. Faucherre, A., Kissa, K., Nargeot, J., Mangoni, M. E. & Jopling, C. Piezo1 plays a role in erythrocyte volume homeostasis. *Haematologica* **99,** 70–75 (2014).
34. Albuisson, J. *et al.* Dehydrated hereditary stomatocytosis linked to gain-of-function mutations in mechanically activated PIEZO1 ion channels. *Nat. Commun.* **4,** 1884 (2013).
35. Zarychanski, R. *et al.* Mutations in the mechanotransduction protein PIEZO1 are associated with hereditary xerocytosis. *Blood* **120,** 1908–1915 (2012).
36. Jin, Y. *et al.* Functional role of mechanosensitive ion channel Piezo1 in human periodontal ligament cells. *Angle Orthod.* **00,** 0–7 (2014).
37. O'Hagan, R., Chalfie, M. & Goodman, M. B. The MEC-4 DEG/ENaC channel of Caenorhabditis elegans touch receptor neurons transduces mechanical signals. *Nat. Neurosci.* **8,** 43–50 (2005).
38. Zhong, L., Hwang, R. Y. & Tracey, W. D. Pickpocket Is a DEG/ENaC Protein Required for Mechanical Nociception in Drosophila Larvae. *Curr. Biol.* **20,** 429–434 (2010).
39. Mauthner, S. E. *et al.* Balboa binds to pickpocket in vivo and is required for mechanical nociception in Drosophila larvae. *Curr. Biol.* **24,** 2920–5 (2014).

40. Drew, L. J. *et al.* Acid-sensing ion channels ASIC2 and ASIC3 do not contribute to mechanically activated currents in mammalian sensory neurones. *J. Physiol.* **556,** 691–710 (2004).

41. Lu, Y. *et al.* The ion channel ASIC2 is required for baroreceptor and autonomic control of the circulation. *Neuron* **64,** 885–97 (2009).

42. Kang, L. J., Gao, J. W., Schafer, W. R., Xie, Z. X. & Xu, X. Z. S. C. elegans TRP Family Protein TRP-4 Is a Pore-Forming Subunit of a Native Mechanotransduction Channel. *Neuron* **67,** 381–391 (2010).

43. Goodman, M. B. *et al.* MEC-2 regulates C. elegans DEG/ENaC channels needed for mechanosensation. *Nature* **415,** 1039–1042 (2002).

44. Chelur, D. S. *et al.* The mechanosensory protein MEC-6 is a subunit of the C. elegans touch-cell degenerin channel. *Nature* **420,** 669–673 (2002).

45. Tabarean, I. V, Juranka, P. & Morris, C. E. Membrane stretch affects gating modes of a skeletal muscle sodium channel. *Biophys. J.* **77,** 758–774 (1999).

46. Yu, F. H., Yarov-Yarovoy, V., Gutman, G. a & Catterall, W. a. Overview of molecular relationships in the voltage-gated ion channel superfamily. *Pharmacol. Rev.* **57,** 387–395 (2005).

47. Nassar, M. A. *et al.* Nociceptor-specific gene deletion reveals a major role for Na. *Pnas* **101,** (2004).

48. Cox, J. J. *et al.* An SCN9A channelopathy causes congenital inability to experience pain. *Nature* **444,** 894–898 (2006).

49. Calabrese, B., Tabarean, I. V, Juranka, P. & Morris, C. E. Mechanosensitivity of N-type calcium channel currents. *Biophys. J.* **83,** 2560–74 (2002).

50. Lyford, G. L. *et al.* alpha(1C) (Ca(V)1.2) L-type calcium channel mediates

mechanosensitive calcium regulation. *Am. J. Physiol. Cell Physiol.* **283,** C1001–8 (2002).

51. Farrugia, G. *et al.* A mechanosensitive calcium channel in human intestinal smooth muscle cells. *Gastroenterology* **117,** 900–5 (1999).
52. Shin, J., Martinez-salgado, C., Heppenstall, P. A. & Lewin, G. R. A T-type calcium channel required for normal function of a mammalian mechanoreceptor. **6,** 724–730 (2003).
53. Catterall, W. A. Voltage-Gated Calcium Channels. (2015). doi:10.1101/cshperspect.a003947
54. Davies, A. *et al.* Functional biology of the $\alpha 2\delta$ subunits of voltage-gated calcium channels. *Trends Pharmacol. Sci.* **28,** 220–228 (2007).
55. Arikkath, J. & Campbell, K. P. Auxiliary subunits: essential components of the voltage-gated calcium channel complex. *Curr. Opin. Neurobiol.* **13,** 298–307 (2003).
56. Wu, J. *et al.* Structure of the voltage-gated calcium channel Cav1.1 complex. *Science (80-.).* **350,** aad2395–aad2395 (2015).
57. Hofmann, F., Flockerzi, V., Kahl, S. & Wegener, J. W. L-Type CaV1.2 Calcium Channels: From In Vitro Findings to In Vivo Function. *Physiol. Rev.* **94,** 303–326 (2014).
58. Sheets, L., Kindt, K. S. & Nicolson, T. Presynaptic CaV1.3 channels regulate synaptic ribbon size and are required for synaptic maintenance in sensory hair cells. *J. Neurosci.* **32,** 17273–86 (2012).
59. Christel, C. J. *et al.* Distinct localization and modulation of Cav1.2 and Cav1.3 L-type Ca2+ channels in mouse sinoatrial node. *J. Physiol.* **590,** 6327–42 (2012).

60. Heginbotham, L. & MacKinnon, R. Conduction properties of the cloned Shaker K+ channel. *Biophys. J.* **65,** 2089–96 (1993).

61. Graf, J., Rupnik, M., Zupancic, G. & Zorec, R. Osmotic swelling of hepatocytes increases membrane conductance but not membrane capacitance. *Biophys. J.* **68,** 1359–63 (1995).

62. Hao, J. *et al.* Kv1.1 channels act as mechanical brake in the senses of touch and pain. *Neuron* **77,** 899–914 (2013).

63. Beyder, A. *et al.* Mechanosensitivity of Nav1.5, a voltage-sensitive sodium channel. *J. Physiol.* **588,** 4969–85 (2010).

64. Wang, J. a *et al.* Membrane trauma and Na+ leak from Nav1.6 channels. *Am. J. Physiol. Cell Physiol.* **297,** C823–34 (2009).

65. Woo, S.-H. *et al.* Piezo2 is the principal mechanotransduction channel for proprioception. *Nat. Neurosci.* **18,** 1756–1763 (2015).

66. Demolombe, S., Duprat, F., Honoré, E. & Patel, A. Slower piezo1 inactivation in dehydrated hereditary stomatocytosis (Xerocytosis). *Biophys. J.* **105,** 833–834 (2013).

67. Bae, C., Gnanasambandam, R., Nicolai, C., Sachs, F. & Gottlieb, P. a. Xerocytosis is caused by mutations that alter the kinetics of the mechanosensitive channel PIEZO1. *Proc. Natl. Acad. Sci. U. S. A.* **110,** E1162–8 (2013).

68. Gottlieb, P. a., Bae, C. & Sachs, F. Gating the mechanical channel Piezo1: a comparison between whole-cell and patch recording. *Channels (Austin).* **6,** 282–289 (2012).

69. Li, C. *et al.* Piezo1 forms mechanosensitive ion channels in the human MCF-7 breast cancer cell line. *Sci. Rep.* **5,** 8364 (2015).

70. Shi, Y., Kirwan, P., Smith, J., Robinson, H. P. C. & Livesey, F. J. Human cerebral cortex development from pluripotent stem cells to functional excitatory synapses. *Nat. Neurosci.* **15,** 477–486 (2012).

71. Munoz-sanjuan, I. & Brivanlou, A. Neural induction, the default model and embryonic stem cells. *Nat. Rev. Neurosci.* **3,** 272–80 (2002).

72. Wichterle, H., Lieberam, I., Porter, J. J. a & Jessell, T. T. M. Directed differentiation of embryonic stem cells into motor neurons. *Cell* **110,** 385–97 (2002).

73. Wichterle, H. & Peljto, M. Differentiation of mouse embryonic stem cells to spinal motor neurons. *Curr. Protoc. Stem Cell Biol.* 1–9 (2008). doi:10.1002/9780470151808.sc01h01s5

74. Ran, F. A. *et al.* Genome engineering using the CRISPR-Cas9 system. *Nat. Protoc.* **8,** 2281–2308 (2013).

75. Lee, S. M. *et al.* PLP2/A4 interacts with CCR1 and stimulates migration of CCR1-expressing HOS cells. *Biochem. Biophys. Res. Commun.* **324,** 768–772 (2004).

76. Breitwieser, G. E. *et al.* Colonic epithelium-enriched protein A4 is a proteolipid that exhibits ion channel characteristics. *Am. J. Physiol.* **272,** C957–65 (1997).

77. Timms, R. T. *et al.* Haploid Genetic Screens Identify an Essential Role for PLP2 in the Downregulation of Novel Plasma Membrane Targets by Viral E3 Ubiquitin Ligases. *PLoS Pathog.* **9,** 1–14 (2013).

78. Sánchez-pulido, L., Martín-belmonte, F., Valencia, A. & Alonso, M. A. MARVEL : a conserved domain involved in membrane apposition events.

27, 599–601 (2002).

79. E.Evans. Entropy-Driven Tension and Bending Elasticity in Condensed-Fluid Membranes. *Phys. Rev. Lett.* **69,** 168–171 (1992).

80. Longo, M. L. & Ly, H. V. Micropipet aspiration for measuring elastic properties of lipid bilayers. *Methods Mol. Biol.* **400,** 421–37 (2007).

81. Horejsi, V. & Vlcek, C. Novel structurally distinct family of leucocyte surface glycoproteins including CD9, CD37, CD53 and CD63. *FEBS Lett.* **288,** 1–4 (1991).

82. Petersen, S. H. *et al.* The role of tetraspanin CD63 in antigen presentation via MHC class II. *Eur. J. Immunol.* **41,** 2556–2561 (2011).

83. Ivanusic, D. In Sweet Harmony: CD63 and HIV-1. *AIDS Res. Hum. Retroviruses* **31,** 1–2 (2015).

84. Lupia, A. *et al.* CD63 Tetraspanin Is a Negative Driver of Epithelial-to-Mesenchymal Transition in Human Melanoma Cells. *J. Invest. Dermatol.* **134,** 2947–2956 (2014).

85. Ivanusic, D. HIV-1 Cell-to-Cell Spread: CD63–gp41 Interaction at the Virological Synapse. *AIDS Res. Hum. Retroviruses* **30,** 844–845 (2014).

86. Lindern, J. J. Von *et al.* Potential Role for CD63 in CCR5-Mediated Human Immunodeficiency Virus Type 1 Infection of Macrophages Potential Role for CD63 in CCR5-Mediated Human Immunodeficiency Virus Type 1 Infection of Macrophages. *J. Virol.* **77,** 3624–3633 (2003).

87. Bae, C., Sachs, F. & Gottlieb, P. a. Protonation of the Human PIEZO1 Ion Channel Stabilizes Inactivation. *J. Biol. Chem.* **290,** 5167–5173 (2015).

88. Martens, J. R., O'Connell, K. & Tamkun, M. Targeting of ion channels to membrane microdomains: Localization of K V channels to lipid rafts.

Trends Pharmacol. Sci. **25,** 16–21 (2004).

89. Martens, J. R. *et al.* Differential targeting of shaker-like potassium channels to lipid rafts. *J. Biol. Chem.* **275,** 7443–7446 (2000).

90. Martens, J. R., Sakamoto, N., Sullivan, S. A., Grobaski, T. D. & Tamkun, M. M. Isoform-specific Localization of Voltage-gated K+Channels to Distinct Lipid Raft Populations: TARGETING OF Kv1.5 TO CAVEOLAE. *J. Biol. Chem.* **276,** 8409–8414 (2001).

91. Brady, J. D. *et al.* Functional role of lipid raft microdomains in cyclic nucleotide-gated channel activation. *Mol. Pharmacol.* **65,** 503–511 (2004).

92. Anderson, R. G. W. A Role for Lipid Shells in Targeting Proteins to Caveolae, Rafts, and Other Lipid Domains. *Science (80-.).* **296,** 1821–1825 (2002).

93. Huang, H., Bae, C., Sachs, F. & Suchyna, T. M. Caveolae Regulation of Mechanosensitive Channel Function in Myotubes. *PLoS One* **8,** 1–15 (2013).

94. Anderson, R. G. The caveolae membrane system. *Annu. Rev. Biochem.* **67,** 199–225 (1998).

95. Maruyama, T. *et al.* (SI) Increasing the efficiency of precise genome editing with CRISPR-Cas9 by inhibition of nonhomologous end joining. *Nat. Biotechnol.* **33,** 1–9 (2015).

96. Wetzel, C. *et al.* A stomatin-domain protein essential for touch sensation in the mouse. *Nature* **445,** 206–209 (2007).

97. Lapatsina, L., Brand, J., Poole, K., Daumke, O. & Lewin, G. R. Stomatin-domain proteins. *Eur. J. Cell Biol.* **91,** 240–245 (2012).

98. Yaffe, Y. *et al.* The MARVEL transmembrane motif of occludin mediates oligomerization and targeting to the basolateral surface in epithelia. *J. Cell*

Sci. **125,** 3545–56 (2012).

99. Arthur, C. P. & Stowell, M. H. B. Structure of synaptophysin: A hexameric MARVEL domain channel protein. *Structure* **15,** 707–714 (2007).

100. Raleigh, D. R. *et al.* Tight junction-associated MARVEL proteins marveld3, tricellulin, and occludin have distinct but overlapping functions. *Mol. Biol. Cell* **21,** 1200–13 (2010).

101. Delic, S. *et al.* Systematic Investigation of CMTM Family Genes Suggest Relevance to Glioblastoma Pathogenesis and CMTM1 and CMTM3 as Priority Targets. *Genes. Chromosomes Cancer* **54,** 433–443 (2015).

102. Zhang, H. *et al.* CMTM3 inhibits cell growth and migration and predicts favorable survival in oral squamous cell carcinoma. *Tumor Biol.* **36,** 7849–7858 (2015).

103. Li, T. *et al.* CMTM4 is frequently downregulated and functions as a tumour suppressor in clear cell renal cell carcinoma. *J. Exp. Clin. Cancer Res.* **34,** 122 (2015).

104. Xiao, Y. *et al.* CMTM5 is reduced in prostate cancer and inhibits cancer cell growth in vitro and in vivo. *Clin. Transl. Oncol.* **17,** 431–437 (2015).

105. Xiong, W. *et al.* TMHS Is an Integral Component of the Mechanotransduction Machinery of Cochlear Hair Cells. *Cell* **151,** 1283–1295 (2015).

106. Beurg, M., Xiong, W., Zhao, B., Müller, U. & Fettiplace, R. Subunit determination of the conductance of hair-cell mechanotransducer channels. *Proc. Natl. Acad. Sci.* **112,** 1589–1594 (2015).

107. Zhao, B. *et al.* TMIE Is an Essential Component of the Mechanotransduction Machinery of Cochlear Hair Cells. *Neuron* **84,** 954–

967 (2014).

108. Pan, B. *et al.* TMC1 and TMC2 Are Components of the Mechanotransduction Channel in Hair Cells of the Mammalian Inner Ear. *Neuron* **79,** 1–12 (2013).

109. Hemler, M. E. Tetraspanin functions and associated microdomains. *Nat. Rev. Mol. Cell Biol.* **6,** 801–811 (2005).

110. Maecker, T., Todd, C. & Levy, S. The tetraspanin facilitators. *FASEB J.* **11,** 428–442 (1997).

111. Levy, S. *et al.* Protein-Protein Interactions in the Tetraspanin Web. *Physiology (Bethesda).* **20,** 218–224 (2005).

112. Yunta, M. & Lazo, P. a. Tetraspanin proteins as organisers of membrane microdomains and signalling complexes. *Cell. Signal.* **15,** 559–564 (2003).

113. Yáñez-Mó, M., Barreiro, O., Gordon-Alonso, M., Sala-Valdés, M. & Sánchez-Madrid, F. Tetraspanin-enriched microdomains: a functional unit in cell plasma membranes. *Trends Cell Biol.* **19,** 434–446 (2009).

114. Li, L. & Ginty, D. D. The structure and organization of lanceolate mechanosensory complexes at mouse hair follicles. *Elife* **2014,** 1–24 (2014).

115. Abraira, V. E. & Ginty, D. D. The Sensory Neurons of Touch. *Neuron* **79,** 618–639 (2013).

116. Rutlin, M. *et al.* The Cellular and Molecular Basis of Direction Selectivity of Ad-LTMRs. *Cell* 1640–1651 (2014).

117. Ying, Q. *et al.* The ground state of embryonic stem cell self-renewal. *Nature* **453,** 519–24 (2008).

118. Girard P. *et al*. A new method for the reconstitution of Membrane Proteins into Giant Unilamellar Vesicles. *Biophysical Journal* **87** 419-429 (1984).

119. Evans E. and Needham J. Physical properties of surfactant bilayer membranes: thermal transitions, elasticity, rigidity, cohesion and colloidal interactions. *J Phys Chem* **91** 4219-4228 (1987).

120. Evans E. and Rawicz W. Entropy-driven tension and bending elasticity in condensed-fluid membranes. *Phys Rev Lett* **17** 2094-2097 (1990)